Evaluation of district heating systems based on exergy analysis

Bewertung von Nahwärmenetzen basierend auf Exergieanalyse

Vom Fachbereich Maschinenbau der Technischen Universität Darmstadt
zur Erlangung des akademischen Grades Doktor-Ingenieur (Dr.-Ing.)
genehmigte Dissertation von Paul Michael Falk aus Mainz
Januar 2018 — Darmstadt — D 17

TECHNISCHE
UNIVERSITÄT
DARMSTADT

Technische Thermodynamik

Evaluation of district heating systems based on exergy analysis
Bewertung von Nahwärmenetzen basierend auf Exergieanalyse

Genehmigte Dissertation von Paul Michael Falk aus Mainz

1. Gutachten: Prof. Dr.-Ing. Peter Stephan
2. Gutachten: Prof. Dr. rer. nat. Liselotte Schebek

Tag der Einreichung: 23. Januar 2017
Tag der Prüfung: 17. April 2017

Darmstadt — D 17

Bitte zitieren Sie dieses Dokument als:
URN: urn:nbn:de:tuda-tuprints-73723
URL: https://tuprints.ulb.tu-darmstadt.de/7372

Dieses Dokument wird bereitgestellt von tuprints,
E-Publishing-Service der TU Darmstadt
https://tuprints.ulb.tu-darmstadt.de
tuprints@ulb.tu-darmstadt.de

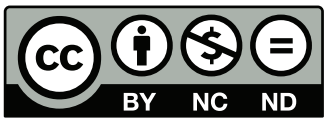

Die Veröffentlichung steht unter folgender Creative Commons Lizenz:
Namensnennung – Keine kommerzielle Nutzung – Keine Bearbeitung 4.0
https://creativecommons.org/licenses/by/4.0/

Erklärung zur Dissertation

Hiermit versichere ich, die vorliegende Dissertation ohne Hilfe Dritter nur mit den angegeben Quellen und Hilfsmitteln angefertigt zu haben. Alle Stellen, die aus Quellen entnommen wurden, sind als solche kenntlich gemacht. Diese Arbeit hat in gleicher oder ähnlicher Form noch keiner Prüfungsbehörde vorgelegen.

Darmstadt, 17. Januar 2018

Paul Michael Falk

Acknowledgements

Die vorliegende Arbeit entstand während meiner Tätigkeit am Institut für Technische Thermodynamik (TTD) der Technischen Universität Darmstadt. Ich bedanke mich herzlich bei Herrn Professor Peter Stephan für die Möglichkeit, diese Arbeit an seinem Fachgebiet durchzuführen, und die inhaltlichen Freiräume, die er geschaffen hat. Für die sehr gute Betreuung meiner Arbeit möchte ich Frank Dammel danken. Er war ein sehr kompetenter Ansprechpartner und hatte stets ein offenes Ohr.
Frau Professor Liselotte Schebek möchte ich für die Übernahme des Korreferats danken.
Meinen Kollegen am TTD danke ich für die tolle Arbeitsatmosphäre. Namentlich erwähnen möchte ich Axel Dietrich, Johannes Oltmanns und Kai Schweickert, mit denen man gut fachlich und überfachlich reden und diskutieren konnte.
Tausend Dank gilt auch Gaby Gunkel für ihre freundliche und hilfsbereite Zusammenarbeit.
Insbesondere der Darmstädter Exzellenz-Graduiertenschule für Energiewissenschaft und Energietechnik, nicht zuletzt für die finanzielle Ermöglichung meiner Arbeit, möchte ich danken. Die interdisziplinäre Struktur und die kollegiale Zusammenarbeit mit Doktoranden aus anderen Fachbereichen haben zum Erfolg meiner Arbeit beitragen.
Für das Ermöglichen meines Forschungsaufenthaltes an der Princeton University danke ich Herrn Professor Peter Stephan, Prof. Forrest Meggers und der Darmstädter Exzellenz-Graduiertenschule für Energiewissenschaft und Energietechnik.
Nicht weniger dankbar bin ich Frank Dammel, Kai Schweickert, Johannes Oltmanns und meiner Frau insbesondere für die gründliche Korrektur meiner Arbeit. Um es mit Kai Schweickert's Worten zu sagen: "Something that nobody could have done any better. I owe them now".
Dankend erwähnen möchte ich auch den hilfreichen fachlichen Austausch mit den Mitgliedern des Internationalen Energieagentur Annex 64.
Ein besonderer Dank gilt den vielen Studenten, die ich betreuen durfte. Durch die anregenden Diskussionen und ihre Mitarbeit haben sie meine Promotion sehr bereichert und vorangebracht. Stellvertretend für alle möchte ich Robert Klemmer, Hendryk Engelbart und Andreas Morbach nennen.
Mein größter Dank jedoch gilt meiner Familie.

Darmstadt, im Januar 2018

Paul Michael Falk

The work was conducted in the framework of the International Energy Agency Annex 64: LowEx Communities - Optimized Performance of Community Energy Supply Systems with Exergy Principles. It was financially supported by the DFG in the framework of the Excellence Initiative, Darmstadt Graduate School of Excellence Energy Science and Engineering (GSC 1070). CARNOT was developed by the Solar-Institut Jülich, Germany, and is available there at no charge. The demand data of the individual buildings was kindly provided by MVV Energie AG Mannheim, Germany.

Abstract

In Germany, 22 % of the total primary energy usage is used for room heating and domestic hot water. Oil and gas are the most common energy sources for heating, while renewable energies are rarely used. In order to reach the climate targets set by the German government, primary energy input must be reduced and more renewable energy should be supplied to cover the energy demand. At the same time, the efficiency of energy usage should be increased. District heating systems offer a good opportunity for using renewable energies in combination with thermal energy storage.

One approach to reducing the primary energy input and increasing the efficiency of usage is the so called exergy concept. It aims at using the energy meaningfully by matching the exergy level of the supply with the exergy level of the demand. Thus, high exergy energy is not used to cover low exergy demand.

Numerous examples of applied exergy analysis of district heating systems and thermal energy storages can be found in the literature. However, an integral approach and assessment of different heating technologies for district heating systems by using energy, exergy, ecological and economical analyses is not known. Further, exergy analyses of thermal energy storages integrated into district heating systems are not publicly available.
Therefore, in this work, dynamical simulation models of district heating systems are developed with the MATLAB/Simulink based toolbox CARNOT. The models are used to investigate different heating technologies and to give a comparative overview.

Kurzzusammenfassung

In Deutschland werden 22 % der eingesetzten Primärenergie zu Heizzwecken und für den Warmwasserbedarf genutzt. Öl und Gas sind dabei die am häufigsten eingesetzten Energieträger, während erneuerbare Energien kaum genutzt werden. Um die Klimaziele der deutschen Bundesregierung zu erreichen und den Energiebedarf zu decken, muss der Primärenergieverbrauch gesenkt und mehr erneuerbare Energien sollten bereitgestellt werden. Gleichzeitig sollte die Effizienz der Energienutzung gesteigert werden. Nahwärmenetze bieten eine gute Gelegenheit erneuerbare Energien in Kombination mit Wärmespeichern zu nutzen.
Ein Ansatz zur Primärenergieeinsparung und zur Effizienzsteigerung ist das so genannte Exergiekonzept. Dabei wird versucht, die eingesetzte Energie sinnvoll zu nutzen und das Exergieniveau der eingesetzten Energie an das Exergieniveau des Bedarfes anzupassen. Dadurch wird keine hoch exergetische Energie benutzt, um niedrig exergetische Bedarfe zu decken.
In Veröffentlichungen gibt es zahlreiche Beispiele von angewandter Exergienanalyse von Nahwärmenetzen und Wärmespeichern. Was jedoch nicht bekannt ist, ist ein ganzheitlicher Überblick und eine Bewertung von verschiedenen Technologien für Nahwärmenetze mit energetischer, exergetischer, ökologischer und ökonomischer Analyse. Des Weiteren sind Exergieanalysen von Wärmespeichern eingebunden in Nahwärmenetze nicht öffentlich zugänglich.
Deshalb werden in der vorliegenden Arbeit mit der MATLAB/Simulink basierten Toolbox CARNOT dynamische Simulationsmodelle von Nahwärmenetzen entwickelt. Die Modelle werden genutzt, um verschiedene Heiztechniken zu untersuchen und einen vergleichenden Überblick zu geben.

Further, a new method to calculate thermal energy storage is developed to separate between the exergy change due to a changing reference temperature and the exergy change due to the mixing of temperature layers.

Six different heat supply scenarios are considered. These are a gas boiler scenario, a combined heat and power scenario, a geothermal heat pump scenario, a combination of a geothermal heat pump and a combined heat and power plant scenario, a solar thermal collector scenario, and a scenario with a combination of an air source heat pump and a geothermal heat pump scenario.
The investigated district heating system consists of a building cluster with 11 buildings and a total annual heat demand of 263.7 MWh. The calculated exergy content of the heat demand is 14.0 MWh. The six different heat supply scenarios are assessed using energy, exergy, ecological and economical analysis.
The results show that the combined heat and power scenario has the highest economical efficiency but a high fossil energy input, while the scenario with a combination of an air source heat pump and a geothermal heat pump has the lowest fossil energy input and global warming potential, but is the most expensive. The geothermal heat pump scenario has the lowest total exergy input and shows the best overall performance. In regards to the performance of a thermal energy storage within a district heating system the findings demonstrate that it is very important to take all parameters affecting the storage into account during the dimensioning of the storage, since it reacts very sensitively.

Overall it is shown that the developed thermal energy storage calculation method and the models are suited to study thermal energy storages and district heating systems.

Außerdem wird eine neue Methode Wärmespeicher zu berechnen entwickelt, die es ermöglicht, zwischen Exergieänderung aufgrund veränderlicher Referenztemperatur und Exergieänderung aufgrund von Durchmischung von Temperaturschichten zu unterscheiden.
In der Arbeit werden sechs verschiedene Szenarien betrachtet. Diese sind ein Gas Szenario, ein Blockheizkraftwerk Szenario, ein geothermisches Wärmepumpen Szenario, eine Kombination des geothermischen Wärmepumpen und des Blockheizkraftwerk Szenario, ein Solarthermiekollektor Szenario und ein Szenario mit einer Kombination aus einer Luft-Wärmepumpe und einer geothermischen Wärmepumpe.
Das untersuchte Nahwärmenetz besteht aus einer Gebäudegruppe mit 11 Gebäuden und einem Jahreswärmebedarf von 263.7 MWh. Der berechnete Exergeinhalt des Wärmebedarfes ist 14.0 MWh. Die sechs verschiedenen Szenarien werden mit Hilfe energetischer, exergetischer, ökologischer und ökonomischer Analyse bewertet.
Die Ergebnisse zeigen, dass das Blockheizkraftwerk Szenario am Kostengünstigsten ist, aber mit einem hohen fossilen Energieaufwand verbunden ist. Das Szenario mit einer Kombination aus einer Luft-Wärmepumpe und einer geothermischen Wärmepumpe hingegen besitzt den niedrigsten fossilen Energieaufwand und Treibhauspotential, ist aber am teuersten. Das geothermische Wärmepumpen Szenario hat den niedrigsten Exergieaufwand und zeigt die beste Gesamtleistung.
In Bezug auf das Verhalten eines Wärmespeichers, der in ein Nahwärmenetz eingebunden ist, zeigen die Ergebnisse die Notwendigkeit alle Parameter, die den Wärmespeicher beeinflussen, in die Auslegung mit einzubeziehen, da er sehr sensibel reagiert.
Insgesamt zeigt sich, dass die entwickelte Wärmespeicher Berechnungsmethode und die Modelle geeignet sind um Wärmespeicher und Nahwärmenetze zu untersuchen.

Contents

Nomenclature

Latin Letters

Letter	Description	Unit
A	annuity	€/(a)
A'	area	m^2
CED	cumulative energy demand	J/(a)
CN	criteria number	–
D	distance	m
E	energy calculated for one year	J
E'	electrical energy without conversion losses considered	J
EX	exergy calculated for one year	J
$\dot{EX}$	exergy flow	W
F'	collector efficiency factor	–
GWP	global warming potential	$kg_{CO_2e}/(a)$
I	radiation	$W/(m^2)$
K	incidence angle modifier	–
L	length	m
LHV	lower heating value	J
M	mass	kg
$\dot{M}$	mass flow	kg/(s)
N	mean number of carbon atoms in a molecule	–
P	power	W
Q	heat	J
$\dot{Q}$	heat flow	W
R	revenue	€
S	entropy	J/(K)
SF	simultaneity factor	–
T	temperature	°C and K
TA	effective transmittance-absorptance product for direct solar radiation at normal incidence	–
W	work	J
WMN	weighted multicriteria number	–
a	annuity factor	–

b	price dynamic cash value factor	–
c	specific heat capacity	J/(kgK)
d	day	d
g	gravity	$m/(s^2)$
h	specific enthalpy	J/(kg)
k	heat loss coefficient	$W/(m^2K)$
m	number of consumers	–
p	pressure	Pa
q	CO_2-equivalents	$kg_{CO_2e}/(J)$
q'	annual CO_2-equivalents	$kg_{CO_2e}/(a)$
r	price change factor	%
t	time	s
v	specific volume	$m^3/(kg)$
w	velocity	m/(s)
z	height	m

Greek Letters

Letter	Description	Unit
β	quality factor	–
Δ	difference	–
ϵ	interest factor	%
η	energy efficiency	%
κ	solar coverage	%
λ	thermal conductivity	W/(mK)
ρ	density	$kg/(m^3)$
σ	constant	$W/(m^2K^4)$
σ_{i}	share of one energy source on the overall electricity mix	%
τ	number of years	–
ϕ	weighting factor	–
ψ	exergy efficiency	%

Subscripts

Symbol	Description
0	state 0
1	state 1
2	state 2

C	capital-related
CH	chemical
D	demand-related
O	operation-related
R	revenue
SB	Stefan-Boltzmann
TES begin	TES load condition at beginning of simulation
TES end	TES load condition at end of simulation
air	air sourced
comb.	combined
destr.	destruction
dfu	diffuse
dir	direct
el	electrical
el.district	electrical district demand
el.fossil	fossil electrical
el.grid	electrical supply to grid
el.mix	electricity mix in grid
el.renew	renewable electrical
fix	fix reference temperature
fossil	fossil
in	input
loss	loss
m	mean
n	nominal
out	output
p	peak
r	return
ref	reference temperature
renewable	renewable
s	supply
system	system
th	thermal
th.district	thermal district demand
u	environment state
var	variable reference temperature
w	water

Abbreviations

Acronym	Description
C	carbon
CO_2	carbon dioxide
CHP	Combined heat and power
C&G	cradle and grave
DHS	district heating system
DHW	domestic hot water
H	hydrogen
HP	heat pump
HTS	heat transfer station
HVAC	heating, ventilation and air conditioning
LCA	life cycle assessment
PV	photovoltaic
PVT	photovoltaic thermal
TES	thermal energy storage
VGHX	vertical ground source heat exchanger

List of Figures

List of Tables

1 Introduction

Backround

Fossil energy resources are decreasing and the climate is changing due to rising CO_2 levels in the atmosphere. Therefore, the German government has committed itself to reducing the overall greenhouse gas emissions by 80 % compared to 1990 and the primary energy demand in the residential sector by 80 % compared to 2008 until the year 2050 [22]. Consequently more renewable energy should be used for the energy supply and the efficiency of usage should be enhanced. In Germany, the residential sector uses 30 % of the primary energy input [133]. Of these 30 % around 75 % are used for room heating [146]. This leads to an actual use of 22 % of the overall primary energy input for room heating and to 10 % of Germany's overall CO_2 emissions [148]. Due to its high energy efficiency and affordable use, the main heat source in German households is the natural gas condensing boiler [132]. Compared to natural gas and fuel oil, alternative heat sources are seldom used [132].
Due to the high primary energy use in the residential sector, many measures are taken to increase the energy efficiency and to decrease overall energy use [143]. However, matching the energy quality level of the supply to the energy quality level of the demand is not discussed publicly. The term "exergy" is only known to very few people. "Exergy" is the share of energy which can be transformed into useful work. Simply put, it defines the share of energy which could be used for a high quality process such as electricity generation. Room heating or domestic hot water (DHW) is considered to be low quality energy demand. Even though the commonly used condensing boiler has a very high energy efficiency, high quality natural gas is used to generate low quality heat. Exergy concepts aim at using the available high quality energy for high quality demands such as lighting or computer usage. Torío defines low exergy systems as "systems that provide acceptable thermal comfort with minimum exergy destruction" [143]. Exergy concepts attempt to use available energy meaningfully, while energy concepts are not focused on energy quality, but just on quantity. In a way, exergy concepts do not necessarily aim at energy savings, but at a more meaningful way of using energy which can result in overall energy savings. Exergy analysis is always coupled with energy analysis and gives a different viewpoint in addition to the energy efficiency. Energy efficiency is a measure for the matching of energy supply and demand in terms of quantity, while exergy efficiency is a measure for the matching of the quality levels of demand and supply. However, exergy analysis should not be compared to energy analysis in terms of better or worse as it simply gives another viewpoint of the same system, making energy use decisions more substantiated. Exergy analysis does not differentiate between fossil and renewable energy although renewable energy is often more preferable from an exergy viewpoint. The reason for this is that geothermal heat and outside air for example are low exergy sources, whereas all fossil fuels are high exergy sources.
In this work, the focus lies on primary energy savings and greenhouse gas emission reductions in the residential sector. Different heating systems are analyzed from different perspectives. First, energy and exergy analysis is used to assess and optimize different heating systems of a building cluster connected via a district heating system (DHS). Then, the optimized systems are analyzed in terms of ecological and economical efficiency. An integrated overview of different heat supply options is given in a concluding

comparison.

Outline of the work

The analysis in this work is conducted using a building cluster connected via a DHS. The different analyzed systems in this work are a gas boiler system as reference case, a combined heat and power (CHP) plant with a gas boiler as backup, a geothermal HP, a CHP plant combined with a geothermal heat pump (HP), solar thermal collectors with a gas boiler as backup, and a scenario consisting of a combination of an air HP and a geothermal HP.
The systems are assessed using real demand and weather data and simulating the building cluster dynamically in the MATLAB/Simulink based toolbox CARNOT.
The outline of this work is as follows: In chapter 2, an introduction into literature is given and the aims of the thesis are deducted. In chapter 3, basics regarding heating systems and exergy analysis are outlined, followed by a description of the used models in chapter 4. Subsequently, a new method for the calculation of the exergy balance of a thermal energy storage (TES) is developed and applied to a TES within a simulated building cluster in chapter 5. After the results are presented in chapter 6, the work is discussed, summarized and an outlook for future work is given. In the appendix, calculation methods and data are given for the model parameters and assumptions.

2 State of the art

In this chapter, basics regarding energy and exergy analysis are discussed, heat generation systems are introduced and a literature review is conducted from which the research tasks for this work are derived.

2.1 Basics

In the following, an introduction into energy and exergy analysis and the heat generation technologies used in this work are given.

Energy analysis

Within an energy analysis the energy flow through a system and through individual components is assessed and the efficiency of each component and of the system as a whole can be quantified. Energy cannot be destroyed or lost, only converted into a different energy type. With energy analysis, the quantity of an energy flow can be determined.

Exergy analysis

Exergy is the maximum work that can be obtained when a system is brought into equilibrium with a reference environment. It is a measure of the quality of energy [118]. Such conversion requires a reversible process, which is the theoretical limit for the optimization of real processes. According to Bejan et al. [13] the total exergy of a system can be divided into physical, kinetic and chemical exergy, while nuclear, magnetic, electrical and surface tension effects are neglected.
In contrast to energy, exergy can be lost and destroyed. Exergy analysis also assesses the input and output flows of a system, but in regards to their exergy content. With exergy analysis, the exergy flow through a system and through the individual components is assessed and the efficiency of each component and of the system as a whole can be quantified. The difference to energy analysis is that during energy analysis the quantity of energy is determined, whereas with exergy analysis the quality of the energy is determined. By taking the quality of energy into account, the energy can be used more meaningful.

Gas boiler

Gas boilers are widely used in building heating systems and DHS as the main heat source as well as for peak loads. Gas boilers provide an excellent energy efficiency above 80 % and are easy to use and maintain. However, their exergetic performance is very poor, because the high exergy content of the natural gas is used to generate low exergy heat instead of a high exergy product like electricity. In terms of exergy, only a direct electrical heater is worse than a gas boiler [9].

Combined heat and power

CHP plants produce heat and electricity at the same time. By using the heat that is produced in the process, the overall efficiency of the plant is increased. Available CHP units include steam turbines, gas turbines, combined cycle gas/steam turbines, reciprocating internal combustion engines, Stirling engines and fuel cells [107]. Gas turbines and combustion engines are the most common types of CHP units. In both types, the exhaust heat generated during the combustion of the fuel is recovered and used to heat a hot water cycle. In the case of the combustion engine, it is also possible to recuperate the lube oil heat. CHP units are available from several kW to MW, which makes them suitable for individual buildings as well as DHS. A good overview of CHP systems is given in [94] and [173].

Heat pumps

A HP uses mechanical energy to transfer heat from a low temperature to a higher temperature using the following process: In a closed loop process a working fluid is evaporated at low pressure and low temperature. The steam is then compressed, producing hot steam at high pressure. Then, the steam is condensed at high pressure. In an expansion valve, which closes the loop, the pressure and the temperature are reduced to make the evaporation at low temperatures possible. In the evaporator, the working fluid absorbs heat at low temperatures, while it emits the heat at higher temperatures in the condenser. Usual heat sources are outside air or geothermal heat. Another option is the implementation of a solar thermal collector to set up a solar assisted HP system in which the evaporator takes the heat from the solar collector [145]. HP are widely used in individual buildings and in combination with geothermal DHS. A good overview of different HP applications is given in [59].

Solar thermal collectors

Solar thermal systems for hot water production usually consist of a solar collector to heat the heat transfer medium and a TES to separate the time of the heat generation from the time of the demand. The incoming solar radiation heats up the heat transfer medium which is led out of the collector to the TES, while at the same time the cool heat transfer medium is directed into the collector. There are many different types of solar thermal collectors including flat-plate, compound parabolic, evacuated tube and parabolic trough collectors [67]. Solar thermal collectors are often used for DHW production in individual buildings. However, large collector fields combined with seasonal storage systems can also supply DHS with hot water [126]. A good overview of solar thermal collectors is given in [67].

Geothermal heat

Geothermal applications use the heat which is stored in the ground to produce hot water. Geothermal heat is usually divided into deep and shallow geothermal heat [135]. Deep geothermal heat produces heat at high temperatures which can be directly used for processes, while shallow geothermal heat usually needs a temperature lift to higher temperatures via a HP. Although there is no fixed separation between shallow and deep geothermal heat, a depth of 400 m is often defined as a limit for shallow geothermal heat [135]. Among building heating technologies, the shallow geothermal heat is more common, with three different heat extraction types. One is an open well system with cold water injection and hot water extraction using two separate boreholes. The second option is a geothermal collector

with horizontal closed loop pipes not deeper than 5 m, while the third is a vertical ground source heat exchanger (VGHX) with a closed loop pipe. VGHX commonly use three different types of pipes in the building heating applications, which are U-pipes, double-U-pipes and coaxial pipes [135]. Geothermal heat is used to heat individual buildings as well as DHS. A good overview of geothermal systems is given in [37].

Photovoltaic

Photovoltaic (PV) collectors transform incoming solar radiation into electricity using the photovoltaic effect of semi-conducting materials in solar cells. A good overview of PV technology is given in [108]. PV collectors do not only generate electricity, more than 50 % of the incoming solar radiation is transformed into heat [29]. The PV collector's efficiency decreases with increasing collector temperature. By cooling the collector not only the electrical efficiency can be increased, but by making the heat available for hot water generation, the overall component efficiency can be increased. This concept is called photovoltaic thermal (PVT) collector. The PVT collector generates electricity, while the coolant ensures good working conditions for the solar cells and at the same time making the generated heat available for later use. A good overview of PVT collectors and technology is given in [29].

Thermal Energy Storage

TES are usually used as either short term buffer TES or as seasonal TES. Buffer TES are usually built as insulated cylindrical steel tanks located above ground and used to store heat in the range of hours to a few days to decouple the production from the demand.
Seasonal TES also decouple the production from the demand but over a longer period of time, often from the warm summer months till the heating period. Seasonal TES are usually categorized in four different types, namely a hot water tank, an aquifer storage, a water/gravel pit storage and a geothermal borehole storage [14]. The decision of when to use which type of TES is dependent on the needed temperature level of the TES and the geological location specifics. A good overview of the different TES characteristics is given in [126].

2.2 Literature review

In the field of heat supply systems many studies have been conducted focusing on the heat supply technology, buildings and district heating systems. Studies put their focus on energy analysis, exergy analysis, economic analysis or a combination of the aforementioned. The content of this work is the evaluation of district heating systems based on exergy analysis. Therefore, an overview of studies relevant to this topic is given in the following. Studies regarding individual heating components, as can be found for example in [28; 38; 56; 61; 66; 69; 101–105; 139; 145], are not considered here since the focus of the present work is not the optimization of individual components but the assessment of the component integration into a larger system.
Studies on building scale usually deal with the description or analysis of one or more heat generation systems and the effects on the heated building. In contrast, analyses on district scale deal with larger energy systems consisting of several buildings or building clusters with often several heat generation components as well as TES. In the present work, a focus is also put on the design and implementation of TES into DHS. Therefore, studies regarding the performance of TES both as individual components as well as implemented within large DHS are also presented below.

On building scale, Terés-Zubiaga et al. [137] study the primary energy input of a flat within a multi-family building in Spain. They consider two reference cases (case I and II) and three improved cases (cases III - V). Case I is the flat without any renovations as it was built in 1960, without insulation and using electrical heating for space heating. Case II is the flat with basic restorations including facade insulation and central heating using a gas boiler and high temperature radiators. The improved cases III - V all include increased insulation but different heat generation systems. Case III uses a HP together with low temperature floor heating, solar thermal collectors and PV modules and a condensing boiler as backup heat source. Case IV uses a CHP plant as the source for heat and electricity as well as PV modules and a low temperature heating system with radiators. Case V uses a HP in combination with a low temperature heating system with radiators. Further, solar thermal collectors and PV modules are installed and a condensing boiler is used as backup heat source. It is shown that for both reference cases the main exergy destruction occurs in the primary energy conversion to electricity, and further from the conversion from electricity and natural gas to heat. The biggest exergy destruction in case III and V takes place during the primary energy conversion to electricity and in case IV in the CHP plant. All improved cases benefit from the better insulation and the low temperature heating system, making the use of HP possible. Significant in case III and IV is the exergy destruction in the auxiliary condensing boiler, especially considering its small overall energy input. Using exergy analysis, the components with the main exergy destruction could be identified and the primary energy input could be decreased by almost 15.0 %.

Ortiz et al. [95] model a solar assisted heating, ventilation and air conditioning (HVAC) system for an educational building. In this system, solar thermal collectors are used to provide low temperature heating and high temperature cooling for the building. By implementing a hot and a cold TES, the solar assisted HVAC system is able to supply 90 % of the heating demand and to reduce the energy demand for cooling by approximately 40 %.

Lohani [80; 81] conducts an energy and exergy analysis of different building heating systems at two different reference temperatures. One is the dynamic ambient temperature and the other is 8.0 °C. The investigated heating systems are a condensing boiler, ground source HP and an air HP. Findings show that the ground source HP performs better than the condensing boiler and the air source HP, both energy- and exergy-wise.

Yumrutaş et al. [175] present a model to simulate a solar assisted ground source HP system with an underground TES. The heating system is coupled with a building to simulate the heating demand during winter. The experimental setup is found in [174] where Yumrutaş et al. present the results of an analysis of a solar assisted HP system with floor heating and a TES. Both the model and the experiment are aimed at energy analysis.

Badescu [4–7] presents a model of a solar assisted HP system for a building at the University of Bucharest. The solar assisted HP system is compared to a system with the same settings but with an additional TES. The implementation of the TES results in up to 50 % of HP energy savings compared to the same HP system without the TES. He also conducts exergy analysis to determine the components of the system with the highest exergy destruction.

Hepbasli [57] conducts an energy and exergy analysis of a solar assisted DHW TES in combination with a ground source HP system for a residential building. Exergy efficiencies of the individual components as well as the whole system are given.

On district scale, Dalla Rosa et al. [34] present a concept of a low energy DHS which can supply a district of 10 energy-efficient apartments and 5 energy-efficient buildings. A main finding of their study is that human behavior can lead to up to 50 % higher heating demand and 60 % higher peak loads than expected in standard calculations of the demand patterns of energy-efficient buildings. They conclude

that a fully renewable energy supply system needs a large initial investment but has costs in the range of standard fossil fuel based systems in the long run. They further demonstrate that a low temperature DHS shows better results than a low flow DHS.
Felsmann et al. [45] analyze the influence of low DHS temperatures on different types of CHP plants. They show that lowering the return temperature can improve the system performance, but there is a trade-off between lower temperatures and increased pump power. Lowering the system temperatures is not always possible due to existing plant components, but it is a promising approach for new systems.
Çomaklı et al. [30] analyze the DHS of the university campus of the Atatürk University, Turkey. They study the exergy losses in the system pipes and find that the total exergy losses relative to the overall exergy content of the heating system is 16 %. The energy conversion from the power plant to the primary cycle was not within the system boundary.
Torío and Schmidt [141] investigate different system concepts in order to improve the performance of a waste heat DHS. As a result they find that decreasing the supply temperature from 95 °C to 57.7 °C increases the exergy efficiency of the system from 32 % to 39.3 % and that decreasing the return temperature has a similar effect. The energy efficiencies remain nearly constant at around 80 % independent of the system configuration.
Østergaard et al. [96] develop a model to describe the transition from fossil fuels to 100 % renewable energy for all sectors of energy demand using locally available energy sources such as wind power and geothermal heat for the city of Frederikshavn in Denmark. The main change in the energy system is the use of geothermal heat in combination with an absorption HP which runs on the steam of a waste incineration plant. It is shown that the energy consumption of Frederikshavn could be decreased by 25 % and the carbon dioxide emissions by even 75 % by changing the heat production system to geothermal heat. If energy saving measures of the end user were considered, the reductions could be even higher.
Ozgener et al. [97–99] conduct energy and exergy analyses of geothermal DHS in the regions of Manisa, Balikesir and Izmir in Turkey. Results demonstrate that exergy losses mainly result from losses in pumps, heat exchangers, and re-injection sections of the geothermal water [100]. The energy efficiencies were found to be 41.9 %, 55.5 % and 45.9 % respectively. The exergy efficiencies were found to be 46 %, 49.4 % and 64.1 % respectively. In addition, the authors investigate the influence of a varying reference temperature on the energy and exergy efficiencies in [100], where two correlations are developed to predict the efficiencies of the geothermal DHS in Izmir.
Bargel [9] develops an exergy based analysis model to compare different heat supply system technologies while taking a varying outdoor temperature into account. He aims at giving a comparative overview of DHS heating technologies, by simulating individual building heating supply as well as DHS. On the demand side, four different building types are investigated. On the supply side, a gas boiler, direct electrical heating, a CHP, a HP and waste heat is considered. The main outcomes are that combustion-based technologies have the lowest exergetic efficiencies and that for CHP a high electrical efficiency should be top priority, followed by the highest possible overall efficiency. It is further concluded that auxiliary energy flows cannot be neglected, which is especially true for well insulated buildings, and that efficient DHW generation can be crucial for the overall efficiency. Another outcome is that DHS should operate at low temperatures, but general statements regarding the overall efficiency are difficult to issue and that the main advantage of a DHS is the flexibility of modernizing the plants. Bargel also evaluates an increasing share of renewable resources in electrical power generation and the results indicate that the exergetic efficiencies of all scenarios increase, especially for HP and direct electrical heating.
Noussan et al. [91] model the integration of a CHP plant coupled to a TES into an existing DHS. They vary the CHP plant and TES size as well as the mode of operation. They find that the installation of a TES can lead to an increase in the overall efficiency of up to 8.6 % and that energy efficiency and economic

efficiency are conflicting characteristic numbers. They also find a high dependency of the economic efficiency on national policies and financial incentives.
Rosen et al. [119; 121] apply energy and exergy analysis to a CHP-based DHS project in Edmonton, Alberta, Canada. Investigated is a district heating and cooling project for which three central chilling alternatives are considered. The first is the base case, with an electrical chiller, while the other two cases replace the electrical chiller with a single-effect and a double-effect absorption chiller. The alternatives are assessed regarding energy and exergy efficiency and the overall energy and exergy efficiencies are found to vary from 83 % to 94 % and 28 % to 30 % respectively.
Nuytten et al. [92] study the flexibility of a CHP DHS with two different storage concepts. The aim of the study is to determine whether a large centralized TES or small decentralized TES in the individual buildings offer more flexibility in terms of operating the CHP plant. They simulate 100 residential dwellings in Flanders, Belgium, and conclude that a centralized TES offers more flexibility in operating the system than decentralized TES. The reason for this is that in the decentralized scenario, a "weakest link situation" is created where the operation of the entire system is dependent on the dwelling with the highest heat demand at any given time.
Wang et al. [165] model and optimize a DHS with CHP plants fed by natural gas and biomass, a TES and and a solar thermal plant. The optimization parameter is the overall cost. It is found that the TES efficiency is a crucial parameter for the operation of the CHP plant in combination with the fluctuating renewable energies.
Sibbitt et al. [129] compare the results of five years of monitoring data of a solar thermal DHS with a seasonal TES to the simulation results of the model used in the design process of the system. The seasonal TES is a geothermal borehole TES. The results display good agreement of the simulation model and the monitoring data, achieving a solar fraction of 97 %.
Buoro et al. [27] optimize the electrical, heating and cooling supply of a cluster of nine industrial facilities. Different system scenarios are investigated including an individual building scenario, a DHS with CHP, and a DHS with CHP but also a centralized solar thermal plant and a TES. The optimization parameter is the cost. They show that a DHS with a solar thermal plant offers a 5 % annual cost reduction as well as a 15 % primary energy demand reduction.
Lindenberger et al. [78] model a solar thermal DHS with a seasonal TES. They study different cases of backup heating in case the solar thermal energy is not sufficient for the heating demand. The cases include the integration of a condensing boiler, HP and a CHP plant into the system and are compared to a base case consisting of a condensing boiler. They find that the CHP plant has a high economic efficiency, whereas a CHP plant combined with the solar thermal DHS leads to a cost increase of 120 % while at the same time reducing emissions in the range of 20 % to 30 %, together with fossil fuel savings of approximately 40 %.

An overview of the development of solar DHS systems in Germany is given in [10; 33; 83; 126] with a focus on the performance and design of the seasonal TES. Several operating solar DHS are described and performance energy values are given. The case studies are also presented in [85] in more detail. Information regarding simulation, design and operation of solar DHS in Germany is given, again with a focus on seasonal TES. The analysis however focuses only on energy.
Fisch et al. [46] review solar DHS and give an overview of operating systems and the scale of costs associated with implementing a TES. They find that the costs of the installation of a seasonal TES are twice the installation costs of a short term TES.
In [131] and [40] an overview of the current state of solar DHS in Denmark is given with a focus on the operating system and the implementation of TES. The optimization parameters are costs and energy savings.

Verda and Colella [151] present a model to simulate the performance and integration of a seasonal TES into an existing DHS with a CHP plant. By adding a seasonal TES to the system the CHP running-time can be increased and the use of auxiliary boilers decreased. As a case study they consider a DHS in Italy and find that up to 12 % of the primary energy can be saved and the total costs be reduced by up to 5 %. These savings are possible by increasing the CHP running-time and thus also increasing the electricity production of the system and decreasing the use of the auxiliary boilers at the same time.
On TES scale, Rosen and Dincer [115] apply exergy analysis to different types of TES including aquifer system, stratified TES and cold TES and illustrate the usefulness of exergy analysis by determining optimal discharge periods.
Haller et al. [53] review methods to determine the stratification efficiency of a TES and apply the different methods to a simulation model. They conclude that the methods to determine the stratification efficiency should be further developed to separate the exergy losses accompanying the heat loss from the exergy destruction due to destratification.
Haller et al. [54] present a method to determine the ability of a TES to stratify and maintain stratified temperature layers. They compare the results of simulations with experiments using a 0.8 m^3 TES. However, their method only includes exergy destruction due to destratification and exergy loss through heat loss. A changing reference temperature for the exergy calculation is not considered.
Panthalookaran et al. [106] suggest a new method for the characterization of TES which combines the first and second law of thermodynamics. They apply the method to a large-scale seasonal heat storage and find it useful in deriving TES design insights.
Cruickshank and Harrison [32] experimentally determine the heat loss and the internal heat transfer of a TES. They find no temperature gradient in horizontal direction and the highest heat loss in their setting occurs at the bottom of the TES. They conclude that it is important to use accurate heat loss parameters in simulations in order to make acceptable predictions with a TES model.
Cruickshank [31] experimentally and numerically investigates configurations of three series- and parallel-connected TES. Results indicate that the parallel configuration stored more energy than the series configuration during charging. The parallel configuration also has a higher cumulative exergy content than the series configuration.
Rosen [117] describes how stratification can increase the exergy storage capacity of a TES. He introduces six temperature-distribution models for stratified TES, differing in complexity. He concludes that for most situations a three-zone temperature-distribution model may represent a good compromise between result accuracy and calculation effort.
Rosen et al. [120] investigate the increase in exergy content of a stratified TES compared to a fully mixed storage for a wide range of temperature profiles of storage fluids. Their results indicate that exergy storage capacity increases with the level of stratification and that the percentage increase in exergy storage capacity is greatest for TES near ambient temperature.

2.3 Aim of this thesis

As presented in section 2.2 many studies have been conducted regarding heating systems for individual buildings as well as for DHS. Some focus on a single heat generation system, others give an overview of several different systems. While all studies conduct an energy analysis, some also investigate the use of exergy or the costs. Exergy analysis of individual TES or their implementation into buildings can also be found. But regarding the exergy analyses of TES, the influence of a varying reference temperature on the exergy content of a TES is not investigated or discussed. In order to integrate renewable energies

into the heat supply of building clusters or larger DHS, storage systems are needed. However, regarding the integration of a TES into a DHS, only energy analyses could be found. Although Bargel [9] gives a comparative overview of heating systems for individual buildings as well as DHS, a DHS with a TES is not investigated from an exergy perspective. Furthermore, no approach could be found which takes energy, exergy, ecological and economic analyses into account within the same study of a DHS.
The aim of this thesis is therefore to address these academic voids. The integration of a TES into a DHS is assessed from an exergy perspective, the dependency of the exergy content of the TES on a changing reference environment is analyzed, and a method to describe that phenomenon is developed. Further, an integral assessment of different DHS heat generation technologies and their application is conducted, including energy, exergy, ecological and economical analysis.
In short, the following main research tasks are identified as aims of this thesis.

- Development of a method to describe the change of exergy content of a TES for variable reference temperatures
- Discussion of the integration of a TES in a DHS
- Energy, exergy, ecological and economical assessment and comparison of heat supply systems for DHS

To assess and compare different heat supply systems and the TES integration, several heat supply scenarios are defined, analyzed and optimized and the following situation is considered. A gas boiler DHS consisting of a building cluster with 11 buildings with a supply temperature of $T_s = 90\,°C$ has to be renewed. For the building cluster a demand for room heating, DHW and electricity is preassigned. While the building cluster demand will be kept constant, the heat supply system is to be replaced by an alternative at a lower supply temperature. Both electricity and heat supply are investigated, but the emphasis is on the different heat supply options. Therefore, the following six different scenarios are designed and compared in this work:

- Gas scenario: a gas boiler with lower supply temperatures.
- CHP scenario: a CHP plant with a gas boiler as backup and a small buffer TES.
- Geo scenario: a ground sourced HP and a buffer TES.
- CHP+Geo scenario: a CHP plant, a ground sourced HP and a buffer TES.
- Solar scenario: solar thermal collectors, a seasonal TES and a gas boiler as backup.
- Power to heat (P2H) scenario: an air and a ground sourced HP, PV modules and a seasonal and buffer TES.

These systems will be analyzed and optimized regarding energy and exergy use and finally an ecological and economic analysis will be conducted. It is important to emphasize that the optimization of the scenarios is done only for energy and exergy analysis. The subsequent ecological and economical analysis is meant to assess the different scenarios, but is not used to optimize them. A special focus will be on the integration of TES in particular concerning TES for renewable energies. Four characteristic numbers out of the four different analysis types will be taken to assess the overall result. Another part of the work will focus on the investigation of the dependency of the exergy content of a TES on a varying reference temperature and the development of a method to describe the change of exergy content.

3 Methods

In this chapterm details regarding the assessment methods used in this work are presented. Furthermore, characteristic numbers used to assess the heat supply scenarios are defined.

3.1 Energy and exergy analysis

The steps to conduct an energy and exergy analysis are as follows:

- Definition of the system boundaries
- Definition of the reference environment
- Definition of the system components and of the input and output flows of each
- Determination of the energy content of all flows
- Determination of the exergy content of all flows
- Analysis and Conclusion

3.1.1 System boundary

The choice of the appropriate system boundary is crucial for the meaning of the results. Depending on the system boundary, energy and exergy losses are either included or omitted in the results. It is therefore essential to clearly define the system boundary of this work in order to interpret the results. But before the system boundary of this work is determined, several possible system boundary choices are introduced. First, two options for the system boundary on the demand side are presented and then three options for the system boundary on the supply side.

Demand side system boundary

A common general characterization of an exergy system is the use of efficiencies which are defined as the useful output or the demand divided by the input, here the exergy efficiency $\psi = demand/input$. The efficiency can be increased by minimizing the input and/or by maximizing the useful output.
Two possible definitions of the useful output and therefore of the demand side system boundary of a DHS are

(1) the room heating demand at room temperature and the DHW demand at water temperature [140].

(2) the state of the water at the heat transfer station (HTS) in front of the building [97].

These two different system boundaries lead to different results and to different optimizing strategies. Given that both systems would have the same input, the system with boundary (1) would have a smaller

exergy efficiency than (2), because the exergy destruction from the HTS into the building would be considered for (1), but omitted for (2). The optimization strategy for (1) would therefore be to minimize the exergy input into the system. However, for (2) the optimization strategy would aim at increasing the useful output and therefore increasing the district heating temperature level in order to increase the efficiency. However, this would also lead to higher heat loss and would be counterproductive in terms of overall energy input.

Supply side system boundary

Regarding the system boundary on the supply side, different options are possible to either include or omit energy conversion processes that precede the actual system components. Torío [144] discusses two different system boundaries regarding incoming solar radiation:

(A) a “technical boundary” which includes the conversion from incoming solar radiation into heat or electricity.

(B) a “physical boundary” which omits the conversion from the incoming solar radiation into heat or electricity and only considers heat or electricity as entering the system.

Option (A), which includes the conversion from incoming solar radiation into heat or electricity leads to a high exergy destruction at the system boundary and is useful if the solar thermal collector or the PV module is the focus of a study or optimization. This high exergy destruction at the system boundary dominates the results and makes it hard to compare it to other systems or to evaluate the overall impact of optimizing measures for other system components.
Option (B), which omits the conversion from the incoming solar radiation into heat or electricity, is useful if the focus of a study is not the individual component, but its integration into a larger system. The negligence of the solar radiation can be tolerated, because the incoming solar radiation can only be used at the time of income and not be stored for later. The concept of storing energy is used by Jentsch [65], who introduced the storability criterion regarding the supply side system boundary. The storability criterion differentiates between energy in a storable and a non storable form. Only energy in a storable form is regarded as input into the system. Following that approach, solar radiation would not be storable, but the heat in form of hot water generated by a solar thermal collector would be. The system boundary defined by the storability criterion is similar to option (B), but also defines the system boundary for other forms of energy. It defines electricity as non storable and makes it necessary to put the system boundary beyond the power plants to include the conversion processes from primary energy into electricity. However, since the storability criterion does define electricity as non storable, it is not applicable for PV collectors or wind turbines, since neither solar radiation nor wind are directly storable.

Chosen system boundary

On the demand side, the system boundary option (1) is chosen in this work, because the thermal comfort in terms of room heating and DHW is the actual demand of a user in a building, not the water at the HTS in front of the building. Bargel [9] also states that it is important to use the minimal exergy demand as the useful output, because otherwise a comparison of different systems is not possible. Specifically for this work, the exergy demand for room heating and DHW is calculated using a heat demand temperature of 20 °C and 40 °C respectively.

In general, the system boundary is chosen according to the storability criterion on the supply side. However, for the forms of energy not included in the storability criterion, the system boundary is chosen according to option (B). Therefore, primary energy is considered as input into the system. Only in the case of solar radiation, the produced hot water and the electricity is taken as input into the system [44]. In order to demonstrate the chosen system boundary, all possible input and useful output flows are displayed in figure 3.1, even though they may not occur in every investigated scenario in this work. The term "compensated grid electricity" in figure 3.1 is defined in section 3.1.5.

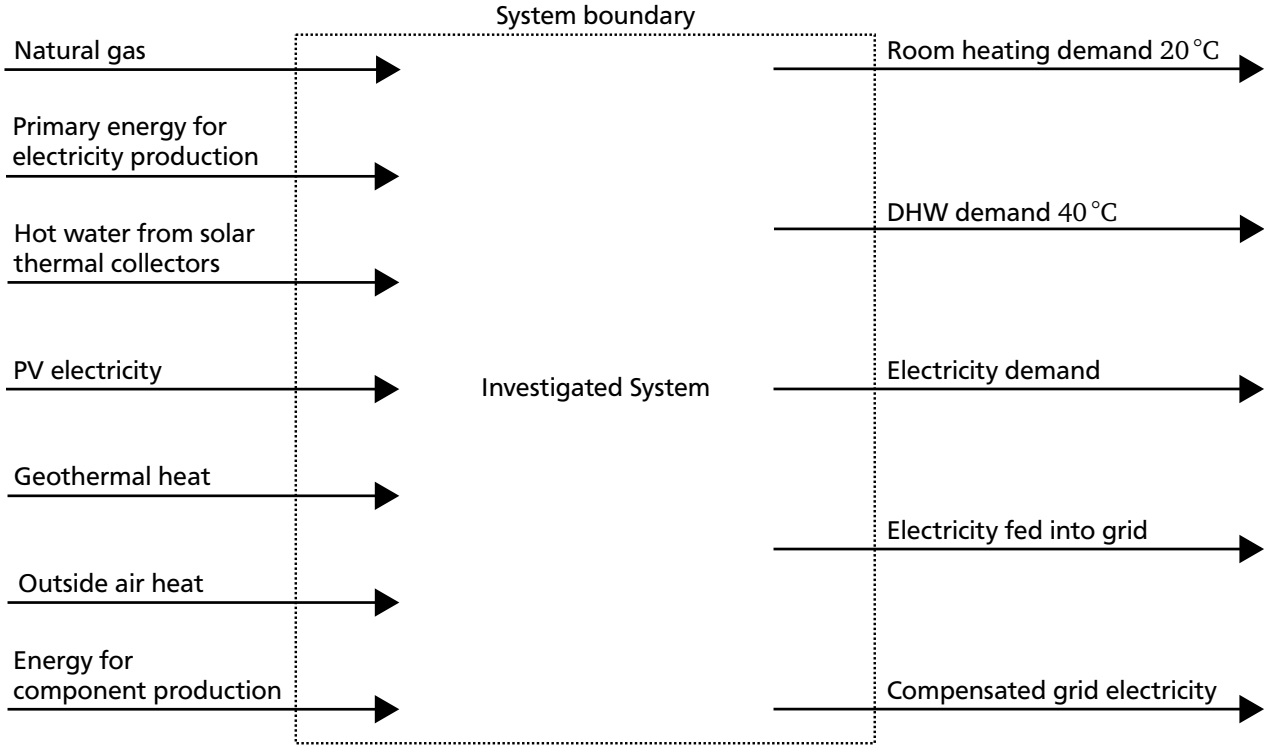

Figure 3.1: System boundary with input and output flows.

3.1.2 Reference environment

As introduced in section 3.1, a reference environment has to be defined to determine the exergy content of a system. In the International Energy Agency Annex 49 guidebook [142], different options regarding the reference environment are discussed, which must meet certain criteria. The reference environment

- must be in thermodynamic equilibrium,
- must be in chemical equilibrium,
- must not be changed by the analyzed system.

Different options in the built environment are considered and discussed in [142]. These are:

- Universe at nearly zero Kelvin.
  The universe at nearly zero Kelvin is in equilibrium and not changed by the analyzed system. However, it is not in direct contact with the system, but rather shielded by the Earth's atmosphere.

- Indoor air inside the building.
  The indoor air does not meet the above introduced criteria, since it is not in thermodynamic equilibrium and is changed by the analyzed system.

- Undisturbed ground.
  The undisturbed ground is a commonly used reference environment for exergy analyses. It is in equilibrium and not changed by the analyzed system.

- Ambient air surrounding the building.
  The ambient air surrounding the building can also be seen as in equilibrium and it is not changed by the analyzed system. Further, the surrounding air is in direct contact with the building and acts as the environment to which the heat losses in a building occur. It is therefore recommended as the reference environment in the building sector [142].

Following the recommendations of the Annex 49 guidebook [142], the current ambient air surrounding the building is chosen as the reference environment. In this work, only the ambient air temperature is needed as a reference environment, because the model setup does not include air pressure and humidity. Since the ambient air temperature outside the building changes continuously over the year, the reference temperature for the exergy calculation also changes continuously. This has a significant impact on storage processes, since heat stored over a longer period of time can change its exergy content just because of the changing outdoor air temperature. This is especially significant for seasonal TES, where heat is stored during high reference temperatures and used during cold reference temperatures, thus leading to a possible increase in exergy content over time. This phenomenon is discussed in more detail in subsection 5.1.

3.1.3 Exergy definitions of energy flows

In the built environment, mainly physical and chemical exergy are of importance. Physical exergy includes the exergy of a mass flow and the exergy of heat, while the exergy of fuels is included in chemical exergy.

Exergy of a massflow

According to [134] the exergy flow $\dot{EX}$ of a mass flow $\dot{M}$ is defined by

$$-\dot{EX} = \dot{M}\left[h_1 - h_\mathrm{u} - T_\mathrm{u}\left(s_1 - s_\mathrm{u}\right) + \frac{w_1^2}{2} + g z_1\right], \tag{3.1}$$

where h_1 and h_u are the specific enthalpies in state 1 and the environment state, T_u is the temperature of the environment, s_1 and s_u are the entropies in state 1 and the environment, respectively. w_1 is the velocity, g is the gravity and z_1 is the height in state 1. In a heating system the mass usually flows in a closed loop within the system boundaries and the kinetic and potential energy cannot be used to produce useful work. Therefore, the kinetic and potential energy of the flow $\dot{M}$ in equation 3.1 are neglected in this work.

Exergy of heat

The exergy flow of a heat flow $\dot{Q}$ is defined by [134]

$$-\dot{EX} = \left(1 - \frac{T_u}{T}\right)\dot{Q}\,. \tag{3.2}$$

The term in the brackets is often referred to as the "Carnot-Factor".

Exergy of electricity

The exergy content of electricity is equal to its energy content, $E_{el} = EX_{el}$, because electrical energy can be completely transformed into any other type of energy.

Exergy of natural gas

Bargel [9] based the calculation of the exergy content of fuel mainly on Hepbasli's [58] work and derived equations to calculate the exergy content of natural gas. Hepbasli [58] defines a constant ratio β_{LHV} of the chemical exergy EX_{CH} and the lower heating value LHV which can be used to determine the chemical exergy of liquid and solid fuels. β is also referred to as the proportionality constant, quality factor or exergy coefficient. The relation is given by

$$\beta_{LHV} = \frac{EX_{CH}}{LHV}\,. \tag{3.3}$$

Hepbasli [58] cites Szargut [136], who proposed the following equation for the calculation of the exergy coefficient of natural gas:

$$\beta_{LHV} = 1.0334 + 0.0183\frac{H}{C} - 0.0694\frac{1}{N_C}\,, \tag{3.4}$$

where H/C is the atomic ratio of hydrogen and carbon elements and N_C is the mean number of carbon atoms in the molecule [58].
The assumption that natural gas is pure methane with the chemical structure CH_4 leads to $H/C = 4$ and $N_C = 1$ and therefore to an exergy coefficient $\beta_{LHV}(CH_4) \approx 1.04$ for the lower heating value [9].
The definition of β_{LHV} with the use of the lower heating value leads to a $\beta_{LHV} > 1$ for the common fuels, such as coal, natural gas, oil and wood [58]. This also leads to a chemical exergy higher than the lower heating value $EX_{CH} > LHV$.
The energy efficiency η_i of a power plant is defined as the produced electricity divided by the energy input in form of the lower heating value,

$$\eta_i = \frac{E_{el}}{LHV}\,. \tag{3.5}$$

The exergy efficiency ψ_i of a power plant is defined as the produced electricity divided by the exergy input in form of the chemical exergy,

$$\psi_i = \frac{E_{el}}{EX_{CH}}\,. \tag{3.6}$$

For most fuels, the definition of equations 3.5 and 3.6 will lead to $\eta_i > \psi_i$, which seems unusual but it originates in the definition of the chemical exergy with the lower heating value.

Table 3.1: Electricity mix in 2012.

	Hard coal	Lignite	Nuclear	Gas	Oil	Renewable
σ_i	18 %	26 %	16 %	12 %	1 %	23 %
η_i	46 % [74]	42 % [109]	30 % [116]	54.7 % [55]	54.7 %	100 %
ψ_i	45 % based on [116]	41 % based on [116]	30 % [116]	52.6 % [55]	52.6 %	100 %

3.1.4 Conversion efficiency of grid electricity production

In the investigated scenarios, electricity is drawn from the electricity grid to supply appliances and to meet the demand of the buildings. For the calculation of the primary energy demand that produces the electricity, the German electricity mix from 2012 [2] is taken into account. The conversion efficiency from primary energy source to electricity, the energy efficiency η_{el} and exergy efficiency ψ_{el} can be calculated using

$$\eta_{el} = \frac{\Sigma_i \sigma_i \eta_i}{\Sigma_i \sigma_i} \tag{3.7}$$

and

$$\psi_{el} = \frac{\Sigma_i \sigma_i \psi_i}{\Sigma_i \sigma_i} \,, \tag{3.8}$$

where σ_i is the share of one energy source on the overall electricity mix and η_i and ψ_i are its corresponding energy and exergy conversion efficiencies. The values for σ_i, η_i and ψ_i are given in table 3.1. The sum of the distribution shares only adds up to 96 % instead of 100 %, because energy sources other than the ones listed in table 3.1 are neglected. It is assumed that the exergy conversion efficiencies of hard coal and lignite are one percentage point lower than their energy efficiencies based on Rosen's efficiency values for the Nanticoke Generation Station in Canada [116]. It is further assumed that oil and gas have the same conversion efficiencies and that renewable energies have an efficiency of 100% based on the chosen system boundary as discussed in section 3.1.1 [44].
With equation 3.7 and 3.8 the energy and exergy conversion efficiency of the German electricity mix in 2012 can be calculated to $\eta_{el} = 56.4\,\%$ and $\psi_{el} = 55.6\,\%$. Because the chemical exergy of most fuels is slightly higher than their lower heating value, there is a small difference between the value of the energy and exergy efficiency [116].

3.1.5 Compensated grid electricity

In this work, different types of heat supply systems are compared. However, in some scenarios not only heat, but also electricity is generated. The generated electricity is used to cover the electricity demand of the building cluster, to run system components and the excess electricity, the so called net electricity, is fed into the electricity grid. This results in two different types of energy as a useful product in the scenarios. The two types of energy make the modeled scenarios difficult to compare, because the numerator in the efficiency calculation would be different. As already stated in section 3.1.1, the efficiency is defined as the ratio of the useful output of a system to the input. Therefore, if the useful output is not the same, different systems are not comparable. In order to make the scenarios analyzed in this work comparable, a so called compensated grid electricity is introduced [111]. The compensated grid electricity ensures that the numerator in all systems stays constant. This is achieved by designing all

scenarios in a way that they all feed the same amount of electricity into the grid. In scenarios with no or little net electricity generation the needed differential electricity is drawn from the grid.
If, for example, a scenario with a CHP plant feeds 70.0 MWh/(a) of net electricity into the electricity grid and is then substituted by a scenario with solar thermal collectors, no electricity is generated which could be fed into the grid. Therefore, a power plant outside the investigated scenario would need to generate 70.0 MWh/(a) more electricity to make up for the electricity that the CHP plant no longer generates. The compensated grid electricity is this extra electricity that the grid has to supply. Therefore, the additional primary energy needed to produce that extra electricity is attributed to the scenario which produces no or less net electricity than the scenario with the highest electricity feed into the grid.

3.2 Ecological analysis

Life cycle assessment (LCA) is a method to assess all environmental impacts connected with a product and is defined in the DIN EN ISO 14040 [63]. While applying LCA, the whole life cyle of a product, "from-cradle-to-grave", is assessed regarding its environmental impact. This includes the production of raw materials, the manufacturing, the utilization and the disposal. The different steps of a LCA according to the DIN EN ISO 14040 are as follows:

- Goal and scope definition:
  The goal and the reason for the study, the depth, the system boundaries, the functional unit, rules and assumptions, and the kind of impact assessment and valuation are defined [71].

- Inventory analysis:
  All relevant input and output flows related to the product are taken into account in regards to the life cycle of the product. One part of the inventory analysis is the cumulative energy demand CED which lists all energy input during the life cycle of a product [71].

- Impact assessment:
  The results of the inventory analysis are linked with impact categories. This link creates a relationship between the data from the inventory analysis and the environmental impact.

- Interpretation:
  The results from the inventory analysis and the impact assessment are discussed regarding the defined goals. Significant parameters are also identified.

In the following, the four steps of LCA are described for this work:

- Goal and scope definition:
  The goal of the LCA is the integral assessment of different heat supply systems for a building cluster. The system boundary is described in section 3.1.1 and details to the modeled systems and components are given in chapter 4. For all components “from-cradle-to-grave” data is used, except for the CHP, for which only “from-cradle-to-gate” data was available. It is assumed that the impact of the disposing of the CHP is negligible. In the analysis only those components are taken into account that differentiate one scenario from the other. This means that the district pumps for example, which are the same in every scenario, are not taken into account to compare the impact of each scenario. Further, the LCA is only conducted after the energy and exergy analysis and is not an optimization parameter in this work. Only the result of the optimization of the energy and exergy analysis is assessed.

- Inventory analysis:
  The inventory analysis is part of the energy analysis in this work. During the energy analysis the CED is calculated, which includes the "cradle and grave" (C&G) annualized energy demand ($E_{\mathrm{C\&G}}$) for producing and disposing of the scenario components and the annual energy input. Due to a lack of data, a cumulative exergy demand cannot be calculated. For the exergy analysis, only the exergy flows during the time of usage are taken into account.

- Impact assessment:
  As impact factors in this work, the CED and the GWP 100 are chosen. The GWP 100 is a measure for the global warming potential (GWP) of emitted gases in CO_2 equivalents for a time horizon of 100 years [60]. In this work it is used to assess the GWP of the production and disposing processes of the components used in a scenario and to assess the GWP of the input flows of electricity and natural gas. The GWP 100 makes it possible to assess the effect the different scenarios have on climate change relative to each other in the scenario comparison. A detailed definition of the terms that are included in the CED and GWP 100 can be found in equation 3.20 and 3.23.

- Interpretation:
  The results of the LCA are presented and discussed in the results in chapter 6 and 7 in form of the CED and GWP 100. In this work the GWP 100 will be referred to as GWP.

3.3 Economic analysis using the annuity method

The economical analysis is carried out using the annuity method according to VDI 2067 [152]. With the help of the annuity method, die initial investment and the demand-related costs can be merged and accounted for as equal payments over the whole life cycle of the system. The costs are divided into:

- capital-related,
- demand-related,
- operation-related,
- other costs.

In this work, the capital-related, the demand-related and the operation-related costs are considered. Since some scenarios in this work also sell electricity, the revenue is also taken into account.

3.3.1 Capital-related costs

The annuity of the capital-related costs A_{C} is determined using

$$A_{\mathrm{C}} = A_0 a \ , \tag{3.9}$$

where A_0 is the investment cost and a is the annuity factor which can be calculated using

$$a = \frac{\epsilon - 1}{1 - \epsilon^{-\tau}} \ , \tag{3.10}$$

where ϵ is the interest factor and τ is the number of years of the investigated period.

3.3.2 Demand-related costs

The annuity for the demand-related costs A_{D} is determined using

$$A_{\mathrm{D}} = a\left(A_{\mathrm{D,el}} b_{\mathrm{D,el}} + A_{\mathrm{D,gas}} b_{\mathrm{D,gas}}\right) , \tag{3.11}$$

where $A_{\mathrm{D,el}}$ and $A_{\mathrm{D,gas}}$ are the costs for grid electricity and natural gas in the first year, while $b_{\mathrm{D,el}}$ and $b_{\mathrm{D,gas}}$ are the price dynamic cash value factors for grid electricity and natural gas. $b_{\mathrm{D,i}}$ can be calculated using the general equation

$$b_{\mathrm{D,i}} = \frac{1 - \left(\frac{r_{\mathrm{i}}}{\epsilon}\right)^{\tau}}{\epsilon - r_{\mathrm{i}}} , \tag{3.12}$$

where r_{i} is the application dependent price change factor, which depends on the different prices for gas and electricity. The price change factor takes the price development into account.

3.3.3 Operation-related costs

The annuity for the operation-related costs such as maintenance and operation A_{O} is determined using

$$A_{\mathrm{O}} = A_0 f_{\mathrm{O}} a b_{\mathrm{O}} , \tag{3.13}$$

where f_{O} is the sum of the percentage factors for maintenance and operation found in [152] and b_{O} is the price dynamic cash value factor calculated with equation 3.12.

3.3.4 Revenue

Some of the investigated scenarios in this work feed electricity into the electricity grid and therefore not only have costs but also revenue. The annuity of the revenue $A_{\mathrm{N,R}}$ can be calculated using,

$$A_{\mathrm{R}} = R_1 a b_{\mathrm{R}} , \tag{3.14}$$

where R_1 is the revenue in the first year, a is the annuity factor calculated with equation 3.10 and b_{R} is the price dynamic cash value factor calculated with equation 3.12.

3.3.5 Annuity of total annual payments

The annuity of the total annual payments is determined using

$$A = A_{\mathrm{C}} + A_{\mathrm{D}} + A_{\mathrm{O}} - A_{\mathrm{R}} . \tag{3.15}$$

In general the annuity can be $A < 0$ or $A > 0$. In this work heat supply scenarios are investigated and, because the produced heat is not sold but used, the annuity will always be $A > 0$. The smallest annuity is most favorable from an economic perspective.

3.4 Characteristic numbers

The characteristic numbers used to assess the different systems are introduced in the following. All characteristic numbers are calculated with annualized quantities.

3.4.1 Solar fraction

The solar fraction κ_{Solar} is the share of solar energy in the total energy supplied to the DHS. In this work it is used for the Solar scenario, in which the solar thermal collectors charge the TES, from which the solar energy is supplied to the DHS. The solar fraction κ_{Solar} is defined as

$$\kappa_{\text{Solar}} = \frac{E_{\text{TES to DHS}}}{E_{\text{E to DHS}}} \,. \tag{3.16}$$

$E_{\text{TES to DHS}}$ describes the energy supplied from the TES to the DHS, therefore not including TES losses, and $E_{\text{E to DHS}}$ is the total energy supplied to the DHS.

3.4.2 Energy and exergy analysis

The optimization of the different systems is based on energy and exergy analysis, which are introduced in the following.

Energy efficiency

The energy efficiency of a system η_{system} is defined as the ratio of the useful output and the input

$$\eta_{\text{system}} = \frac{E_{\text{th.district}} + E_{\text{el.district}} + E_{\text{el.grid}} + \Delta E_{\text{el}}}{E_{\text{C\&G}} + E_{\text{renew}} + E_{\text{gas}} + E_{\text{el.renew}} + E_{\text{el.fossil}} + \Delta E_{\text{el.renew}} + \Delta E_{\text{el.fossil}} + E_{\text{TES begin}} - E_{\text{TES end}}} \,. \tag{3.17}$$

$E_{\text{th.district}}$ is the thermal energy demand of the building group, $E_{\text{el.district}}$ is the electrical energy demand of the building group, $E_{\text{el.grid}}$ is the electrical energy fed into the electricity grid in case excess electrical energy is produced and ΔE_{el} is the compensated grid electricity introduced in section 3.1.5. $E_{\text{C\&G}}$ is the C&G energy of the system components, E_{renew} is the renewable energy input such as solar or geothermal heat, depending on the scenario design as shown in further detail in section 4.4.1 to 4.4.6. E_{gas} is the natural gas input, $E_{\text{el.renew}}$ and $E_{\text{el.fossil}}$ are the renewable and fossil primary energies needed to run the appliances, $\Delta E_{\text{el.renew}}$ and $\Delta E_{\text{el.fossil}}$ are the renewable and fossil energies needed to produce the compensated grid electricity and $E_{\text{TES begin}}$ and $E_{\text{TES end}}$ are the energy content of the TES at the beginning and end of the investigated period. It was made sure that for every scenario for the simulated period of a year, the energy content of the TES at the beginning and end of the simulation is equal, $E_{\text{TES begin}} = E_{\text{TES end}}$. Therefore, $E_{\text{TES begin}}$ and $E_{\text{TES end}}$ are neglected in the equations of this work.

Exergy efficiency

The exergy efficiency of a system ψ_{system} is defined as the ratio of the useful output and the input

$$\psi_{\text{system}} = \frac{EX_{\text{th.district}} + EX_{\text{el.district}} + EX_{\text{el.grid}} + \Delta EX_{\text{el}}}{EX_{\text{in}}} \,. \tag{3.18}$$

$EX_{\text{th.district}}$ describes the thermal exergy demand of the building group, $EX_{\text{el.district}}$ is the electrical energy demand of the building group, $EX_{\text{el.grid}}$ is the electrical energy fed into the electricity grid in case excess electrical energy is produced and ΔEX_{el} is the compensated grid electricity introduced in section 3.1.5. EX_{in} is the exergy input into the system.
EX_{in} consists of fossil and renewable exergy, but due to a lack of data the exergy needed for producing and disposing of the system components is not considered in the exergy analysis. EX_{in} can be written as

$$EX_{\text{in}} = EX_{\text{gas}} + EX_{\text{renew}} + EX_{\text{el.renew}} + EX_{\text{el.fossil}} + \Delta EX_{\text{el.renew}} + \Delta EX_{\text{el.fossil}} \,, \tag{3.19}$$

where EX_{gas} is the exergy of the gas input, EX_{renew} is the renewable exergy used in a scenario, $EX_{\text{el.renew}}$ and $EX_{\text{el.fossil}}$ are the primary renewable and fossil exergy needed to produce electricity. $\Delta EX_{\text{el.renew}}$ and $\Delta EX_{\text{el.fossil}}$ are the primary renewable and fossil exergy needed to produce the compensated grid electricity. Again, the exergy content of the TES at the beginning and the end of the simulation are equal, $EX_{\text{TES begin}} = EX_{\text{TES end}}$ and are therefore neglected in the equations of this work. Further details regarding EX_{in} in the specific scenarios can be found in section 4.4.1 to 4.4.6.

3.4.3 Ecological analysis

During the ecological analysis, the cumulative energy demand and the global warming potential are assessed, which are both calculated on an annual basis.

Cumulative energy demand

The annual CED for a scenario is defined as

$$CED = E_{\text{C\&G}} + E_{\text{gas}} + E_{\text{renew}} + E_{\text{el.renew}} + E_{\text{el.fossil}} + \Delta E_{\text{el.renew}} + \Delta E_{\text{el.fossil}} \,, \tag{3.20}$$

where $E_{\text{C\&G}}$ is the annualized C&G energy of the components in a scenario, E_{gas} is the energy of the used gas, E_{renew} is the renewable energy used in a scenario, $E_{\text{el.renew}}$ and $E_{\text{el.fossil}}$ are the primary renewable and fossil energy needed to produce electricity, $\Delta E_{\text{el.renew}}$ and $\Delta E_{\text{el.fossil}}$ are the the primary renewable and fossil energy needed to produce the compensated grid electricity, while all energy quantities are calculated on an annual basis.
The CED can be differentiated by renewable and fossil fraction to

$$CED_{\text{renew}} = E_{\text{C\&G.renew}} + E_{\text{renew}} + E_{\text{el.renew}} + \Delta E_{\text{el.renew}} \tag{3.21}$$

and

$$CED_{\text{fossil}} = E_{\text{C\&G.fossil}} + E_{\text{gas}} + E_{\text{el.fossil}} + \Delta E_{\text{el.fossil}} \,. \tag{3.22}$$

Global Warming Potential

The annual global warming potential GWP of a scenario is defined as,

$$GWP = q'_{\mathrm{C\&G}} + E_{\mathrm{gas}}\, q_{\mathrm{gas}} + \left(E'_{\mathrm{el.renew}} + E'_{\mathrm{el.fossil}} + \Delta E'_{\mathrm{el.renew}} + \Delta E'_{\mathrm{el.fossil}}\right) q_{\mathrm{el.mix}}\,, \tag{3.23}$$

where $q'_{\mathrm{C\&G}}$ are the annualized specific C&G emission of CO_2 equivalents of the components needed in a scenario, stated with the unit $\mathrm{kg}_{\mathrm{CO_2e}}$. These CO_2 equivalents include all the different greenhouse gas emissions for producing and disposing of the components needed in a scenario. q_{gas} is the specific CO_2 emission of natural gas and $q_{\mathrm{el.mix}}$ are the specific CO_2 emissions of the electricity grid, stated in $\mathrm{kg}_{\mathrm{CO_2e}}$/kWh. Here, only the greenhouse gas CO_2 is accounted for with its CO_2 equivalent of 1. The specific q-values have to be multiplied with the energy input as stated in equation 3.23. E_{gas} is the energy of natural gas used in a scenario, $E'_{\mathrm{el.renew}}$ and $E'_{\mathrm{el.fossil}}$ is the amount of grid electricity from renewable and fossil energies used in a scenario without the primary energy conversion losses. $\Delta E'_{\mathrm{el.renew}}$ and $\Delta E'_{\mathrm{el.fossil}}$ is the grid electricity from renewable and fossil energies used for the compensated grid electricity in a scenario, again without the primary energy conversion losses. When comparing the GWP of the different scenarios investigated in this work, the scenario with the smallest GWP is the most ecologically advantageous.

3.4.4 Economic analysis

The given period for the economic analysis is 20 years. All components are assumed to have a life cycle of 20 years and the costs of disposal are neglected. It is further assumed that the whole DHS with all its components does not have any liquidation proceeds. The characteristic number regarding the economic analysis is the annuity of the total annual payments A_{N} as introduced in 3.3.5. When comparing the annuity of the different scenarios investigated in this work, the scenario with the smallest annuity is the most economically advantageous.

3.4.5 Weighted multicriteria number

In this work, the efficiency of different heat supply systems is investigated using energy, exergy, ecological and economical analysis. The results show system components and designs which could be improved to enhance the efficiency. However, an improvement regarding one assessment category is likely to affect the other assessment categories as well. One system might be very efficient regarding costs, but not very efficient regarding exergy use. This makes it difficult to draw an overall conclusion of the results. Therefore a weighted multicriteria number (WMN) is introduced to make it possible to combine the results of the four different assessment categories into one result number. The WMN is calculated for each scenario and is defined in a way, that the higher the WMN, the better the overall system performance is. The four different characteristic numbers that are combined in the WMN are:

- Energy analysis: Fossil energy input CED_{fossil} as defined in equation 3.22
- Exergy analysis: Total exergy input EX_{in} as defined in equation 3.19
- Ecological analysis: GWP as defined in equation 3.23
- Economical analysis: Total annuity A_{N} as defined in equation 3.15

The weighed multicriteria number is defined as

$$WMN = \phi_{\mathrm{CED_{fossil}}} CN_{\mathrm{CED_{fossil}}} + \phi_{\mathrm{EX_{in}}} CN_{\mathrm{EX_{in}}} + \phi_{\mathrm{GWP}} CN_{\mathrm{GWP}} + \phi_{\mathrm{A_N}} CN_{\mathrm{A_N}} \ , \tag{3.24}$$

where ϕ_{i} is the weighting factor and CN_{i} the criteria number (CN) regarding the four assessment categories. The four different ϕ_{i} have to be chosen so that

$$\Sigma \phi_{\mathrm{i}} = 1 \ . \tag{3.25}$$

In order to calculate CN_{i}, the lowest characteristic number out of all scenarios has to be identified and then divided by the characteristic number of the investigated scenario so that all CN_{i} are

$$0 \leq CN_{\mathrm{i}} \leq 1 \ . \tag{3.26}$$

As an example on how to calculate CN_{i} and WMN the detailed calculation is displayed for the Gas scenario. For this purpose equation 3.24 is transformed into

$$\begin{aligned} WMN_{\mathrm{Gas}} &= \phi_{\mathrm{CED_{fossil}}} CN_{\mathrm{CED_{fossil},Gas}} + \phi_{\mathrm{EX_{in}}} CN_{\mathrm{EX_{in},Gas}} + \phi_{\mathrm{GWP}} CN_{\mathrm{GWP,Gas}} + \phi_{\mathrm{A_N}} CN_{\mathrm{A_N,Gas}} \\ &= \phi_{\mathrm{CED_{fossil}}} \frac{CED_{\mathrm{fossil,min}}}{CED_{\mathrm{fossil,Gas}}} + \phi_{\mathrm{EX_{in}}} \frac{EX_{\mathrm{in,min}}}{EX_{\mathrm{in,Gas}}} + \phi_{\mathrm{GWP}} \frac{GWP_{\mathrm{min}}}{GWP_{\mathrm{Gas}}} + \phi_{\mathrm{A_N}} \frac{A_{\mathrm{N,min}}}{A_{\mathrm{N,Gas}}} \ . \end{aligned} \tag{3.27}$$

4 Model of heat supply scenarios

In this chapter the simulation model is presented. This includes the used simulation software, the individual heat supply scenarios, the layout of the building cluster and the heat distribution network. Furthermore, the demand and weather data is characterized, typical demand days are shown and details regarding the modeling of individual components and their dimensioning are given.

4.1 Heat and electricity demand and investigated building cluster

For the heat demand and weather real data is available while for the electricity demand standardized load profiles are used for the simulation.

4.1.1 Building cluster

The investigated system consists of a building cluster with 11 buildings connected via a DHS. Real demand data for room heating demand and DHW demand is available in 5 min – 15 min time steps for the year 2013. The demand data of the individual buildings was kindly provided by MVV Energie AG Mannheim, Germany [70; 90]. However, in reality this specific building cluster does not exist. The buildings are not connected via a DHS, nor do they share the same neighborhood. This is an assumption of this work in order to develop the method on an example with practical relevance.
The building types with the heated space, annual heat and DHW demand are shown in table 4.1. The system layout is shown in figure 4.1.
The combined annual heat demand of the building cluster is 263.7 MWh. Together with the heat demand

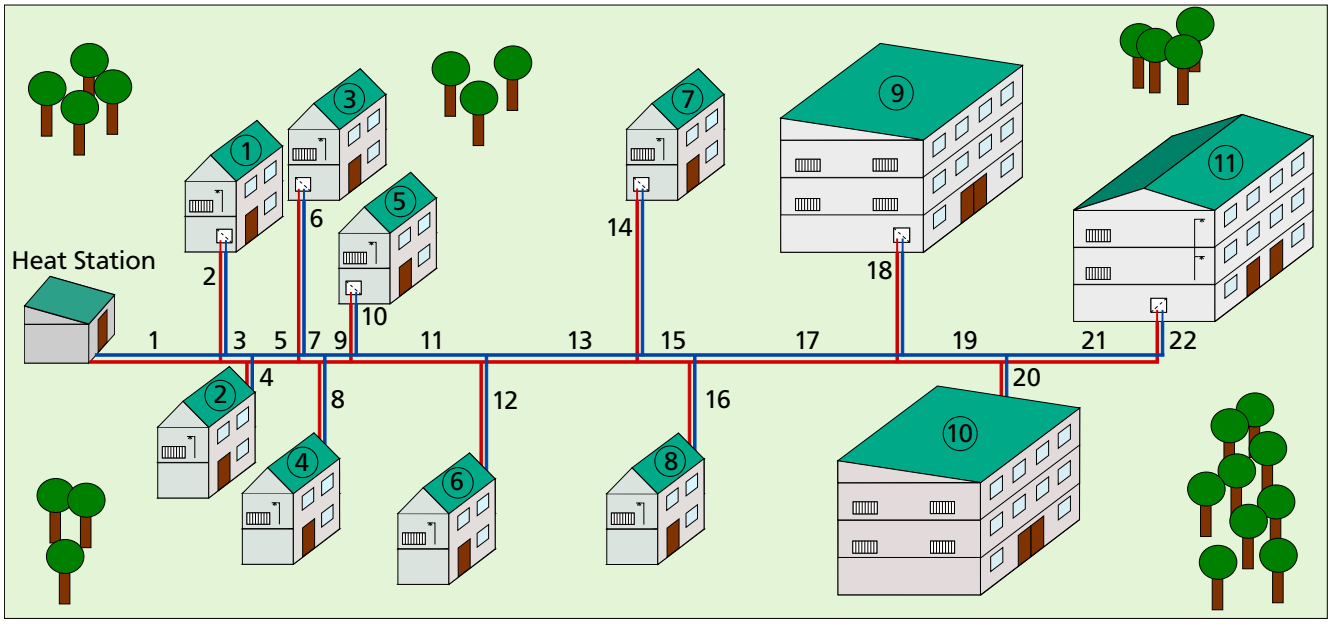

Figure 4.1: System layout of the investigated building cluster. Numbering see table 4.1 and table 4.2.

temperatures specified in section 3.1.1 and the reference temperature specified in section 3.1.2, the exergy content of the annual heat demand is calculated to 14.0 MWh. The building cluster consists of nine residential buildings, a youth center and a community library. All buildings are considered to have floor heating and flow heaters. By assuming that direct flow heaters are installed in each building, legionella forming is avoided independently from the supply temperature.
The simultaneity factor SF describes the reduction of the actual demand power of a DHS compared to the sum of the nominal power of the individual consumers [170]. It is defined as

$$SF = \frac{\sum_{i=1}^{m} P_i(t)}{\sum_{i=1}^{m} P_{n,i}}, \tag{4.1}$$

where $\sum_{i=1}^{m} P_i(t)$ is the sum of the needed power of the consumers at the time t, $\sum_{i=1}^{m} P_{n,i}$ is the sum of the nominal powers P_n and m is the number of consumers. The simultaneity factor of the investigated building cluster is 0.86 [70], which matches the results of Winter et al. [170] who investigated the simultaneity factor for small and medium sized DHS. Because the demand data is available for these buildings, the buildings itself are not modeled. The system is only modeled till the HTS in front of the building. Then, using the demand data, a temperature drop of the DHS water is calculated.

Table 4.1: Building types used in the building cluster.

	Type	Heated space in m^2	Heat demand in MWh/a	DHW demand in MWh/a
1)	Single family house	165	25.4	1.4
2)	Semidetached house	138	16.1	0.4
3)	Single family house	120	11.8	5.0
4)	End-terrace house	165	18.5	0.5
5)	Single family house	160	22.4	1.6
6)	Single family house	200	21.7	2.7
7)	End-terrace house	115	15.5	1.1
8)	Single family house	190	11.9	1.6
9)	Youth Center	unknown	26.5	10.8
10)	Library	unknown	30.3	4.8
11)	Multi-family house	230	31.3	2.4

In figure 4.2 the daily mean heat load for the whole building cluster is shown for the year 2013. The heat load is high in winter and low in summer.

4.1.2 Typical days

In figure 4.3 the heat load profile of buildings 3, 4 and 10 is shown for February 15th 2013, which is a typical day for the heat load profile. Building 3 has a low mean heat load with high fluctuating amplitudes throughout the whole 24 hours with high peaks during the day. The mean heat load of Building 4 is higher with rather low amplitudes throughout the day, with a peak in the evening and a lower mean heat load during the night. The curve of building 10 is above that of building 4 and it shows some fluctuation during the day but is in general smoother than the curve of building 3.
The room heating load and DHW load for the week from February 10th till 16th for building 4 is shown

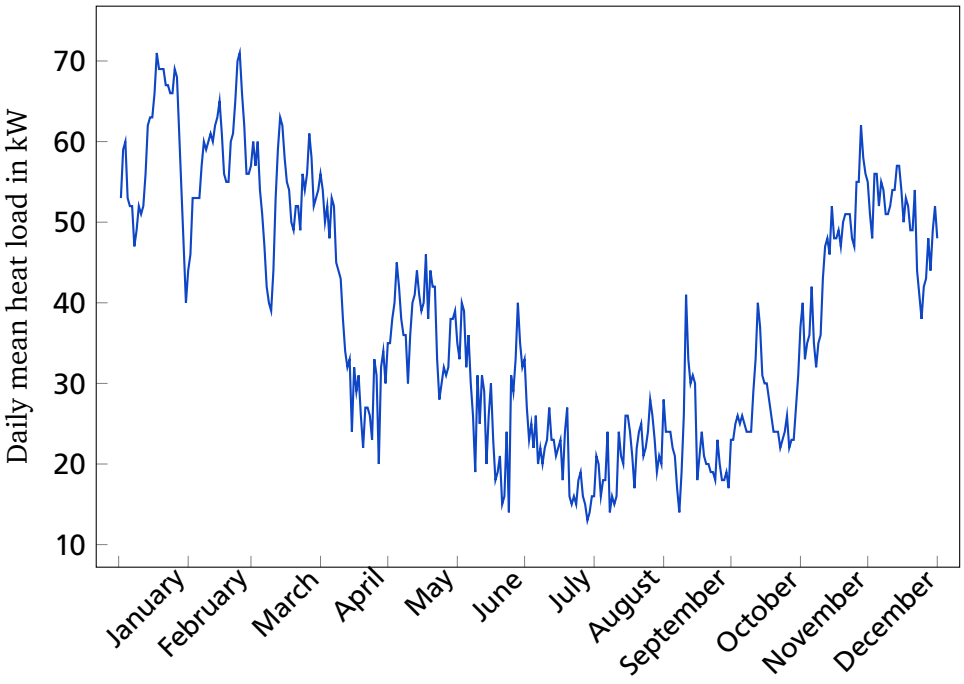

Figure 4.2: Daily mean heat load profile for the building cluster for 2013.

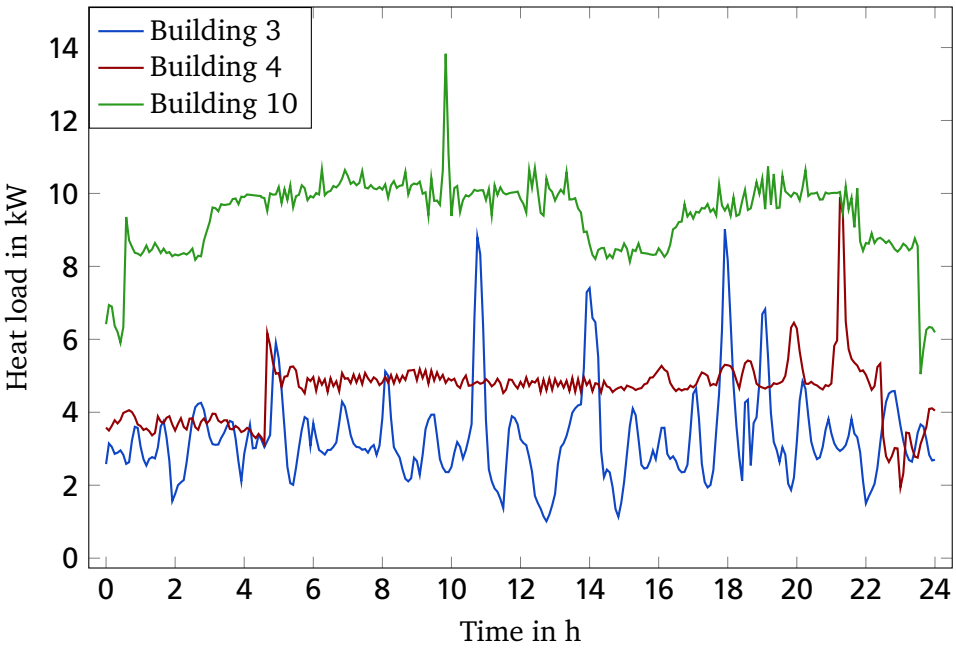

Figure 4.3: Heat load profile for buildings 3, 4 and 10 on 15.02.2013.

in figure 4.4. The room heating load is low during the night, stays on a rather constant higher level during the day and peaks in the evening. There is DHW demand during lunchtime and in the evening, but most of the time the DHW load is zero.

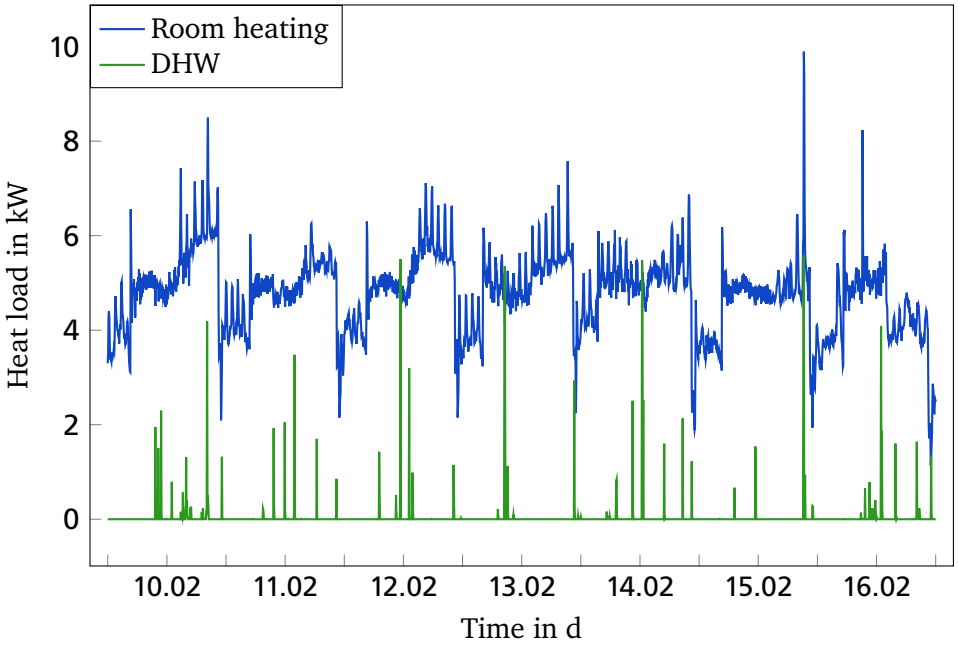

Figure 4.4: Heat load profile for the week from the 10.02.2013 till the 16.02.2013 for building 4.

4.1.3 Electricity demand

Since the electricity demand of the 11 buildings was not available, it is estimated with the help of standardized load profiles. Standardized load profiles are available for different building- and user types and can be upscaled to match a certain annual demand. Morbach [87] used the standardized load profiles of the Bundesverband der Energie- und Wasserwirtschaft [26] to create the electricity load profile for the building cluster with an annual electricity demand of 59.4 MWh. This demand does not include the electricity demand for heat generation and distribution or the compensated grid electricity. The load profile for a week for the building cluster is displayed in figure 4.5. The load is high in the mornings and evenings and low during the nights.

4.2 Heat distribution grid

The buildings are connected via a DHS in form of a radial distribution system, which distributes heat from the heat station to the individual buildings with one main supply and return line [70]. The system layout is shown in figure 4.1. The overall pipe length is 810 m and the individual pipe lengths and diameters are listed in table 4.2. To meet the desired supply and return temperatures of $T_s = 50\,°C$ and $T_r = 35\,°C$, the district pump is speed-controlled. Further information on the used components in each scenario are given in section 4.4.

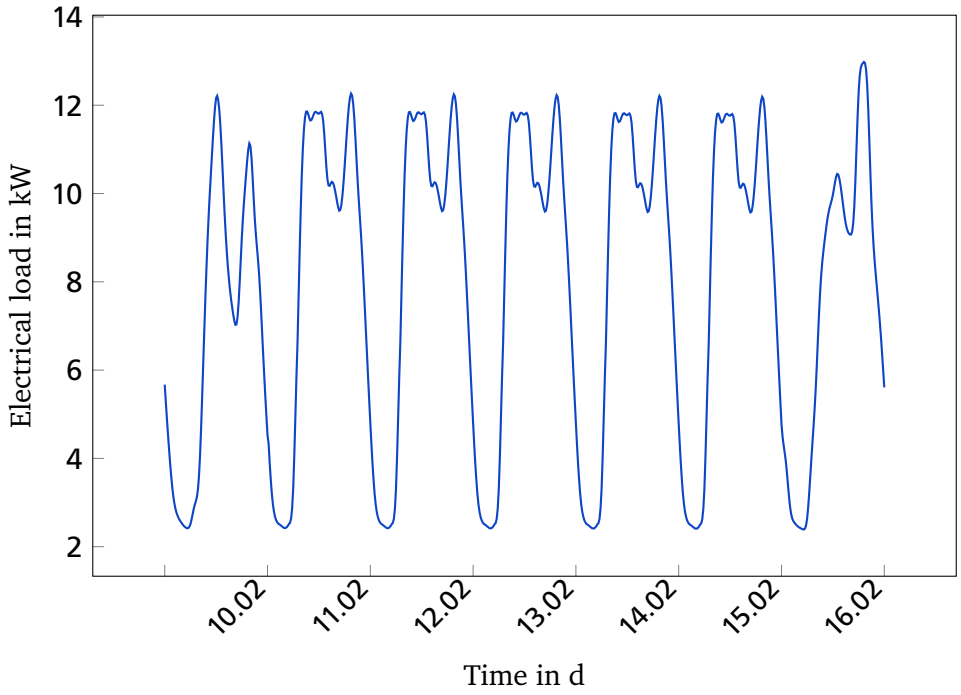

Figure 4.5: Electrical load profile for the week from the 10.02.2013 till the 16.02.2013.

Table 4.2: CaldoPEX [42] pipes used in the DHS.

	Length in m	Diameter in mm
1)	25	50
2)	20	32
3)	5	50
4)	10	32
5)	10	50
6)	30	25
7)	4	50
8)	20	32
9)	6	50
10)	10	32
11)	25	50
12)	25	32
13)	30	50
14)	30	32
15)	10	25
16)	20	32
17)	40	25
18)	20	32
19)	20	25
20)	10	32
21)	30	25
22)	5	25

4.3 Weather data

The weather data used in the model consists of the outdoor temperature and the solar radiation in 30 min time steps from the weather station Mannheim Nord, Germany [76]. Mannheim is located in one of the warmer regions of Germany, with warm summers and mild winters. In figure 4.6 the daily mean outdoor air temperature for the year 2013 is shown. It ranges from a low of −2.7 °C in February to a high of 30.4 °C in June.

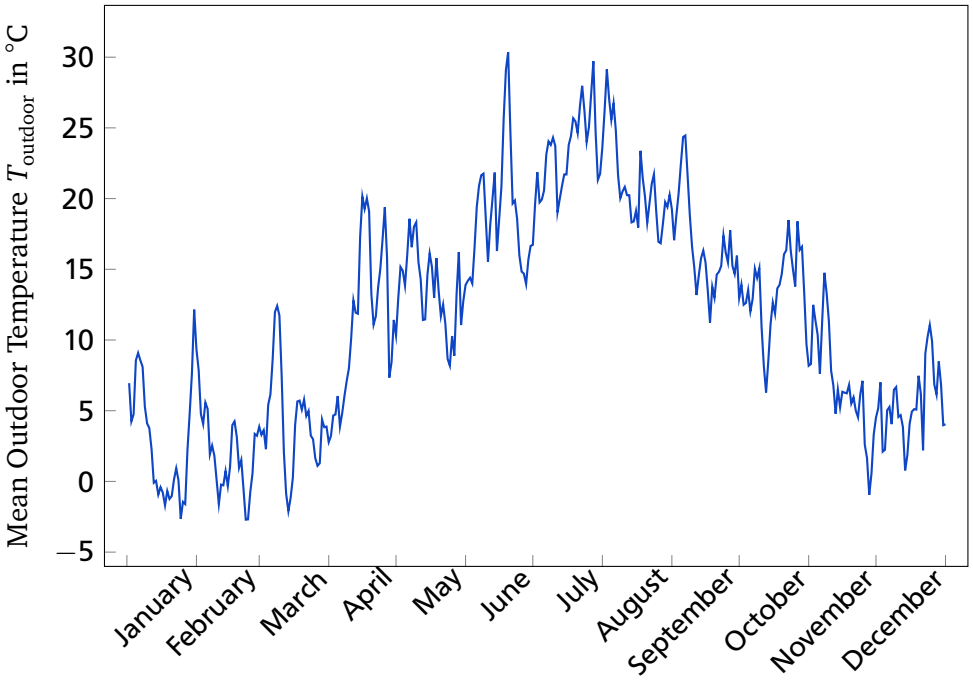

Figure 4.6: Daily mean outdoor air temperature profile for 2013.

4.4 Heat supply scenarios

In the following the different heat supply scenarios are introduced, together with the data of the used components. The dimensioning of the components was done in preliminary studies. The dimensions of the heat generation systems are based on a combination of the needed heating power, TES size and switching frequency.

4.4.1 Gas scenario

The Gas scenario, shown in fig. 4.7, consists of the DHS and a gas boiler [70]. The water is heated by the gas boiler and pumped through the DHS. The component data for the Gas scenario is listed in table 4.3.

Table 4.3: Gas scenario component data.

Component	Dimension	Remarks	Brand	Type	Source
Gas boiler	150 kW	$\eta_{\text{Boiler}} = 95\,\%$	Viessmann	Vitocrossal 200	[163]
District pump	1.1 kW	-	Grundfos	CR10-03 A-A-A-E-HQQE	[48]

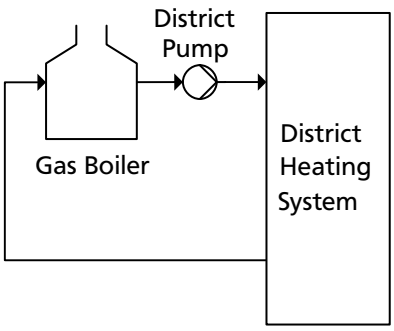

Figure 4.7: Gas scenario layout.

Exergy and energy analysis

The energy efficiency for the Gas scenario η_{Gas} is defined as

$$\eta_{\text{Gas}} = \frac{E_{\text{th.district}} + E_{\text{el.district}} + \Delta E_{\text{el}}}{E_{\text{C\&G}} + E_{\text{gas}} + E_{\text{el.renew}} + E_{\text{el.fossil}} + \Delta E_{\text{el.renew}} + \Delta E_{\text{el.fossil}}} \,. \tag{4.2}$$

$E_{\text{th.district}}$ is the thermal energy supplied to the district buildings, $E_{\text{el.district}}$ is the electrical energy supplied to the district buildings, ΔE_{el} is the compensated grid electricity introduced in section 3.1.5, $E_{\text{C\&G}}$ is the C&G energy of the scenario components, E_{gas} is the natural gas needed for the gas boiler, $E_{\text{el.renew}}$ and $E_{\text{el.fossil}}$ are the renewable and fossil primary energies needed to run the pump and $\Delta E_{\text{el.renew}}$ and $\Delta E_{\text{el.fossil}}$ are the renewable and fossil energies needed to produce the compensated grid electricity.
The exergy efficiency for the Gas scenario ψ_{Gas} is defined as

$$\psi_{\text{Gas}} = \frac{EX_{\text{th.district}} + EX_{\text{el.district}} + \Delta EX_{\text{el}}}{EX_{\text{gas}} + EX_{\text{el.renew}} + EX_{\text{el.fossil}} + \Delta EX_{\text{el.renew}} + \Delta EX_{\text{el.fossil}}} \,, \tag{4.3}$$

where $EX_{\text{th.district}}$ is the thermal exergy supplied to the district buildings, $EX_{\text{el.district}}$ is the electrical exergy supplied to the district buildings, ΔEX_{el} is the compensated grid electricity introduced in section 3.1.5, EX_{gas} is the natural gas needed for the gas boiler, $EX_{\text{el.renew}}$ and $EX_{\text{el.fossil}}$ are the renewable and fossil primary exergies needed to run the pump and $\Delta EX_{\text{el.renew}}$ and $\Delta EX_{\text{el.fossil}}$ are the renewable and fossil exergies needed to produce the compensated grid electricity.

4.4.2 Combined heat and power scenario

The CHP scenario, shown in fig. 4.8, consists of the DHS, a CHP plant, a buffer TES and an auxiliary gas boiler [87]. The CHP plant generates electricity and heats the TES. The TES is used to cover peak demands and to reduce the nominal power of the CHP plant. From the TES the water is pumped into the DHS. During peak loads the gas boiler can additionally heat the supply water to make sure the desired supply temperature T_{s} is met. The return water is either heated in the TES again or is used in a mixing loop in case the TES temperature is higher than T_{s}. The produced electricity is used for the building cluster demand and the excess electricity is fed into the electricity grid and serves as a baseline for the calculation of the needed compensated grid electricity in the other scenarios. The component data for the CHP scenario is listed in table 4.4.

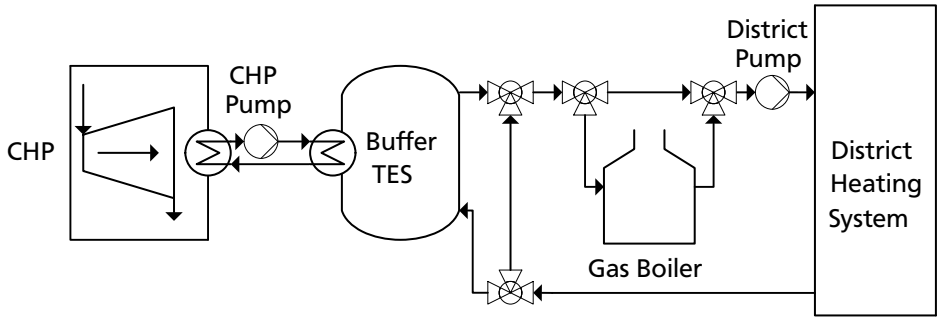

Figure 4.8: CHP scenario layout.

Table 4.4: CHP scenario component data.

Component	Dimension	Remarks	Brand	Type	Source
CHP	39 kW_{th}	$\eta_{el+th} = 95\,\%$	Viessmann	Vitobloc EM 20/39	[159]
Gas boiler	150 kW	$\eta_{Boiler} = 95\,\%$	Viessmann	Vitocrossal 200	[163]
TES	10 m^3	$k = 0.6\,W/m^2K$	Lorenz GmbH	Typ PSG 10000	[82]
District pump	1.1 kW	-	Grundfos	CR10-03 A-A-A-E-HQQE	[48]
CHP pump	1.1 kW	-	Grundfos	CR10-03 A-A-A-E-HQQE	[48]

Exergy and energy analysis

The energy efficiency for the CHP scenario η_{CHP} is defined as

$$\eta_{CHP} = \frac{E_{th.district} + E_{el.district} + E_{el.grid}}{E_{C\&G} + E_{gas} + E_{el.renew} + E_{el.fossil}} . \tag{4.4}$$

The exergy efficiency for the CHP scenario ψ_{CHP} is defined as

$$\psi_{CHP} = \frac{EX_{th.district} + EX_{el.district} + EX_{el.grid}}{EX_{gas} + EX_{el.renew} + EX_{el.fossil}} . \tag{4.5}$$

4.4.3 Geothermal scenario

The Geo scenario, shown in fig. 4.9, consists of the DHS, a VGHX, a HP and a buffer TES [43]. The HP is used to lift the temperature level of the geothermal energy from the primary to the secondary loop, which in turn heats the TES. The temperature difference between supply and return temperature in the primary loop between VGHX and HP is chosen to be 2.5 K and in the secondary loop between HP and TES 15.5 K based on the the preliminary studies [43]. The component data for the Geo scenario is listed in table 4.5. No gas boiler is needed because of the high nominal power of the HP.

Exergy and energy analysis

The energy efficiency for the Geo scenario η_{Geo} is defined as

$$\eta_{Geo} = \frac{E_{th.district} + E_{el.district} + \Delta E_{el}}{E_{C\&G} + E_{geo} + E_{el.renew} + E_{el.fossil} + \Delta E_{el.renew} + \Delta E_{el.fossil}} . \tag{4.6}$$

The exergy efficiency for the Geo scenario ψ_{Geo} is defined as,

$$\psi_{Geo} = \frac{EX_{th.district} + EX_{el.district} + \Delta EX_{el}}{EX_{geo} + EX_{el.renew} + EX_{el.fossil} + \Delta EX_{el.renew} + \Delta EX_{el.fossil}} . \tag{4.7}$$

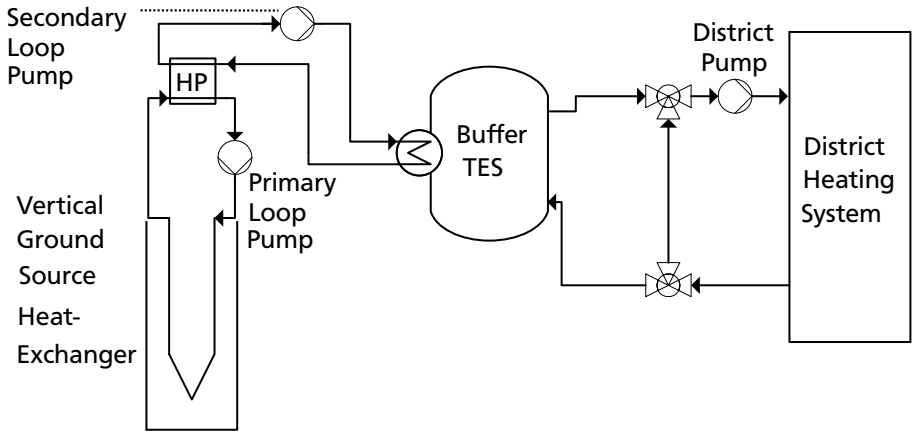

Figure 4.9: Geo scenario layout.

Table 4.5: Geo scenario component data.

Component	Dimension	Remarks	Brand	Type	Source
HP	93 kW	-	Viessmann	Vitocal 300 G	[158]
VGHX	12*96 m	double-U-pipe	-	-	[130]
TES	60 m^3	$k = 0.6\,W/(m^2K)$	Dehoust	-	[35]
District pump	1.1 kW	-	Grundfos	CR10-03 A-A-A-E-HQQE	[48]
Primary pump	1.3 kW	-	Grundfos	MAGNA 80-120 F	[49]
Secondary pump	0.1 kW	-	Grundfos	ALPHA2 15-60	[50]

4.4.4 Combined heat and power and geothermal scenario

The CHP+Geo scenario, shown in fig. 4.10, consists of the DHS, a CHP plant, a VGHX, a HP and a buffer TES [87]. The heat produced by the CHP plant and the HP heats the TES. The VGHX heats the fluid in the primary loop. The HP lifts the energy of the fluid in the primary loop to the higher temperature level of the secondary loop, which is then used to charge the TES. The produced electricity is used to run the HP and to supply the building cluster with electricity, while the excess is fed into the electricity grid. The temperature difference between supply and return temperature in the primary loop between VGHX and HP is chosen to be 1.0 K and in the secondary loop between HP and TES 15.5 K with the help of a parameter study and values from literature in the preliminary studies [87]. The component data for the CHP+Geo scenario is listed in table 4.6.

Exergy and energy analysis

The energy efficiency for the CHP+Geo scenario $\eta_{\mathrm{CHP+Geo}}$ is defined as

$$\eta_{\mathrm{CHP+Geo}} = \frac{E_{\mathrm{th.district}} + E_{\mathrm{el.district}} + E_{\mathrm{el.grid}} + \Delta E_{\mathrm{el}}}{E_{\mathrm{C\&G}} + E_{\mathrm{gas}} + E_{\mathrm{geo}} + E_{\mathrm{el.renew}} + E_{\mathrm{el.fossil}} + \Delta E_{\mathrm{el.renew}} + \Delta E_{\mathrm{el.fossil}}}\,, \tag{4.8}$$

where E_{geo} is the energy input into the VGHX.
The exergy efficiency for the CHP+Geo scenario $\psi_{\mathrm{CHP+Geo}}$ is defined as,

$$\psi_{\mathrm{CHP+Geo}} = \frac{EX_{\mathrm{th.district}} + EX_{\mathrm{el.district}} + EX_{\mathrm{el.grid}} + \Delta EX_{\mathrm{el}}}{EX_{\mathrm{gas}} + EX_{\mathrm{geo}} + EX_{\mathrm{el.renew}} + EX_{\mathrm{el.fossil}} + \Delta EX_{\mathrm{el.renew}} + \Delta EX_{\mathrm{el.fossil}}}\,, \tag{4.9}$$

where EX_{geo} is the exergy input into the VGHX.

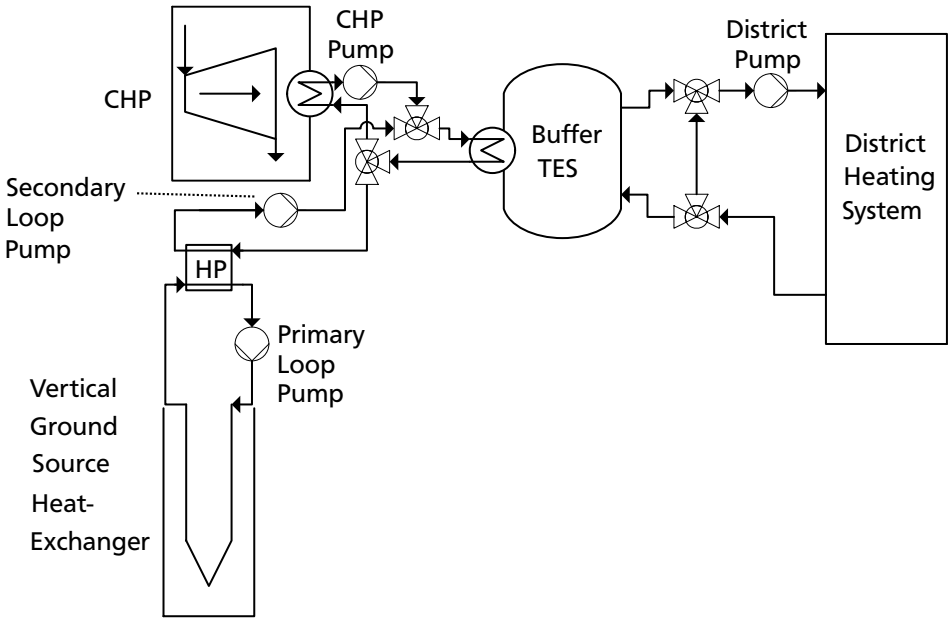

Figure 4.10: CHP+Geo scenario layout.

Table 4.6: CHP+Geo scenario component data.

Component	Dimension	Remarks	Brand	Type	Source
CHP	20.1 kW_{th}	$\eta_{el+th} = 95\,\%$	Viessmann	Vitobloc EM 9/20	[160]
HP	42.8 kW	-	Viessmann	Vitocal 300 G BW 301.A45	[161]
VGHX	6*96 m	double-U-pipe	-	-	[130]
TES	90 m^3	$k = 0.6\,W/(m^2K)$	Dehoust	-	[35]
District pump	1.1 kW	-	Grundfos	CR10-03 A-A-A-E-HQQE	[48]
CHP pump	1.1 kW	-	Grundfos	CR10-03 A-A-A-E-HQQE	[48]
Primary pump	1.3 kW	-	Grundfos	MAGNA 80-120 F	[49]
Secondary pump	0.1 kW	-	Grundfos	ALPHA2 15-60	[50]

4.4.5 Solar scenario

The Solar scenario, shown in fig. 4.11, consists of the DHS, solar thermal collectors, a seasonal TES and a backup gas boiler [70]. The solar thermal collectors heat the water of the TES. The TES stores the heat from summer till autumn, when the heat is needed in the buildings. From the TES, the water is pumped into the DHS. When the TES temperature is below T_s, the gas boiler additionally heats the supply water to make sure the needed heat is supplied. The return water is either heated in the TES again, is used in a mixing loop in case the TES temperature is higher than T_s or is bypassed by the TES in case that the TES temperature is below T_r. The component data for the Solar scenario is listed in table 4.7.

Table 4.7: Solar scenario component data.

Component	Dimension	Remarks	Brand	Type	Source
Solar thermal collectors	500 m^2	facing south at an angle of 40°	Viessmann	Vitosol 200 F	[70; 162]
Gas boiler	150 kW	$\eta_{\text{Boiler}} = 95\,\%$	Viessmann	Vitocrossal 200	[163]
TES	800 m^3	$k = 0.6\,\text{W}/(\text{m}^2\text{K})$	-	Custom made	[70]
District pump	1.1 kW	-	Grundfos	CR10-03 A-A-A-E-HQQE	[48]
Solar pump	1.1 kW	-	Grundfos	CR10-03 A-A-A-E-HQQE	[48]
Solar Pipes	810 m	Supply and return	Enerpipe	CaldoPEX	[42]

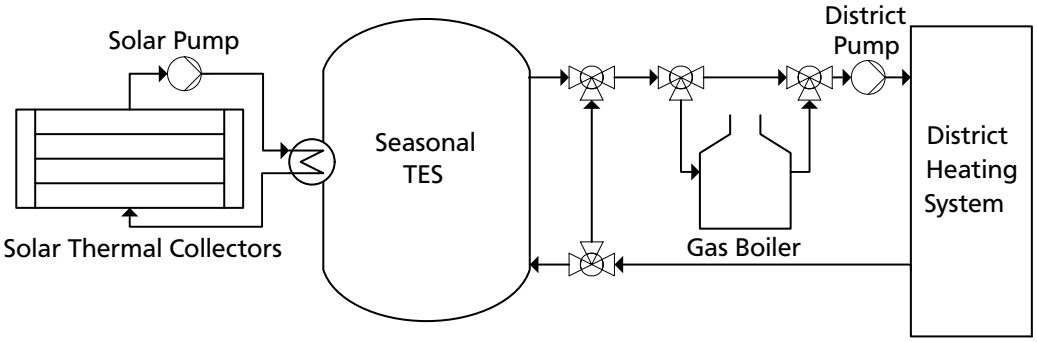

Figure 4.11: Solar scenario layout.

Exergy and energy analysis

The energy efficiency for the Solar scenario η_{Solar} is defined as

$$\eta_{\text{Solar}} = \frac{E_{\text{th.district}} + E_{\text{el.district}} + \Delta E_{\text{el}}}{E_{\text{C\&G}} + E_{\text{gas}} + E_{\text{solar}} + E_{\text{el.renew}} + E_{\text{el.fossil}} + \Delta E_{\text{el.renew}} + \Delta E_{\text{el.fossil}}}, \tag{4.10}$$

where E_{solar} is the heat input into the solar fluid.
The exergy efficiency for the Solar scenario ψ_{Solar} is defined as

$$\psi_{\text{Solar}} = \frac{EX_{\text{th.district}} + EX_{\text{el.district}} + \Delta EX_{\text{el}}}{EX_{\text{gas}} + EX_{\text{solar}} + EX_{\text{el.renew}} + EX_{\text{el.fossil}} + \Delta EX_{\text{el.renew}} + \Delta EX_{\text{el.fossil}}}, \tag{4.11}$$

where EX_{solar} is the exergy increase of the solar fluid through the solar thermal collectors.

4.4.6 Power to heat scenario

The P2H scenario, shown in fig. 4.12, consists of the DHS, a VGHX with a HP, an air source HP, a seasonal TES, a buffer TES and PV modules [17]. The PV modules power the two HP. The system uses two different heat sources depending on the time of year. The air/water HP runs during the "summer period" from 01.05.2013 till 15.09.2013 to make use of the warm outdoor air. During the rest of the year, the "winter period", the ground source HP generates the needed heat using the VGHX. During the "winter period" the VGHX heats the fluid in the primary loop and the HP lifts the energy to the higher temperature level of the secondary loop. During the "summer period", when the PV output is high and the heat demand is low, the air/water HP uses the PV electricity and the heat from the outside air to heat the seasonal TES and the buffer TES when needed. In autumn, the seasonal TES supplies the buffer TES with warm water. The excess electricity produced by the PV modules is either used to cover the electricity demand of the building cluster or is fed into the electricity grid.

Exergy and energy analysis

The energy efficiency for the P2H scenario η_{P2H} is defined as

$$\eta_{\text{P2H}} = \frac{E_{\text{th.district}} + E_{\text{el.district}} + E_{\text{el.grid}} + \Delta E_{\text{el}}}{E_{\text{C\&G}} + E_{\text{air}} + E_{\text{geo}} + E_{\text{PV}} + E_{\text{el.renew}} + E_{\text{el.fossil}} + \Delta E_{\text{el.renew}} + \Delta E_{\text{el.fossil}}}, \tag{4.12}$$

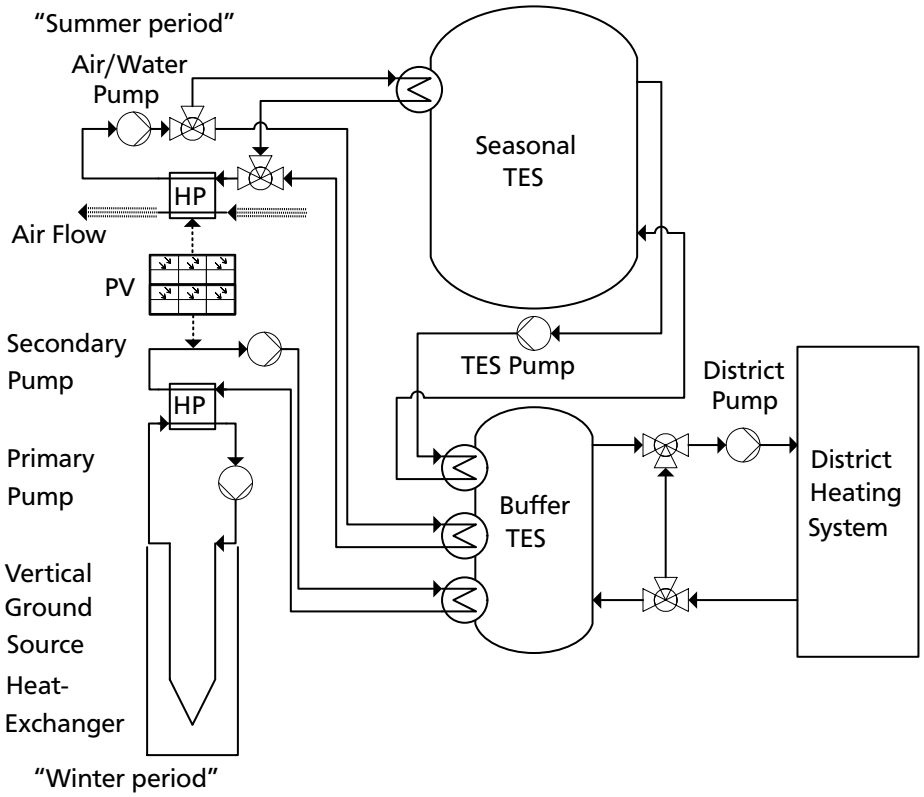

Figure 4.12: P2H scenario layout.

where E_{air} is the energy supplied by the airflow through the air HP and E_{PV} is the electricity produced by the PV modules.

The exergy efficiency for the P2H scenario ψ_{P2H} is defined as

$$\psi_{\text{P2H}} = \frac{EX_{\text{th.district}} + EX_{\text{el.district}} + EX_{\text{el.grid}} + \Delta EX_{\text{el}}}{EX_{\text{geo}} + EX_{\text{PV}} + EX_{\text{el.renew}} + EX_{\text{el.fossil}} + \Delta EX_{\text{el.renew}} + \Delta EX_{\text{el.fossil}}}\,, \tag{4.13}$$

where EX_{PV} is the electricity produced by the PV modules. The exergy of the air flow through the HP is zero since the exergy in this work is calculated with the outdoor air state as reference environment and thus, EX_{air} is not included in equation 4.13.

4.5 Simulation software

In order to optimize or study the performance of a system, the International Energy Agency Annex 49 [143] concludes that dynamic analysis is required, because storage effects need to be taken into account. Three software tools are commonly used by different user groups.
Polysun [150] is a software for the dynamic simulation of buildings and energy generation components. A hydraulic scheme is designed and can be simulated with different control strategies. The software incorporates a weather database, many default systems and a large selection of different energy components such as PV modules, solar thermal plants, CHP plants and geothermal HP.
TRNSYS (TRansient SYstem Simulation) [138] is a simulation software initially designed to simulate solar collectors. Today it is a software with a modular structure which can simulate the building demand and consists of a large library for different energy components such as CHP plants, fuel cells and wind

Table 4.8: P2H scenario component data.

Component	Dimension	Remarks	Brand	Type	Source
PV modules	98 kW_p	500 m^2	LG	LG Solarmodul LG320N1C-G4 NeON 2 Cello	[77]
HP	93 kW	-	Viessmann	Vitocal 300 G	[158]
VGHX	12*96 m	double-U-pipe	-	-	[130]
Air HP	11*16.0 kW	Cascade	Rotex	HPSU hitemp 16.0 kW	[122]
Seasonal TES	1200 m^3	$k = 0.6\,W/(m^2K)$	-	Custom made	[17; 70]
Buffer TES	90 m^3	$k = 0.6\,W/(m^2K)$	Dehoust	-	[35]
District pump	1.1 kW	-	Grundfos	CR10-03 A-A-A-E-HQQE	[48]
Primary pump	1.3 kW	-	Grundfos	MAGNA 80-120 F	[49]
Secondary pump	0.1 kW	-	Grundfos	ALPHA2 15-60	[50]
Air/Water pump	1.3 kW	-	Grundfos	MAGNA 80-120 F	[49]
TES pump	90 W		Grundfos	MAGNA 40-40 F	[49]

turbines.
CARNOT (Conventional And Renewable eNergy systems Optimization Toolbox) [130] is a MATLAB/Simulink based library which uses the MATLAB/Simulink structure in form of blocksets and their solver, and provides components for the simulation of buildings and energy components and TES and other thermo-hydraulic systems.
Becker et al. [11] compare the aforementioned dynamic building simulation software tools and conclude that Polysun is favorable for the simulation of standard energy systems with components from the Polysun library, since own models are not easily implemented. CARNOT is best used for research, as it has a high complexity, but also a high degree of modeling freedom for new components and systems due to its open source structure. TRNSYS combines aspects of Polysun and CARNOT with easy modeling of standard systems and some freedom of modeling new components.
In this work the system is dynamically modeled using CARNOT [130]. It was developed for the simulation of heating systems by the Solar Institut Jülich, Germany. CARNOT is well suited to study a system as complex as a DHS because it provides the user with a wide range of user definable components as well as the possibility to develop own components through its open source design. The individual components allow for the simulation of hydraulics and heat transfer using physical equations as well as characteristic curves.
In this work, own components in form of embedded MATLAB functions and block diagrams are developed and used for the simulation. The modeled systems are simulated using variable time-steps which are in the range of minutes. However, the software is not intended to study individual components and physical effects in detail, but rather the interaction and controlling of multiple components in a larger system.

4.6 Modeled components in CARNOT

In the following, details to the individual modeled components in CARNOT are given.

Gas boiler

The CARNOT gas boiler is a simple model which transfers the constant nominal power to the water and calculates the temperature change of the heating water. In the internal storage of the boiler a multinode model is applied to calculate the water conditions. The differential equation for the water temperature of one node in the boiler is given by the following equation [15]:

$$\left(M_{\mathrm{node}} c_{\mathrm{node}}\right) dT_{\mathrm{node}}/dt = K_{\mathrm{loss}}/N \left(T_{\mathrm{amb}} - T_{\mathrm{node}}\right) + \dot{M}_{\mathrm{w}} c_{\mathrm{w}} \left(T_{\mathrm{in}} - T_{\mathrm{node}}\right) + P_{\mathrm{nom}}/N \ , \tag{4.14}$$

where M_{node} is the mass of the node, c_{node} is the heat capacity of the node, T_{node} is the temperature of the node, K_{loss} is the heat loss to the ambient, N is the number of nodes in the boiler, T_{amb} is the ambient temperature, $\dot{M}_{\mathrm{w}}$ is the mass flow rate, c_{w} is the heat capacity, T_{in} is the temperature of the water entering the node and P_{nom} is the nominal boiler power.
At the same time the fuel consumption is calculated, dependent on the fuel type and heating value. Input parameters are among others, the fluid type, boiler power, internal boiler volume, heat capacity of the boiler and initial boiler temperature. In this work the gas boiler is modeled using 3 calculation nodes.

CHP plant

The CHP is modeled using the data points from the characteristic curves of real CHP plants available on the market. Depending on the required thermal or electrical load, the working point of the CHP plant is determined by linearly interpolating between the available data points. The fuel input P_{fuel} is defined as

$$P_{\text{fuel}} = \frac{P_{\text{el}}}{\eta_{\text{el}}} = \frac{\dot{Q}_{\text{th}}}{\eta_{\text{th}}}\,, \tag{4.15}$$

where P_{el} is the electrical output, η_{el} is the electrical efficiency, $\dot{Q}_{\text{th}}$ is the thermal output and η_{th} is the thermal efficiency of the CHP plant.
The CHP should only be modulated between 50 % and 100 % of the given nominal power. For the simulation two interpolation sections of the characteristic curves are defined. The first between 50 % and 75 %, the second between 75 % and 100 %. For a generated thermal output higher than 75 % of the nominal power $\dot{Q}_{\text{th}} \geq 0.75\dot{Q}_{\text{th,n}}$ the interpolation is defined as

$$\eta_{\text{th}}\left(\dot{Q}_{\text{th}}\right) = \frac{\eta_{\text{th,100\,\%}} - \eta_{\text{th,75\,\%}}}{\dot{Q}_{\text{th,100\,\%}} - \dot{Q}_{\text{th,75\,\%}}}\dot{Q}_{\text{th}} + \left(\eta_{\text{th,100\,\%}} - \frac{\eta_{\text{th,100\,\%}} - \eta_{\text{th,75\,\%}}}{\dot{Q}_{\text{th,100\,\%}} - \dot{Q}_{\text{th,75\,\%}}}\dot{Q}_{\text{th,100\,\%}}\right) \tag{4.16}$$

and for a generated thermal output lower than 75 % of the nominal power $\dot{Q}_{\text{th}} \leq 0.75\dot{Q}_{\text{th,n}}$ the interpolation is defined as

$$\eta_{\text{th}}\left(\dot{Q}_{\text{th}}\right) = \frac{\eta_{\text{th,75\,\%}} - \eta_{\text{th,50\,\%}}}{\dot{Q}_{\text{th,75\,\%}} - \dot{Q}_{\text{th,50\,\%}}}\dot{Q}_{\text{th}} + \left(\eta_{\text{th,75\,\%}} - \frac{\eta_{\text{th,75\,\%}} - \eta_{\text{th,50\,\%}}}{\dot{Q}_{\text{th,75\,\%}} - \dot{Q}_{\text{th,50\,\%}}}\dot{Q}_{\text{th,75\,\%}}\right) \tag{4.17}$$

With the working point, the electrical and thermal efficiency of the plant and the resulting thermal and electrical output is calculated. Thermal capacities during start-up, shut-down and load changes are neglected [52]. Input parameters are among others, the CHP nominal power and the operation type, meaning heat- or electricity-controlled operation.

Solar thermal collectors

The used CARNOT solar thermal collector is modeled according to the EN 12975 norm. For the calculation of the temperature change of the solar collector fluid, the incoming solar radiation, the wind speed, the collector surface area, the collector angle and orientation and the heat loss coefficient and the sky temperature are taken into account [15]. The equation for the energy balance of the collector is given by [15]:

$$\begin{aligned}\dot{M}c\left(T_{\text{out}} - T_{\text{in}}\right)/A' = {} & F'(TA)K_{\text{dir}}I_{\text{dir}} + F'(TA)K_{\text{dfu}}I_{\text{dfu}} \\ & - f_1\left(T_{\text{m}} - T_{\text{amb}}\right) - f_2\left(T_{\text{m}} - T_{\text{amb}}\right)^2 - f_3 w_{\text{wind}}\left(T_{\text{m}} - T_{\text{amb}}\right) - f_6 w_{\text{wind}} I_{\text{glb}} \\ & + f_4\left(I_{\text{Longwave}} - \sigma_{\text{SB}}\left(T_{\text{amb}} + 273.15\right)^4\right) - f_5 dT_{\text{m}}/dt\end{aligned} \tag{4.18}$$

A' is the surface area of the collector, F' is the collector efficiency factor, TA is the effective transmittance-absorptance product for direct solar radiation at normal incidence, K_{dir} is the incidence angle modifier for direct solar radiation, I_{dir} is the direct solar radiation on the collector plane, K_{dfu} is the incidence angle modifier for diffuse solar radiation and I_{dfu} is the diffuse solar radiation on the collector plane. f_1 through f_6 are coefficients which can be found in the CARNOT manual [15]. T_{m} is the mean collector node temperature, w_{wind} is the wind velocity and I_{glb} is the global solar radiation on the collector plane. I_{Longwave} is the longwave irradiance with wave length > 3000 nm and σ_{SB} is the Stefan-Boltzmann constant.

HP

The dynamic behavior of the CARNOT HP is modeled using the empirical model of Schwamberger [127], which is based on the German DIN 8900. The heating, source and electricla powers for different temperatures in the primary and secondary loop are given in two-dimensional diagrams, from which the working points of the HP are approximated by linear equations. The outlet temperatures of the cold and hot side of the HP are calculated with differential equations [15]. The differential equation for the cold side is

$$M_{\text{cold}} c_{\text{cold}} dT_{\text{cold,out}}/dt = \dot{Q}_{\text{source}} + \dot{M}_{\text{cold}} c_{\text{cold}} \left(T_{\text{cold,in}} - T\right) + kA' \left(T_{\text{amb}} - T_{\text{cold,out}}\right) \tag{4.19}$$

and for the hot side

$$M_{\text{hot}} c_{\text{hot}} dT_{\text{hot,out}}/dt = \dot{Q}_{\text{heating}} + \dot{M}_{\text{hot}} c_{\text{hot}} \left(T_{\text{hot,in}} - T\right) + kA' \left(T_{\text{amb}} - T_{\text{hot,out}}\right) \ , \tag{4.20}$$

where $\dot{Q}_{\text{source}}$ is the source power input and $\dot{Q}_{\text{heating}}$ power output [15].

VGHX

The CARNOT vertical ground heat exchangers model is a transient model for dynamic simulation. The model is based on equations by Bianchi [16] and is implemented using the state space model of Huber and Schuler [62]. It simulates the heat transfer between soil and heating fluid with a simplified model and gives the result through a step function response. For the calculations, the average annual outdoor temperature, the geothermal temperature gradient, the thermal conductivity and the heat capacity of the ground, the depth and geometry of the geothermal borehole field are taken into account.

PV

The CARNOT PV module calculates electricity generation using the incoming solar radiation, module angle and orientation and module efficiency [15].

TES

The CARNOT TES is modeled as a multiport one-dimensional model. The port can be a simple pipe for example, a heat exchanger, a stratified charging pipe or a direct electrical heater. The inlet and outlet height of the ports can be specified. The TES is subdivided into N nodes and heat conduction and mass bound heat transfer is considered, while convection is combined into an effective axial heat conductivity λ_{eff}. For each node, the following differential equation is solved [15]:

$$\begin{aligned}\left(\rho c\right) dT/dt = {} & kA'_{\text{loss}}/V_{\text{node}} \left(T_{\text{amb}} - T_{\text{node}}\right) + k_{\text{hx}} A'_{\text{hx}}/V_{\text{node}} \left(T_{\text{hx node}} - T_{\text{node}}\right) \\ & + \lambda_{\text{eff}}/D_{\text{h}}^2 \left(T_{\text{node above}} - T_{\text{node}}\right) + \lambda_{\text{eff}}/D_{\text{h}}^2 \left(T_{\text{node below}} - T_{\text{node}}\right) \\ & + \dot{M}_{\text{up}} c/V_{\text{node}} \left(T_{\text{node below}} - T_{\text{node}}\right) + \dot{M}_{\text{down}} c/V_{\text{node}} \left(T_{\text{node above}} - T_{\text{node}}\right) \ , \end{aligned} \tag{4.21}$$

where ρ is the TES fluid density, c the heat capacity, k is the heat loss coefficient, A' the heat loss area, V_{node} is the node volume, k_{hx} is the heat transfer coefficient to a possible heat exchanger, A' is the heat exchanger surface, λ_{eff} is the effective axial thermal conductivity, D_{h} is the distance between two nodes and $\dot{M}$ is the mass flow through the TES. In this work the TES is modeled using 15 calculation nodes.

Pipes

The CARNOT pipes are modeled as multinode models calculating the conduction heat loss through the pipe walls to the ambient. Input parameters are the heat loss coefficient, ambient temperature, initial temperature and heat capacity [15]. The differential equation for one pipe node is

$$\begin{aligned}\left(c_{\text{wall}} L / V_{\text{node}}\right) dT/dt = kA'_{\text{loss}}/V_{\text{node}} \left(T_{\text{amb}} - T_{\text{node}}\right) + \dot{M}c/V_{\text{node}} \left(T_{\text{lastnode}} - T_{\text{node}}\right) \\ + \lambda/D_{\text{h}}^2 \left(T_{\text{nextnode}} - T_{\text{node}}\right) + \lambda/D_{\text{h}}^2 \left(T_{\text{lastnode}} - T_{\text{node}}\right) \ , \quad (4.22)\end{aligned}$$

where L is the pipe length [15]. The pressure drop through the pipes can also be calculated in CARNOT. However, in this work, the pressure drop of the whole pipe network is estimated using typical specific pressure drops from [75].

Buildings

The buildings itself are not modeled in this work because real demand data for the heat demand is available as introduced in section 4.1. The needed mass flow to supply the DHS with a supply temperature $T_{\text{s}} = 50\,°\text{C}$ and a return temperature $T_{\text{s}} = 35\,°\text{C}$ is calculated with the demand data.

4.7 Component dimensioning

Optimal dimensions of the components in each individual scenario are determined through preliminary studies.

Boiler: The CARNOT gas boiler is used with the default settings and a nominal power of 150 kW is chosen to accomodate the maximum needed heating power of the building cluster [70].

CHP plant: The nominal power of the CHP plant in this work is chosen depending on the TES size, and the combination of the overall thermal power of CHP plant and HP in the CHP+Geo scenario. The nominal power stated in table 4.6 is determined with the help of an optimization process aiming at a minimized fossil fuel input [87].

Solar collectors: As surface area for the solar thermal collectors and the PV modules, the available rooftop area of the building cluster is taken. An effective collector area is calculated depending on the rooftop orientation and angle. The effective collector area is 500 m^2 facing south at an angle of 40° [70].

Heat pump: The HP nominal power is chosen according to the recommendations of the Viessmann GmbH & Co. KG to optimize the life span of a HP and to keep the switching frequency to a maximum of three per hour [164]. The HP dimension is dependent on the needed power and the TES size and is chosen according to a three-hour average load of 80 kW [43]. The nominal power stated in table 4.4 and 4.6 are determined with the help of an optimization process aiming at a minimized fossil fuel input.

VGHX: In Germany, shallow geothermal heat is often restricted to a depth of 100 m [149]. A maximum depth of 96 m is taken in this work. The geothermal temperature gradient can vary between

0.01 K/m and 0.2 K/m depending on the location and geothermal conditions [68]. The temperature gradient for the investigated region is 0.0454 K/m [112]. The VGHX pipes are double U-tube pipes and the geometry is chosen depending on the HP size, to accommodate the HP with the needed source power.

TES: The TES volume is defined in the preliminary studies and is chosen to minimize the fossil energy input, to optimize the switching frequency as well as the CHP or HP size.

4.8 Overview of ecological and economic data

In this section an overview of the ecological and economic data is given. For the individual scenarios only the data for the components is given, the data which results from the operation is not shown. Therefore, the following data cannot be used to draw conclusions regarding the overall ecological and economical efficiency. The overall results are shown in chapter 6. The derivation of the data is given in appendix A.1 and A.2.

Ecological data

In table 4.9 the GWP of natural gas and electricity is listed.

Table 4.9: GWP of natural gas and electricity.

	GWP in kg_{CO_2e}/kWh	Source
q_{gas}	0.252	[93]
$q_{el.mix}$ year 2015	0.56	[147]
$q_{el.mix}$ year 2030	0.289	[166]

In table 4.10 the GWP and the C&G data for the individual scenarios is listed.

Economical data

In table 4.11 the initial investment of the individual scenarios are given. The CHP, the CHP+Geo and the P2H scenario sell electricity to the electricity grid and are therefore entitled to an input tax reduction, which is already included in table 4.11. The P2H scenario is entitled to an input tax reduction of 100 % for the PV modules and components [84]. Until recently the input tax reduction for CHP plants was

Table 4.10: Total cradle & grave GWP and $E_{C\&G}$ of the different scenarios.

Scenario	GWP in kg_{CO_2e}/a	$E_{C\&G}$ in kWh/a
Gas scenario	122.3	479.8
CHP scenario	1154.0	1516.8
CHP+Geo scenario	1344.2	4193.9
Geo scenario	872.2	4293.8
Solar scenario	6328.8	22 043.2
P2H scenario	10 799.5	37 517.5

calculated dependent on the produced amount of heat and electricity [36]. This would lead to a partitioning of around 75 % and 35 % for heat and electricity. But according to the verdict of the supreme tax court (Bundesfinanzhof) from 16.11.2016 [19], the input tax reduction has to be calculated dependent on the sale prices of heat and electricity, leading to a partitioning of 14 % and 86 % for heat and electricity, which is used in this work. However, a different possibility would be the partitioning according to the produced exergy. This approach would lead to a partitioning of approximately 20 % and 80 %.
Further information regarding the economical data such as interest rate are given in the appendix tables A.9 till A.23.

Table 4.11: Scenario gross investment.

Scenario	investment in €
Gas scenario	16 805
CHP scenario	77 464
CHP+Geo scenario	201 612
Geo scenario	223 619
Solar scenario	581 340
P2H scenario	1 062 804

5 TES exergy dependency on the reference temperature

In this chapter the dependency of the exergy content of a TES on the reference temperature is discussed and a method is developed to separate between exergy destruction and exergy change due to changing reference temperature.

5.1 Exergy balance of a TES for varying reference temperatures

The exergy balance of a TES for a constant reference temperature is as follows:

$$\left(EX_2 - EX_1\right) = \left(EX_{\text{in}} - EX_{\text{out}}\right) + \left(-EX_{\text{loss}} - EX_{\text{destr.}}\right) \ , \tag{5.1}$$

where EX_2 and EX_1 are the exergy contents of the TES at the end and at beginning of the calculation, EX_{in} and EX_{out} are the exergy flows in and out of the TES, EX_{loss} is the exergy loss attributed to the heat loss and $EX_{\text{destr.}}$ is the exergy destruction due to mixing of the stratified layers, so called destratification. However, in the following it will be shown that the exergy content of a TES is also dependent on the reference temperature. The dependency of the exergy content of the TES on the reference temperature and on stratification is discussed using an exemplary, simplified adiabatic TES. The TES has a volume of $100\,\text{m}^3$, a diameter of 5.57 m and five calculation nodes. The density $\rho_{\text{w}} = 991.9\,\text{kg/m}^3$ and the heat capacity $c_{\text{w}} = 4.182\,\text{kJ/}\left(\text{kgK}\right)$ of water are assumed to be constant. For the following example equation 5.1 is reduced to the change of exergy content of the TES due to exergy destruction. This means, that the TES is adiabatic and has no incoming or outgoing flows:

$$\left(EX_2 - EX_1\right) = -EX_{\text{destr.}} \tag{5.2}$$

The example is designed as a comparison of the TES at different reference temperatures and with different TES layer temperatures as shown in figure 5.1. In every TES configuration shown in figure 5.1 the mean temperature is always 64.6 °C, which means that they all have the same energy content. A base case of a stratified TES with different temperature layers after the TES charging process at a reference temperature of 13.0 °C is compared to three homogeneously mixed TES at three different reference temperatures of 13.0 °C, 15.0 °C and 11.0 °C. Each comparison combination in figure 5.1 and in the following description is named after the reference temperature used for the TES exergy content calculation. The first temperature is always the base case, and the second temperature is the homogeneously mixed TES. The base case and the combinations are described in the following:

- Base case
  The base case is the left bar in each pair of bars in figure 5.1. The exergy content of each temperature layer in the TES of the base case is dependent on its temperature and increases with

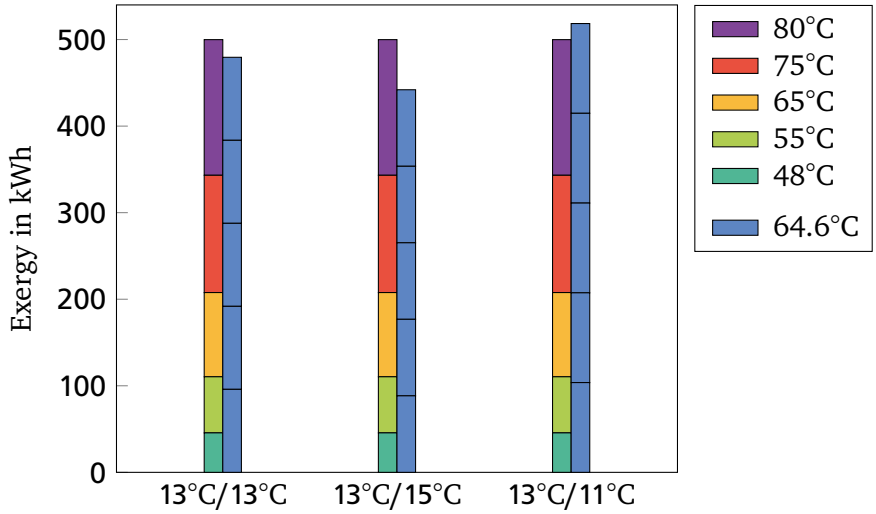

Figure 5.1: Exergy content of a stratified (left bar) and a homogeneous mixed (right bar) TES at different reference temperatures, but with the same mean TES temperature.

increasing temperature and therefore with increasing temperature difference between TES layer temperature and reference temperature. This can be explained with the definition of the exergy of heat in equation 3.2. The exergy content of the layers in the stratified TES range from 45 kWh at 48 °C to 155 kWh at 80 °C and the overall exergy content is 500 kWh.

- 13.0 °C/13.0 °C
  In the combination 13.0 °C/13.0 °C the exergy content of the stratified base case is compared to the exergy content of the homogeneously mixed TES also at a reference temperature of 13.0 °C. The difference to the base case is the mixing of the temperature layers from the base case to the homogeneously mixed TES. The exergy content of the homogeneously mixed TES is 20 kWh lower than the exergy content of the base case. This is due to the exergy destruction which occurs during the destratification of the TES temperature layers. In this case this means that the exergy destruction $EX_{\text{destr.}}$ in equation 5.1 is 20 kWh.

- 13.0 °C/15.0 °C
  In the combination 13.0 °C/15.0 °C the exergy content of the stratified base case is compared to the exergy content of the homogeneously mixed TES at an increased reference temperature of 15.0 °C. The difference to the base case is the mixing of the temperature layers from the base case to the homogeneously mixed TES and the increase of the reference temperature by 2.0 °C. The exergy content of the homogeneously mixed TES is only 440 kWh and thus lower than that of the base case as well as of the homogeneously mixed TES in the 13.0 °C/13.0 °C combination. The exergy content of the homogeneously mixed TES at a reference temperature of 15.0 °C is lower due to two factors. The first one being the above described exergy destruction due to destratification. The second factor is the change of the reference temperature, which is increased by 2.0 °C. The reference temperature increase leads to an even further decrease of exergy content compared to the 13.0 °C/13.0 °C combination. This is due to the definition of the “Carnot-Factor” in equation 3.2 which involves the ratio of the reference temperature and the system temperature.

- 13.0 °C/11.0 °C
  In the combination 13.0 °C/11.0 °C the exergy content of the stratified base case is compared to the exergy content of the homogeneously mixed TES at a decreased reference temperature of 11.0 °C.

The difference to the base case is the mixing of the temperature layers from the base case to the homogeneously mixed TES and the decrease of the reference temperature by 2.0 °C. At 520 kWh the exergy content is the highest of all four discussed TES. Even though exergy is destroyed during destratification, the overall exergy content is increased due to the reference temperature decrease of 2.0 °C. According to equation 3.2 a temperature difference increase between system temperature and reference temperature leads to an exergy increase. In this case, the increase in exergy content, due to lowering the reference temperature, is higher than the exergy decrease due to exergy destruction, which leads to an overall exergy increase.

The example shown in figure 5.1 exemplifies that a stratified TES has a higher exergy content than a homogeneously mixed TES for the same mean TES temperature and reference temperature. Furthermore, the influence of a changing reference temperature on the exergy content of a TES cannot be neglected. Since the current surrounding air is chosen as reference environment in this work as discussed in section 3.1.2, the influence of a changing reference temperature on the exergy content of a TES is addressed below.

5.2 Method development for the separation of exergy destruction and exergy change

In figure 5.1 it is shown that the exergy content of a TES not only depends on the input and output flow, the exergy loss and the exergy destruction as introduced in equation 5.1, but also on the reference temperature. This means that equation 5.1 is only valid for a fixed reference temperature. However, the reference temperature between charging and discharging the TES can change. This is especially significant for seasonal TES. Therefore, equation 5.1 should be changed to include a term which expresses the change of exergy of TES due to a changing reference temperature. To the author's knowledge this has not been done before and is a new approach.
The change of the exergy content due to a changing reference temperature will be called "exergy change" or $EX_{\Delta T_{ref}}$ in this work.
In figure 5.1, no heat loss or in and out going exergy flows are considered. During the actual operation of a TES, in- and outgoing exergy flows, exergy loss, exergy destruction and exergy change can occur at the same time, making it difficult to differentiate between exergy destruction and exergy change. In general, the exergy destruction is calculated with equation 5.1 and hence includes the exergy change as well, combined called $EX_{\mathrm{comb.var}}$. In order to separate the two, the following approach is chosen.
Exergy change does not occur when using a fixed reference temperature. The TES exergy balance for a fixed reference temperature and the standard TES exergy balance for a variable reference temperature are as follows:

$$\left(EX_{2_{\mathrm{fix}}} - EX_{1_{\mathrm{fix}}}\right) = \left(EX_{\mathrm{in}_{\mathrm{fix}}} - EX_{\mathrm{out}_{\mathrm{fix}}}\right) + \left(-EX_{\mathrm{loss}_{\mathrm{fix}}} - EX_{\mathrm{destr.fix}}\right) , \tag{5.3}$$

and

$$\left(EX_{2_{\mathrm{var}}} - EX_{1_{\mathrm{var}}}\right) = \left(EX_{\mathrm{in}_{\mathrm{var}}} - EX_{\mathrm{out}_{\mathrm{var}}}\right) + \left(-EX_{\mathrm{loss}_{\mathrm{var}}} - EX_{\mathrm{comb.var}}\right) . \tag{5.4}$$

In the chosen approach, the exergy destruction $EX_{\mathrm{destr.fix}}$ is calculated with equation 5.3. This exergy destruction is then used as the exergy destruction $EX_{\mathrm{destr.var}}$ for the system with a varying reference temperature $EX_{\mathrm{destr.fix}} = EX_{\mathrm{destr.var}}$. The exergy change $EX_{\Delta T_{ref}}$ is calculated as the difference between $EX_{\mathrm{comb.var}}$ and $EX_{\mathrm{destr.fix}}$:

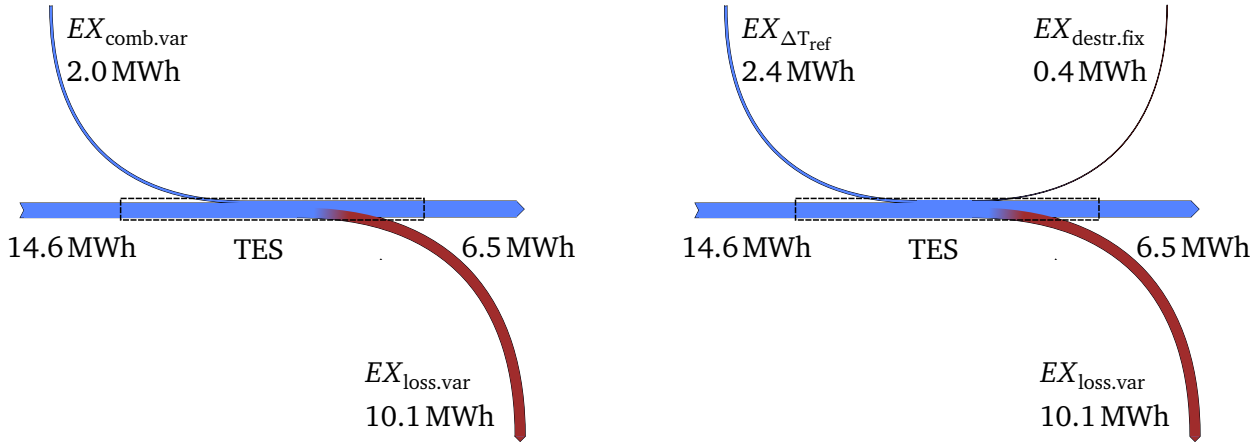

(a) TES with combined exergy destruction and exergy change leading to an overall exergy input.

(b) TES with separated exergy destruction and exergy change .

Figure 5.2: Visualization of the concept of exergy change on a TES using two exergy flow diagrams of the same TES at the same conditions, but with different reference temperatures.

$$EX_{\Delta T_{\text{ref}}} = EX_{\text{comb.var}} - EX_{\text{destr.fix}} \tag{5.5}$$

With $EX_{\Delta T_{\text{ref}}}$ equation 5.4 changes to

$$\left(EX_{2_{\text{var}}} - EX_{1_{\text{var}}}\right) = \left(EX_{\text{in}_{\text{var}}} - EX_{\text{out}_{\text{var}}}\right) + \left(-EX_{\text{loss}_{\text{var}}} - \left(EX_{\text{destr.fix}} + EX_{\Delta T_{\text{ref}}}\right)\right) , \tag{5.6}$$

which now differentiates between exergy destruction and exergy change. In this work, the undisturbed ground temperature is taken as a fixed reference temperature of $T_{\text{ref,fix}} = 13.0\,^{\circ}\text{C}$.
In order to show the results of equation 5.4 and equation 5.6, two exergy flow diagrams are shown in figure 5.2. Here, the exergy flow diagrams of the TES from the Solar scenario, which is introduced in section 4.4.5 are shown. The calculation is carried out for a whole year, with the corresponding changing reference temperature.
In figure 5.2a the exergy flow diagram of a TES, which is calculated with equation 5.4 and a varying reference temperature, is shown. The exergy content of the TES is the same at the start and the end of the calculation, $EX_{2_{\text{var}}} = EX_{1_{\text{var}}}$. The input is $EX_{\text{in}_{\text{var}}} = 14.6\,\text{MW}$ and the output of the TES is $EX_{\text{out}_{\text{var}}} = 6.5\,\text{MW}$. The exergy loss due to heat loss is $EX_{\text{loss}_{\text{var}}} = 10.1\,\text{MW}$. But instead of exergy destruction $EX_{\text{destr.var}}$ decreasing the exergy content of the TES, there is an additional input of $EX_{\text{comb.var}} = 2.0\,\text{MW}$ into the system. This is due to the exergy change which is not separated from the exergy destruction yet and leads to an increase of the exergy content of the TES over the simulation time.
In contrast, figure 5.2b shows the exergy flow diagram of the same TES, but the exergy is calculated with equation 5.6. $EX_{\text{in}_{\text{var}}}$, $EX_{\text{out}_{\text{var}}}$ and $EX_{\text{loss}_{\text{var}}}$ are the same as in figure 5.2a, but the $EX_{\text{comb.var}}$ is now split into $EX_{\text{destr.fix}} = 0.4\,\text{MW}$ and the new introduced exergy change due to changing reference temperature $EX_{\Delta T_{\text{ref}}} = 2.4\,\text{MW}$, thereby differentiating between actual exergy destruction and exergy change due to changing reference temperature.
The exergy change $EX_{\Delta T_{\text{ref}}}$ can have a positive and a negative value as seen in figure 5.1. If the exergy change has a positive value, the TES was charged with low exergy heat, but discharged at a time when its exergy value was higher, due to a lower reference temperature.

6 Results

In this chapter the results of this work are presented. First, the results of the individual scenarios are discussed followed by a comparison of all scenarios. For all scenarios a supply and return temperature of $T_s = 50\,°C$ and $T_r = 35\,°C$ is chosen and the heat loss coefficient for all TES is set to $k = 0.6\,W/(m^2K)$ [70]. A detailed description of the scenarios is given in section 4.4 and information regarding the used components and their dimensioning can be found in table 4.3 till 4.8.

6.1 Scenario Results

In this section results of the individual heat supply scenarios are given and different configurations are discussed for certain scenarios. For each scenario an energy and exergy flow diagram is presented. The color scheme valid for the flow diagrams is given in table 6.1.

Table 6.1: General color scheme for energy and exergy flow diagrams.

Color	Meaning	Color	Meaning	Color	Meaning
=	Fossil energy	=	Renewable energy	=	Heat
=	Electricity	=	Loss/destruction	=	Heat demand
=	Electricity demand	=	Net electricity	=	Compensated grid electricity

The thickness of the individual flow diagram sections is directly proportional to their value in MWh and the scale is the same for every flow diagram, making them directly comparable to each other. During exergy conversion processes, exergy loss due to heat loss and exergy destruction due to energy conversion is shown combined as exergy loss. This simplifies the diagrams, but does not change the result in the overall exergy decrease due to energy conversion. The exergy destruction due to mixing in the mixing valves is not shown individually, but combined with the exergy losses of the pipes, which is another simplification.

6.1.1 Gas scenario

For the Gas scenario different supply and return temperatures are investigated to show the influence of changing temperature levels. In figure 6.1 the pipe losses of the DHS are displayed for different supply and return temperatures. The energy losses increase from 27 MWh to 57 MWh, or an average of 0.8 MWh/(K) with increasing supply and return temperature, while the exergy losses range from 3 MWh to 12 MWh.
Compared to the base case with a supply temperature $T_s = 90\,°C$, the pipe losses are cut in half, for $T_s = 50\,°C$. Therefore, the supply temperature is set to $T_s = 50\,°C$ for all scenarios. Not only can the pipe losses be decreased for lower network temperatures, lower network temperatures also enable renewable energy sources, such as geothermal heat combined with a HP, to feed into the DHS.
In figure 6.2 the energy flow diagram of the Gas scenario is shown with the corresponding data listed in table 6.2. The Gas scenario flow diagram consists of two segments. The heat segment supplied by the

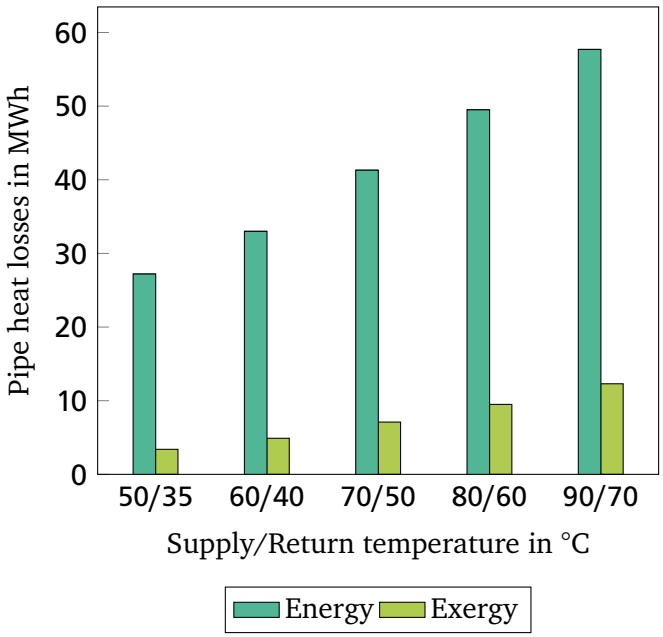

Figure 6.1: Gas scenario district pipe losses for increasing supply and return temperatures.

boiler and the electricity segment supplied by the electricity grid. The only interaction between the two is the electricity for the district pump. The largest energy input is the natural gas for the boiler (I), while the largest energy loss occurs during the primary energy conversion (c). The energy flow diagram shows the straightforward design of the Gas scenario with little energy losses in the heat segment, but also the high overall fossil energy input. The electricity segment is split into the electricity demand (B) and the compensated grid electricity (C) as introduced in section 3.1.5.

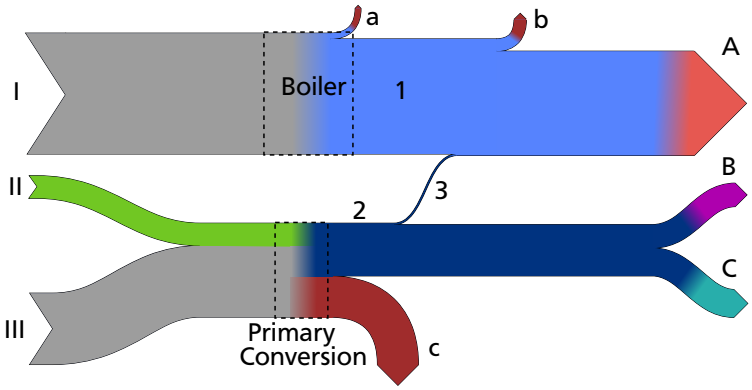

Figure 6.2: Gas scenario energy flow diagram on an annual basis.

In figure 6.3 the exergy flow diagram of the Gas scenario is shown with the corresponding data listed in table 6.3. Compared to the energy flow diagram in figure 6.2, several differences stand out. One is the high exergy loss of the boiler (a) which is by far the largest loss of the system. This is due to the low exergy efficiency of the boiler. While the energy efficiency η_{boiler} is 95 %, the exergy efficiency ψ_{boiler} is only 11 %. Another difference is that the heat segment is much thinner in the exergy flow diagram than in the energy flow diagram. In section 3.1.1, the system boundary was chosen so that room heating at 20 °C and DHW at 40 °C is defined as useful output. This useful output has a low exergy content. Thus the heat segment in figure 6.3 is thinner compared to the segment in figure 6.2. A third difference is the additional loss indicator (c) in the heat segment right before the room demand (A). This is the

Table 6.2: Labeling of the Gas scenario energy flow diagram in figure 6.2.

Number	Description	MWh	Number	Description	MWh
= I	Natural gas	305.6	= a	Boiler loss	14.6
= II	Renewable energy	56.9	= b	DHS pipe loss	31.0
= III	Fossil energy	180.4	= c	Primary conversion loss	103.5
= 1	Boiler to DHS	291.0	= A	Heat demand	263.7
= 2	Grid electricity	133.8	= B	Electricity demand	59.4
= 3	District pump	3.7	= C	Compensated grid electricity	70.7

exergy destruction which occurs when the supplied heat is cooled down from around 50 °C to the room heating demand at 20 °C. The electricity segment is rather unchanged due to the similar energy and exergy efficiencies, as introduced in section 3.1.4, and because the energy content of electricity is equal to its exergy content, as introduced in section 3.1.3. Looking at the exergy flow diagram, the design of the Gas scenario is still straightforward, but the heat segment shows high losses, indicating that the Gas scenario does not have a high exergy efficiency.

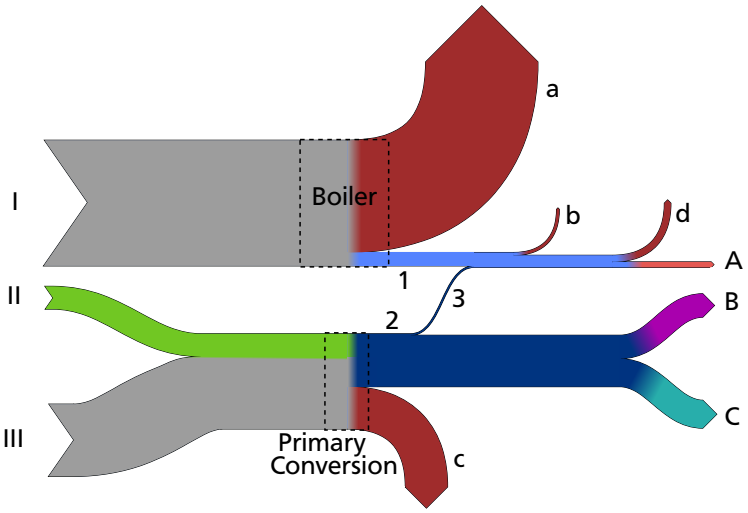

Figure 6.3: Gas scenario exergy flow diagram on an annual basis.

6.1.2 Combined heat and power scenario

In figure 6.4 an overview of the results of the CHP scenario is shown for different TES volumes. In order to make the results for the individual TES volumes comparable, the compensated grid electricity is considered. The useful output is kept constant for the different TES volumes, as introduced in section 3.1.5. It is not shown in the graph, but the electricity fed into the electricity grid increases with increasing TES volume while the compensated grid electricity decreases at the same rate. The total energy input increases with increasing TES volume from 540 MWh at 10 m^3 to almost 700 MWh at 3600 m^3. The total energy input includes the primary energy needed to produce the compensated grid electricity. At the same rate, the TES losses increase from 4 MWh to almost 190 MWh. However, the electrical and thermal output do not increase at the same rate, but rather seem to stay constant after a TES volume of 2250 m^3. This demonstrates that after a TES volume of 2250 m^3 the CHP running-time cannot be increased further, only the losses increase. The reason that the overall energy input still increases after a TES volume of

Table 6.3: Labeling of the Gas scenario exergy flow diagram in figure 6.3.

Number	Description	MWh	Number	Description	MWh
I	Natural gas	317.9	b	DHS pipe loss	7.1
II	Renewable energy	57.7	c	Primary conversion loss	106.9
III	Fossil energy	183.0	d	HTS exergy destruction	16.6
1	Boiler to DHS	34.0	A	Heat demand	14.0
2	Grid electricity	133.8	B	Electricity demand	59.4
3	District pump	3.7	C	Compensated grid electricity	70.7
a	Boiler loss	283.9			

2250 m^3 is that the increasing heat losses of the TES have to be made up for by the backup gas boiler. Even though the CHP plant can produce more electricity with increasing TES volume up to a TES volume of 2250 m^3, the TES losses are higher than the benefit. This is illustrated by the decreasing energy efficiency with increasing TES volume. The energy efficiency η_{CHP} decreases from 80 % at 10 m^3 to 62 % at 3600 m^3. The exergy efficiency ψ_{CHP} also decreases from 33 % to 27 % with increasing TES volume. These results show that in this setting a larger TES has no overall advantage even though the electricity output can be increased up to a certain point. It is not shown here, but even for a TES with a smaller heat loss coefficient, a small TES leads to the highest energy and exergy efficiency. For the comparison with the other scenarios the CHP system with a TES volume of 10 m^3 is chosen.

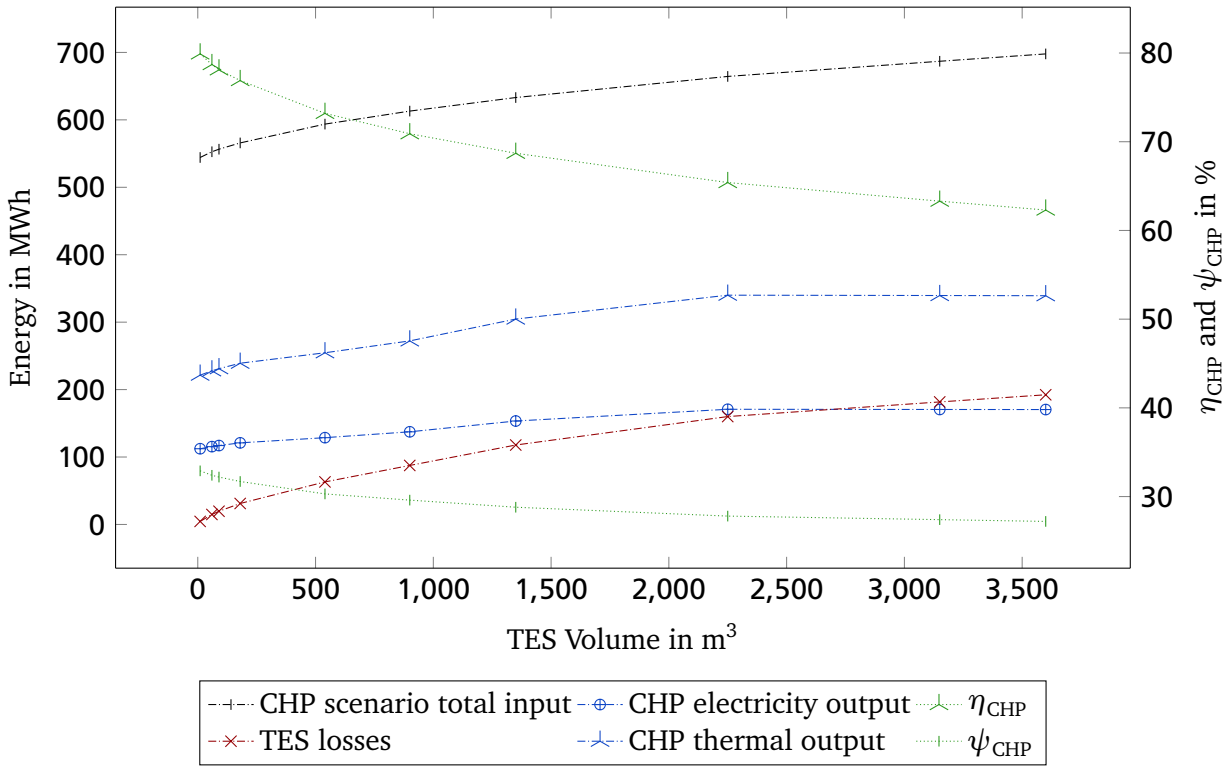

Figure 6.4: CHP scenario result overview showing the performance for different TES volumes.

In figure 6.5 the energy flow diagram of the CHP scenario is shown with the corresponding data listed in table 6.4. Here, two heat and two electricity segments exist. The heat is supplied by both boiler and CHP, with the CHP having the biggest share of heat supply. The largest energy loss occurs within the DHS

Table 6.4: Labeling of the CHP scenario energy flow diagram in figure 6.5.

Number	Description	MWh	Number	Description	MWh
I	Natural gas	431.3	10	Total electricity	133.8
II	Renewable energy	9.6	11	District pump	3.7
III	Fossil energy	30.6	a	CHP loss	17.1
1	CHP input	352.0	b	CHP to TES loss	2.3
2	Boiler input	79.3	c	TES loss	4.5
3	Boiler to DHS	75.5	d	Boiler loss	3.8
4	CHP to TES	221.5	e	DHS pipe loss	32.5
5	TES to DHS	217.0	f	Primary conversion loss	17.5
6	Total to DHS	292.5	A	Heat demand	263.7
7	CHP pump	2.3	B	Electricity demand	59.4
8	CHP electricity	111.1	C	Net electricity	70.7
9	Grid electricity	22.7			

pipes (e) and the TES loss (c) is rather small at 4.5 MWh compared to the energy input (4) of 220 MWh. The electricity segment is supplied by the CHP (8) and the electricity grid (9), with the CHP having the biggest share again. The absolute losses in the primary conversion (f) and the CHP (a) are similar, but the electricity produced by the CHP is five times the amount of grid electricity, showing the higher overall efficiency of the CHP compared to the electricity grid. The net electricity output (C) is the base line for the compensated grid electricity in the other scenarios.

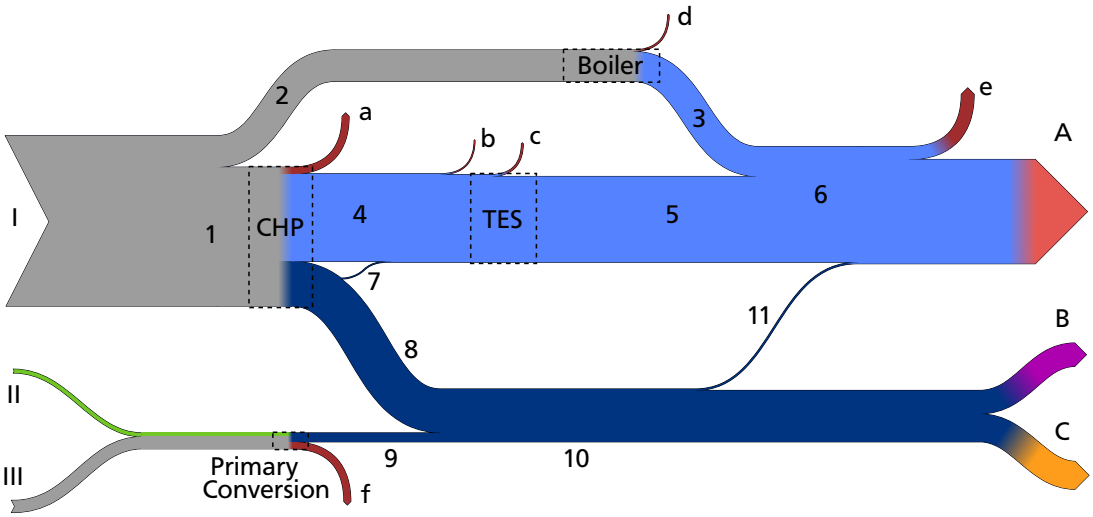

Figure 6.5: CHP scenario energy flow diagram on an annual basis.

In figure 6.6 the exergy flow diagram of the CHP scenario is shown with the corresponding data listed in table 6.5. Noticeable are the high exergy losses of the boiler (e) and the CHP (a). On the heat segment in the TES the exergy change (*) is separated from the exergy destruction (c) and the exergy loss (d) as introduced in section 5.2. The exergy destruction at the HTS (g) is higher than the exergy loss in the district pipes (f). The exergy loss (a) of the CHP is higher than its output, indicating that the CHP has a lower overall exergy efficiency than the electricity grid.

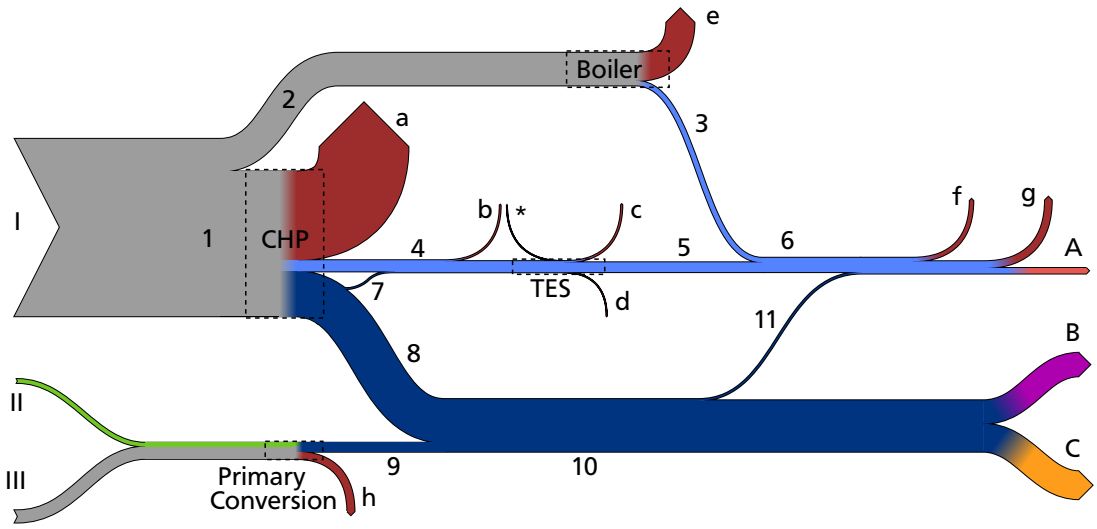

Figure 6.6: CHP scenario exergy flow diagram on an annual basis.

Table 6.5: Labeling of the CHP scenario exergy flow diagram in figure 6.6.

Number	Description	MWh	Number	Description	MWh
= I	Natural gas	448.5	= 10	Total electricity	133.8
= II	Renewable energy	9.8	= 11	District pump	3.7
= III	Fossil energy	30.9	= a	CHP loss	224.3
= 1	CHP input	366.0	= b	CHP to TES loss	2.3
= 2	Boiler input	82.5	= c	TES exergy destruction	3.1
= 3	Boiler to DHS	11.5	= d	TES loss	0.5
= 4	CHP to TES	28.2	= e	Boiler loss	71.0
= 5	TES to DHS	24.7	= f	DHS pipe loss	8.8
= 6	Total to DHS	36.2	= g	HTS exergy destruction	17.1
= *	Exergy change	0.1	= h	Primary conversion loss	18.0
= 7	CHP pump	2.3	= A	Heat demand	14.0
= 8	CHP electricity	111.1	= B	Electricity demand	59.4
= 9	Grid electricity	22.7	= C	Net electricity	70.7

Table 6.6: Labeling of the Geo scenario energy flow diagram in figure 6.7.

Number	Description	MWh	Number	Description	MWh
= I	Geothermal heat	235.6	= a	Primary loop loss	2.8
= II	Renewable energy	93.2	= b	HP loss	9.2
= III	Fossil energy	295.7	= c	Secondary loop loss	0.4
= 1	HP to TES	308.6	= d	TES loss	16.4
= 2	TES to DHS	292.2	= e	DHS pipe loss	32.2
= 3	Grid electricity	219.2	= f	Primary conversion loss	169.7
= 4	Primary loop pump	2.8	= A	Heat demand	263.7
= 5	HP electricity	82.2	= B	Electricity demand	59.4
= 6	Secondary loop pump	0.4	= C	Compensated grid electricity	70.7
= 7	District pump	3.7			

6.1.3 Geothermal scenario

In figure 6.7 the energy flow diagram of the Geo scenario is shown with the corresponding data listed in table 6.6. The Geo scenario only has one heat and one electricity segment. The largest energy loss occurs during the primary energy conversion (f) and the combined renewable energy input (I and II) is larger than the fossil energy input (III). Comparing the energy flow diagram of the Geo scenario to the energy flow diagram of the CHP+Geo scenario in figure 6.12 a difference in the electricity demand of the primary loop pump (4/8) is noticeable. This is due to different temperature spreads between the supply and return temperature of the primary loop for the two scenarios as introduced in section 4.4. The smaller temperature difference for the CHP+Geo scenario leads to a higher primary pump electricity demand, but the HP can save energy because of a smaller necessary temperature lift which makes this setting advantageous for the CHP+Geo scenario. In the Geo scenario however, a bigger temperature difference between the supply and return in the primary loop leads to a better performance, because the chosen HP can handle a greater temperature difference and pump power can be saved in this specific scenario.

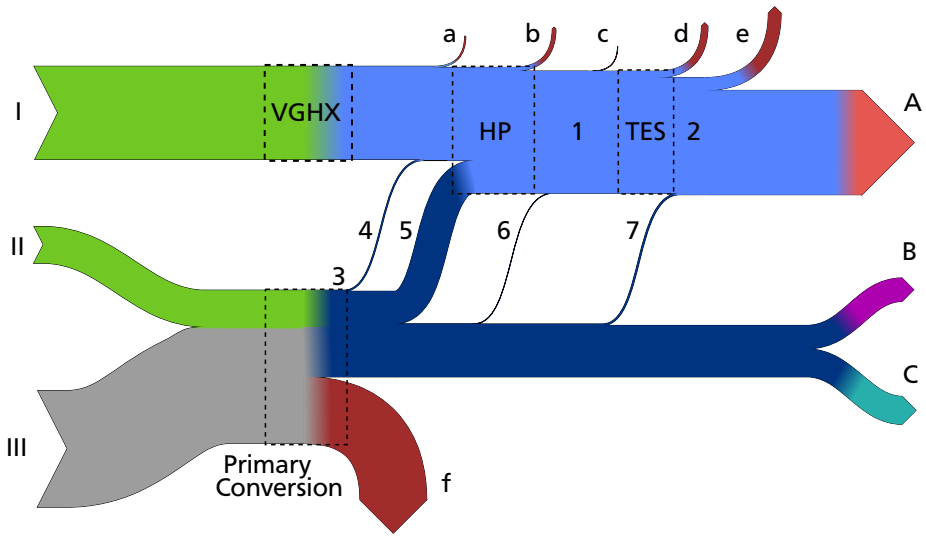

Figure 6.7: Geo scenario energy flow diagram on an annual basis.

Table 6.7: Labeling of the Geo scenario exergy flow diagram in figure 6.8.

Number	Description	MWh	Number	Description	MWh
= I	Geothermal heat	6.0	= b	Primary loop loss	2.8
= II	Renewable energy	94.5	= c	HP loss	45.5
= III	Fossil energy	300.0	= d	Secondary loop loss	0.4
= 1	HP to TES	39.9	= e	TES exergy destruction	1.6
= 2	TES to DHS	36.2	= f	TES loss	2.2
= *	Exergy change	0.1	= g	DHS pipe loss	9.3
= 3	Grid electricity	219.2	= h	HTS exergy destruction	16.6
= 4	Primary loop pump	2.8	= i	Primary conversion loss	175.3
= 5	HP electricity	82.2	= A	Heat demand	14.0
= 6	Secondary loop pump	0.4	= B	Electricity demand	59.4
= 7	District pump	3.7	= C	Compensated grid electricity	70.7
= a	VGHX exergy destruction	2.8			

In figure 6.8 the exergy flow diagram of the Geo scenario is shown with the corresponding data listed in table 6.7. Again, the geothermal heat input (I) is low exergy and exergy is destroyed in the VGHX. The HP shows a great exergy loss during the process, while the exergy change (*), the exergy destruction (e) and the exergy loss (f) of the TES are small.

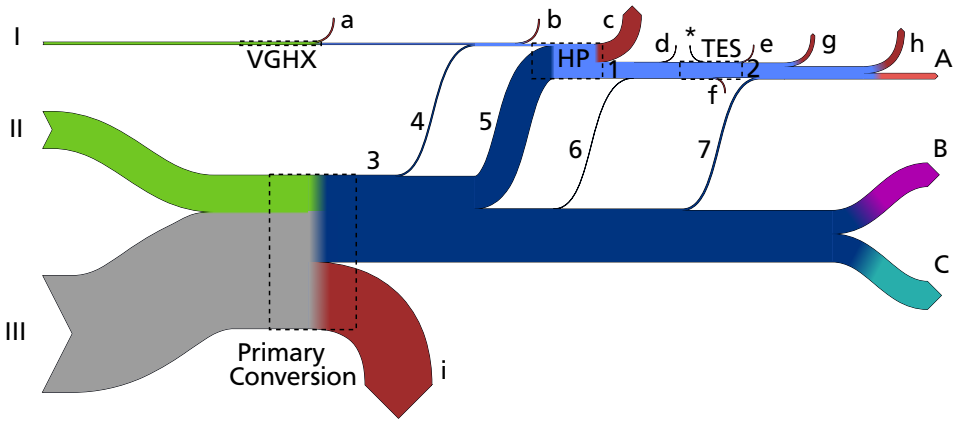

Figure 6.8: Geo scenario exergy flow diagram on an annual basis.

6.1.4 Combined heat and power and geothermal scenario

For the CHP+Geo scenario the share of geothermal HP power on the overall heat production capacity has been varied. The share of geothermal HP power is defined as the ratio of the nominal power of the HP and the nominal power of the CHP and the HP combined, $Share\ of\ geothermal\ HP\ power = P_{HP}/(P_{CHP} + P_{HP})$. Due to the specific HP and CHP combinations, the share is in odd numbers and not in even percentages. 0 % means that there is no HP installed in the scenario and 100 % means that it is a scenario without running a CHP. In table 6.8 the nominal power of the used HP and CHP are listed.
The energy supply and demand for the CHP+Geo scenario is depicted in figure 6.9. On the useful output or demand side the heat and electricity demands stay constant, whereas the compensated grid electricity increases at the same rate the electricity fed into the electricity grid decreases. The overall useful elec-

Table 6.8: Composition of the share of geothermal energy.

	0.0 %	19.4 %	42.5 %	68.0 %	100.0 %
HP power in kW	0.0	14.0 [153]	28.8 [153]	42.8 [153]	56.1 [155]
CHP power in kW	79.0 [128]	58.0 [89]	39.0 [156]	20.1 [157]	0.0

tricity output therefore stays constant, as explained in section 3.1.5. On the supply side the total fossil energy input decreases with increasing geothermal share, because the input of natural gas decreases. At the same time, the input of grid electricity increases. This is due to the decreasing electricity production of the CHP and the increasing need for electricity for the HP and for the compensated grid electricity. The input of renewable energy also increases, both through grid electricity and in form of geothermal heat, so that overall the energy input increases.

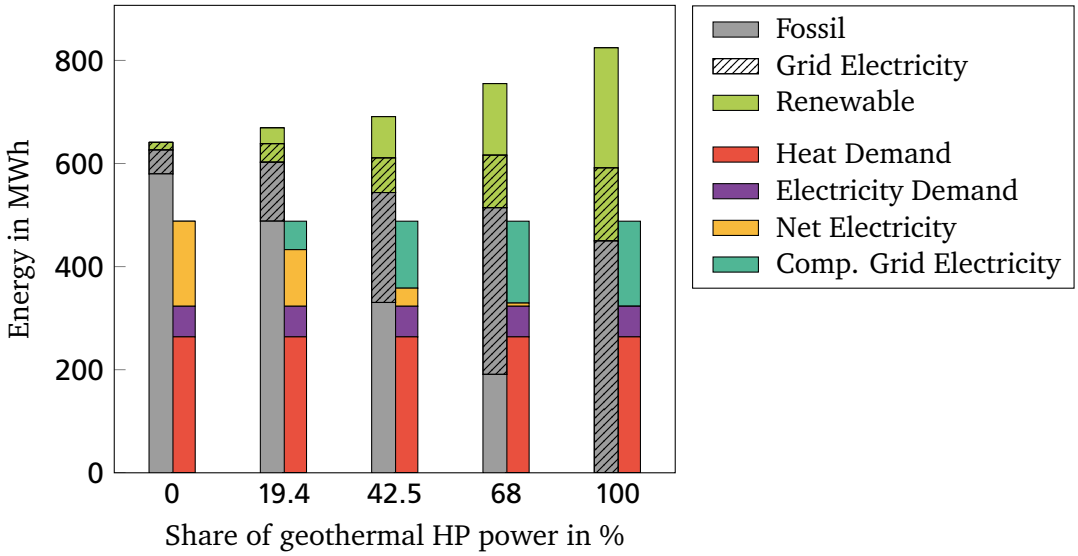

Figure 6.9: CHP+Geo scenario energy input and output for an increasing share of geothermal HP power.

The same development for increasing geothermal share is found in figure 6.10, where the exergy input and output of the CHP+Geo scenario is shown. Again, the useful output stays constant, but here the exergy content of the heat demand is lower compared to figure 6.9 because the exergy demand of room heating at 20 °C is much lower than its energy demand. The overall exergy input decreases because of the low exergy content of geothermal heat. However, for a share of 42.5 % and 68 %, the exergy input is the same due to a lower seasonal performance factor of the HP in combination with a lower electrical efficiency of the CHP plant for the HP and CHP combination for a share of 68 %.
The energy and exergy efficiencies of the CHP+Geo scenario are shown in figure 6.11. In accordance with figure 6.9 and 6.10, the energy efficiency decreases with increasing geothermal share, while the exergy efficiency increases. Energy-wise the system without HP would be the most efficient, while exergy-wise it would be the other way round. Since the two cases with 0 % and 100 % HP are already included in the CHP scenario and the Geo scenario, one of the three remaining cases will be compared to the other scenarios. Due to its low fossil energy input, the CHP+Geo scenario with a share of geothermal energy of 68 % is chosen.
In figure 6.12 the energy flow diagram of the CHP+Geo scenario is displayed with the corresponding data listed in table 6.9. Again, two heat and two electricity segments exist. The heat is supplied by the CHP and the geothermal HP, while the electricity segment is fed by the CHP and the electricity grid.

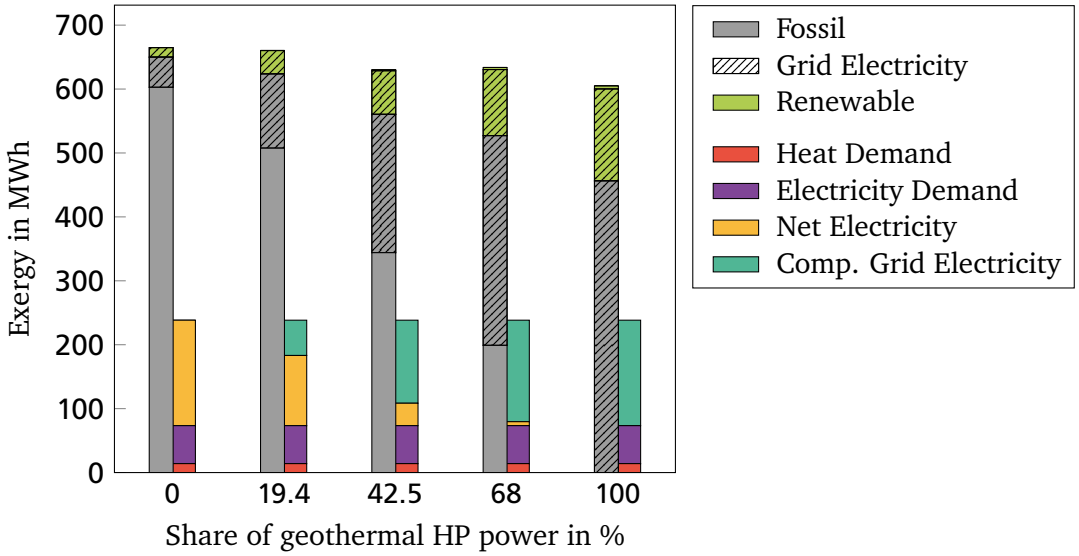

Figure 6.10: CHP+Geo scenario exergy input and output for an increasing share of geothermal HP power.

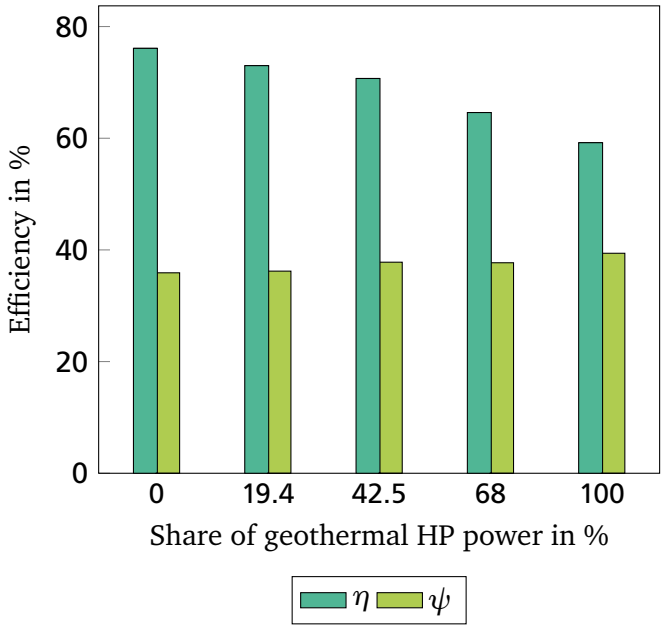

Figure 6.11: CHP+Geo scenario efficiency for an increasing share of geothermal HP power.

Table 6.9: Labeling of the CHP+Geo scenario energy flow diagram in figure 6.12.

Number	Description	MWh	Number	Description	MWh
I	Natural gas	190.8	11	Secondary loop pump	0.1
II	Geothermal heat	139.4	12	District pump	3.7
III	Renewable energy	61.8	a	CHP loss	9.4
IV	Fossil energy	196.3	b	CHP to TES loss	2.3
1	CHP to TES	127.5	c	Primary loop loss	12.2
2	HP to TES	187.0	d	HP loss	3.4
3	Total to TES	314.6	e	Secondary loop loss	0.1
4	TES to DHS	291.6	f	TES loss	23.0
5	CHP pump	2.3	g	DHS pipe loss	31.6
6	CHP electricity	51.6	h	Primary conversion loss	112.5
7	Grid electricity	145.6	A	Heat demand	263.7
8	Primary loop pump	12.2	B	Electricity demand	59.4
9	HP electricity	51.1	C	Net electricity	6.2
10	Total electricity	197.2	D	Compensated grid electricity	64.5

The amount of grid electricity (7) is higher than for the CHP scenario in figure 6.5, because the CHP does not produce as much electricity (6). This is because of the geothermal HP, which supplies 60 % of the heat (2) and in turn reduces the CHP running-time and installed capacity. The highest energy loss occurs in the primary energy conversion (h), followed by the DHS pipe loss (g) and the TES loss (f). The CHP scenario net electricity is taken as a base line for the electricity which has to be fed into the electricity grid. Since the CHP plant in the CHP+Geo scenario does not produce as much electricity as the CHP scenario, its useful electricity output is split into electricity demand (B), net electricity (C) and compensated grid electricity (D).

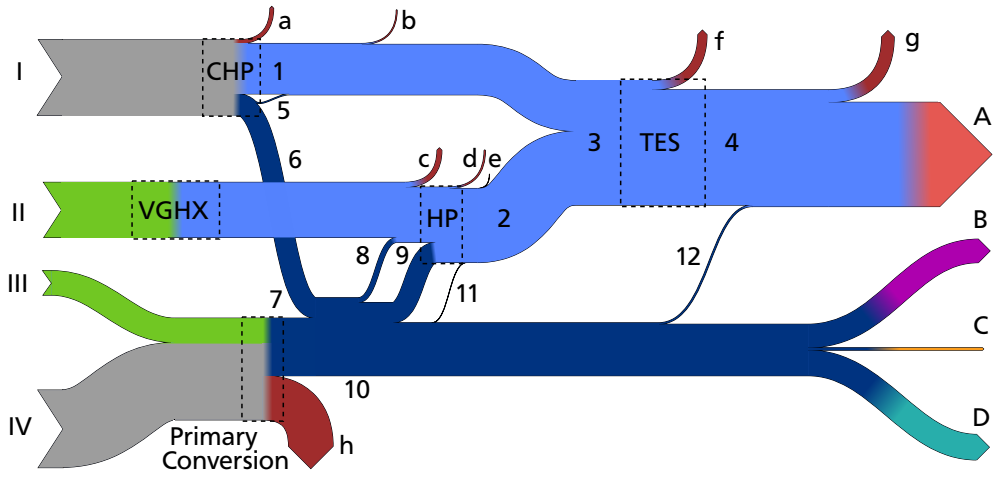

Figure 6.12: CHP+Geo scenario energy flow diagram on an annual basis.

In figure 6.13 the exergy flow diagram of the CHP+Geo scenario is shown with the corresponding data listed in table 6.10. The geothermal heat input (II) is much smaller in terms of exergy compared to its energy content shown in figure 6.12. Since the temperature of the geothermal heat is very close to the reference temperature, its exergy content is low, indicating that geothermal systems are low exergy sources. In the VGHX, exergy destruction (c) occurs during the heat transfer from the surrounding

Table 6.10: Labeling of the CHP+Geo scenario exergy flow diagram in figure 6.13.

Number	Description	MWh	Number	Description	MWh
I	Natural gas	198.4	12	District pump	3.7
II	Geothermal heat	4.2	a	CHP loss	128.3
III	Renewable energy	62.7	b	CHP to TES loss	2.3
IV	Fossil energy	199.1	c	VGHX exergy destruction	1.0
1	CHP to TES	16.2	d	Primary loop loss	12.2
2	HP to TES	24.5	e	HP loss	29.8
3	Total to TES	40.7	f	Secondary loop loss	0.1
4	TES to DHS	36.0	g	TES loss	2.8
*	Exergy change	0.01	h	TES exergy destruction	1.9
5	CHP pump	2.3	i	DHS pipe loss	9.1
6	CHP electricity	51.6	j	HTS exergy destruction	16.6
7	Grid electricity	145.6	k	Primary conversion loss	116.2
8	Primary loop pump	12.2	A	Heat demand	14.0
9	HP electricity	51.1	B	Electricity demand	59.4
10	Total electricity	197.2	C	Net electricity	6.2
11	Secondary loop pump	0.1	D	Compensated grid electricity	64.5

ground into the heat transfer fluid of the VGHX. The highest exergy loss occurs at the CHP (a) followed by the primary energy conversion loss (k). Again the TES shows the exergy change (*) as input separated from the exergy destruction (h) and the exergy loss (g). Compared to the energy flow diagram in figure 6.12, the HP has a high loss (e) during the transformation of electricity into heat.

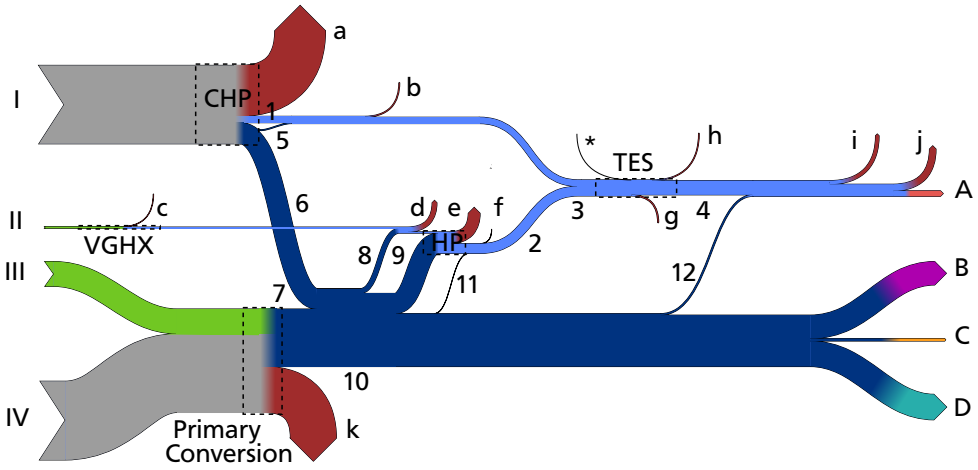

Figure 6.13: CHP+Geo scenario exergy flow diagram on an annual basis.

6.1.5 Solar scenario

In figure 6.14 the results of the Solar scenario are depicted for different TES volumes. The input of renewable energy increases from 145 MWh at a TES volume of 25 m^3 to 275 MWh at 4000 m^3. In the beginning a very steep increase takes place due to two factors. The first one is, that for smaller TES the percentage of increased volume per increased TES cubic meter is higher than for larger TES. The

second factor is the constant solar thermal collector size, which will eventually lead to a saturation of possible renewable input. The total fossil fuel input is not to be confused with the CED. The CED of the Solar scenario will be demonstrated in section 6.2. The total fossil fuel input has a different trend curve than the renewable energy input. It decreases slightly at the beginning to a minimum of 420 MWh at a TES volume of 800 m^3 and increases again afterwards due to increasing heat losses and decreasing TES temperatures. The solar fraction κ_{Solar} has an opposite trend compared to the fossil energy input. It increases for small TES volumes and has a slight maximum of 22 % also at 800 m^3 and decreases afterwards with increasing TES volume. The exergy efficiency ψ_{Solar} is rather constant at 28 % and decreases only slightly with increasing TES volume. The energy efficiency η_{Solar} decreases from 69 % at a TES volume of 25 m^3 to 55 % at 4000 m^3. It is the highest for small TES volumes, because the sum of fossil and renewable input is the smallest there. However, since one of the target figures is the minimization of fossil energy input, a TES volume of 800 m^3 is chosen for the comparison of the Solar scenario.

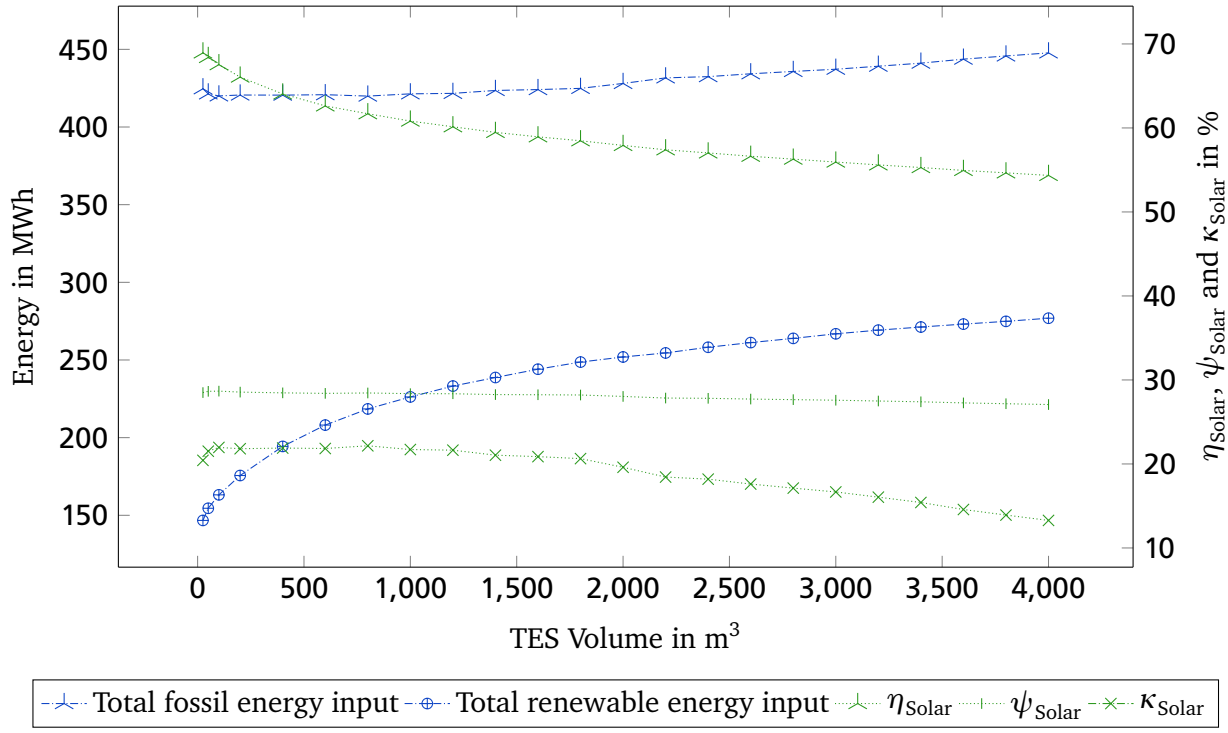

Figure 6.14: Solar scenario result overview showing the performance for different TES volumes.

In figure 6.15 the energy flow diagram of the Solar scenario is shown with the corresponding data listed in table 6.11. There are two heat segments, one supplied by the solar thermal collectors and the other by the boiler. The TES shows a large energy loss (c) due to the long seasonal storage period, which results in the boiler having the larger share of the heat supply (4). Since the transformation from solar radiation to heat is outside the system boundary, no energy losses occur in the solar thermal collectors.
In figure 6.16 the exergy flow diagram of the Solar scenario is shown with the corresponding data listed in table 6.12. Similar to geothermal heat, the exergy content of hot water (II) is low compared to its energy content. The boiler still has the highest share of the heat supply, but it also has the highest exergy loss (a), showing its low exergy efficiency. The exergy destruction of the HTS (f) is higher than the DHS pipe loss (e)m and the TES loss (d). The exergy change (*) is separated from the exergy destruction (c) and serves as an exergy input.

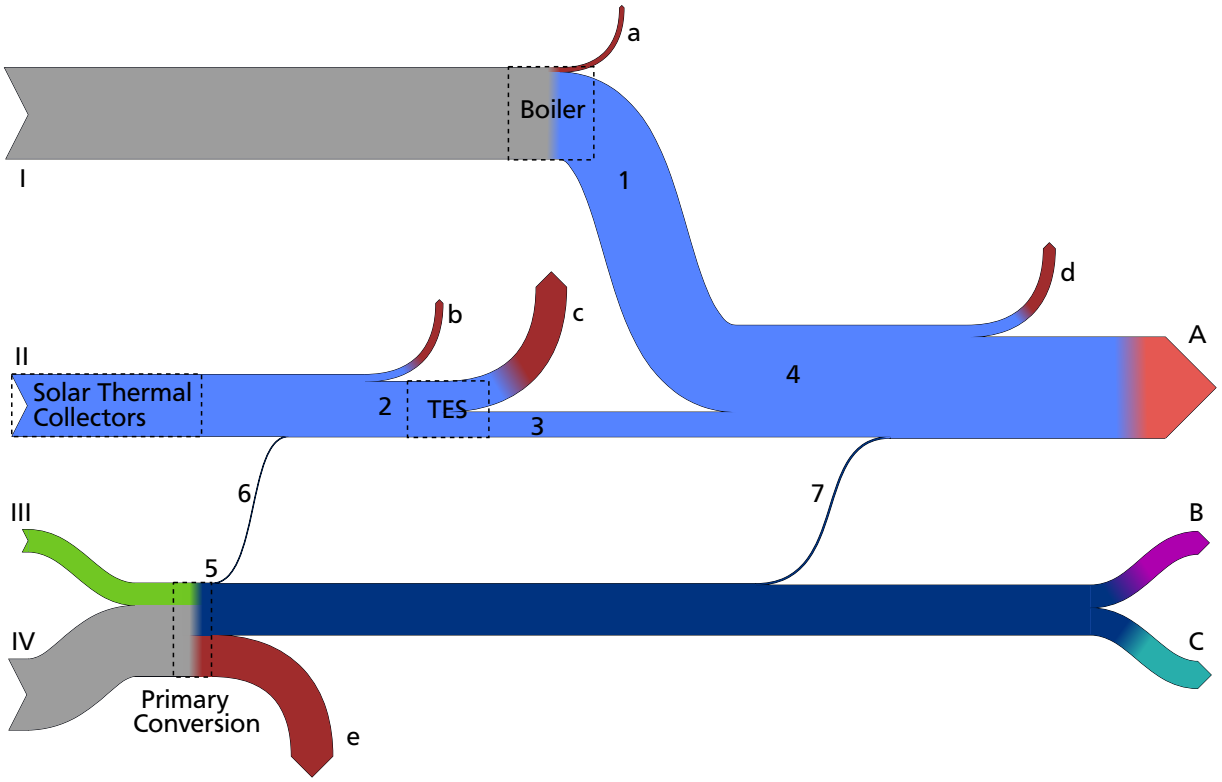

Figure 6.15: Solar scenario energy flow diagram on an annual basis.

Table 6.11: Labeling of the Solar scenario energy flow diagram in figure 6.15.

Number	Description	MWh	Number	Description	MWh
= I	Natural gas	237.6	= 7	District pump	3.7
= II	Solar heat	160.9	= a	Boiler loss	11.4
= III	Renewable energy	57.4	= b	Solar pipe loss	18.5
= IV	Fossil energy	182.3	= c	TES loss	79.4
= 1	Boiler to DHS	226.2	= d	DHS pipe loss	30.6
= 2	Solar to TES	143.8	= e	Primary conversion loss	104.5
= 3	TES to DHS	64.4	= A	Heat demand	263.7
= 4	Total to DHS	290.6	= B	Electricity demand	59.4
= 5	Grid electricity	135.2	= C	Compensated grid electricity	70.7
= 6	Solar pump	1.4			

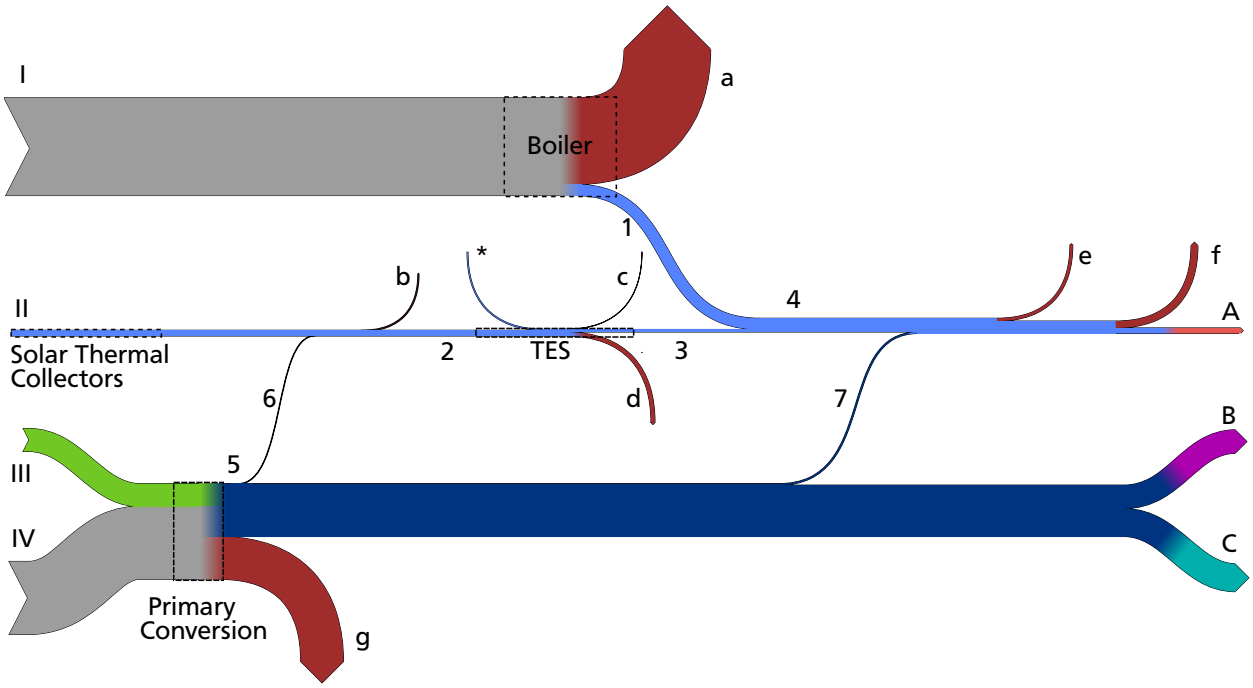

Figure 6.16: Solar scenario exergy flow diagram on an annual basis.

Table 6.12: Labeling of the Solar scenario exergy flow diagram in figure 6.16.

Number	Description	MWh	Number	Description	MWh
= I	Natural gas	247.1	= 7	District pump	3.7
= II	Solar heat	16.4	= a	Boiler loss	218.8
= III	Renewable energy	58.3	= b	Solar pipe loss	3.2
= IV	Fossil energy	184.8	= c	TES exergy destruction	0.4
= 1	Boiler to DHS	28.3	= d	TES loss	10.1
= 2	Solar to TES	14.6	= e	DHS pipe loss	7.1
= 3	TES to DHS	6.5	= f	HTS exergy destruction	17.4
= 4	Total to DHS	34.8	= g	Primary conversion loss	107.9
= *	Exergy change	2.4	= A	Heat demand	14.0
= 5	Grid electricity	135.2	= B	Electricity demand	59.4
= 6	Solar pump	1.4	= C	Compensated grid electricity	70.7

6.1.6 Power to heat scenario

In figure 6.17 the energy flow diagram of the P2H scenario is shown with the corresponding data listed in table 6.13. The energy flow diagram consists of two heat and two electricity segments. The heat is supplied by an air source HP (I) and a ground source HP (II). The electricity is drawn from the electricity grid and the PV modules (III). The air HP supplies the seasonal TES and the buffer TES (2). The seasonal TES shows a large energy loss (c), while the buffer TES energy loss (h) is rather small. The purpose of this scenario is the use of the PV electricity for heat generation. Therefore, the high energy losses are accepted to bridge the time gap between heat generation in summer, to heat use during the heating period. The highest loss occurs, again, during the primary energy conversion (j). The ground source HP only supplies the buffer TES. The control mechanism between the two HP and the two TES is introduced in section 4.4.6. The transformation from solar radiation into electricity is outside the system boundary and therefore the PV (III) does not show any energy loss. The P2H scenario also produces some net electricity (C).

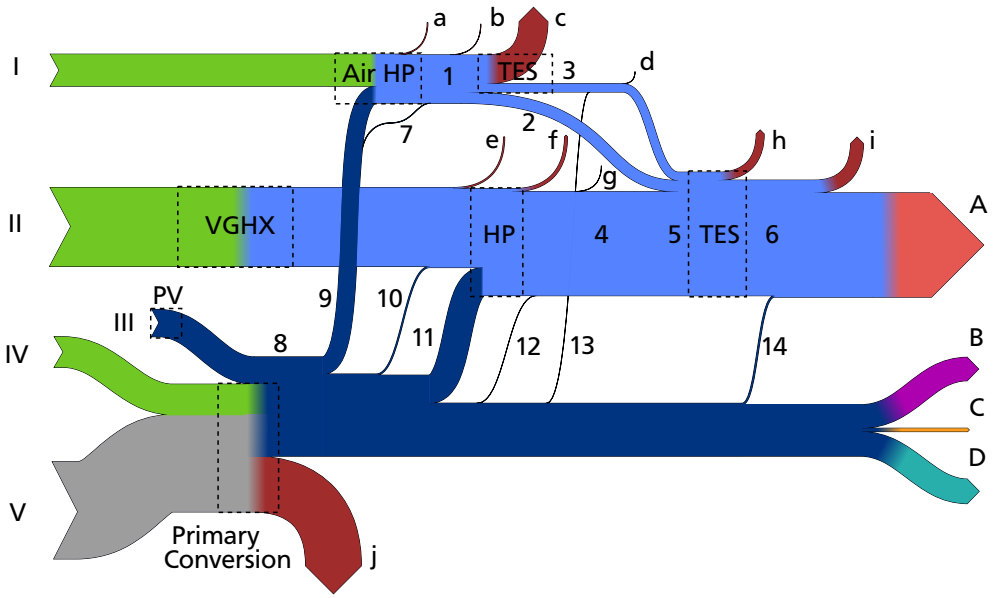

Figure 6.17: P2H scenario energy flow diagram on an annual basis.

In figure 6.18 the exergy flow diagram of the P2H scenario is shown with the corresponding data listed in table 6.14. The two HP show large exergy losses (a and h), while the two TES both have exergy change as input (+ and *). The input into the air HP is non existent as the outside air is taken as reference environment and therefore the air input does not have an exergy content. The exergy of the geothermal heat (I) is low and exergy is destroyed in the VGHX (f).

6.2 Scenario comparison

In this section the results of the individual scenarios are compared to each other.

6.2.1 Results of the comparison

The results are compared regarding energy, exergy, ecological and economical efficiency.

Table 6.13: Labeling of the P2H scenario energy flow diagram in figure 6.17.

Number	Description	MWh	Number	Description	MWh
I	Outside air heat	80.9	13	TES pump	0.06
II	Geothermal heat	199.5	14	District pump	3.7
III	PV electricity	69.0	a	Air HP loss	1.7
IV	Renewable energy	77.4	b	Air HP to TES loss	0.5
V	Fossil energy	245.6	c	Seasonal TES loss	72.5
1	Air HP to TES	121.9	d	Seasonal TES to buffer TES loss	0.06
2	Air HP to buffer TES	28.5	e	Primary loop loss	3.0
3	Seasonal TES to buffer TES	20.9	f	HP loss	7.5
4	HP to buffer TES	262.8	g	Secondary loop loss	0.3
5	Total to buffer TES	312.2	h	Buffer TES loss	20.0
6	Buffer TES to DHS	292.2	i	DHS pipe loss	32.2
7	Air/water pump	0.5	j	Primary conversion loss	140.9
8	Total electricity	251.1	A	Heat demand	263.7
9	Air HP electricity	43.2	B	Electricity demand	59.4
10	Primary loop pump	3.0	C	Net electricity	8.5
11	HP electricity	70.8	D	Compensated grid electricity	62.2
12	Secondary loop pump	0.3			

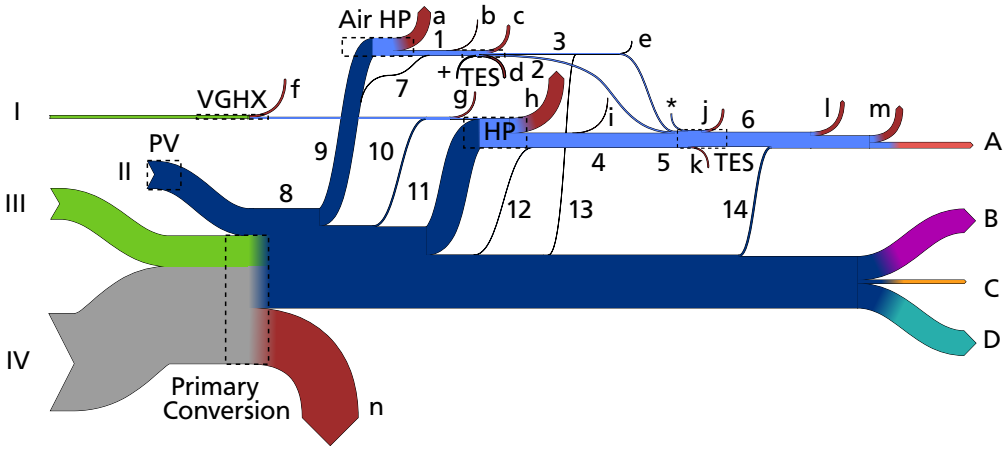

Figure 6.18: P2H scenario exergy flow diagram on an annual basis.

Table 6.14: Labeling of the P2H scenario exergy flow diagram in figure 6.18.

Number	Description	MWh	Number	Description	MWh
I	Geothermal heat	6.4	14	District pump	3.7
II	PV electricity	69.0	a	Air HP loss	31.1
III	Renewable energy	78.5	b	Air HP to TES loss	0.5
IV	Fossil energy	249.2	c	Seasonal TES exergy destruction	4.3
1	Air HP to TES	11.6	d	Seasonal TES loss	3.9
2	Air HP to buffer TES	2.7	e	Seasonal TES to buffer TES loss	0.06
3	Seasonal TES to buffer TES	2.3	f	VGHX exergy destruction	4.2
4	HP to buffer TES	35.9	g	Primary loop loss	3.0
5	Total to buffer TES	40.9	h	HP loss	37.1
6	Buffer TES to DHS	35.8	i	Secondary loop loss	0.3
+	Exergy change seasonal TES	1.6	j	Buffer TES exergy destruction	4.5
*	Exergy change buffer TES	1.9	k	Buffer TES loss	2.5
7	Air/water pump	0.5	l	DHS pipe loss	9.0
8	Total electricity	251.1	m	HTS exergy destruction	16.5
9	Air HP electricity	43.2	n	Primary conversion loss	145.6
10	Primary loop pump	3.0	A	Heat demand	14.0
11	HP electricity	70.8	B	Electricity demand	59.4
12	Secondary loop pump	0.3	C	Net electricity	8.5
13	TES pump	0.06	D	Compensated grid electricity	62.2

Energy

In figure 6.19 the energy input and output of the individual scenarios are shown. On the input side the cumulative energy demand CED is shown, subdivided into fossil energy, renewable energy, grid electricity and C&G energy. On the output side the energy is subdivided into heat demand, electricity demand, net electricity which is the excess electricity fed into the grid, and the compensated grid electricity as introduced in section 3.1.5. The energy output is kept constant at 390 MWh in order to make the different scenarios comparable. Therefore, the compensated grid electricity increases at the same rate as the net electricity decreases.

The Gas scenario has the highest fossil fuel input in form of natural gas and grid electricity. The CHP scenario has the lowest overall energy input and also the lowest grid electricity input, but the highest fossil fuel input in form of natural gas. It also produces the most net electricity with 70 MWh and sets the standard the compensated grid electricity has to meet in the other scenarios. The CHP+Geo scenario has a higher share of renewable energies and grid electricity and a lower natural gas input than the CHP scenario. The Geo scenario only has fossil fuel input in form of grid electricity, but of all scenarios the highest share of grid electricity. The Solar scenario has a lower natural gas input than the Gas and the CHP scenario. The input of C&G energy is significant, mainly because of the seasonal TES and the solar thermal collectors, as displayed in table A.7. The P2H scenario has the highest overall energy input of 710 MWh and the highest renewable energy input, but also the lowest fossil fuel input with 280 MWh. In the P2H scenario a lot of components are needed, which leads to a substantial amount of C&G energy, as listed in table A.8.

Overall, the CHP scenario has the lowest energy input, while the P2H scenario has the highest. At the

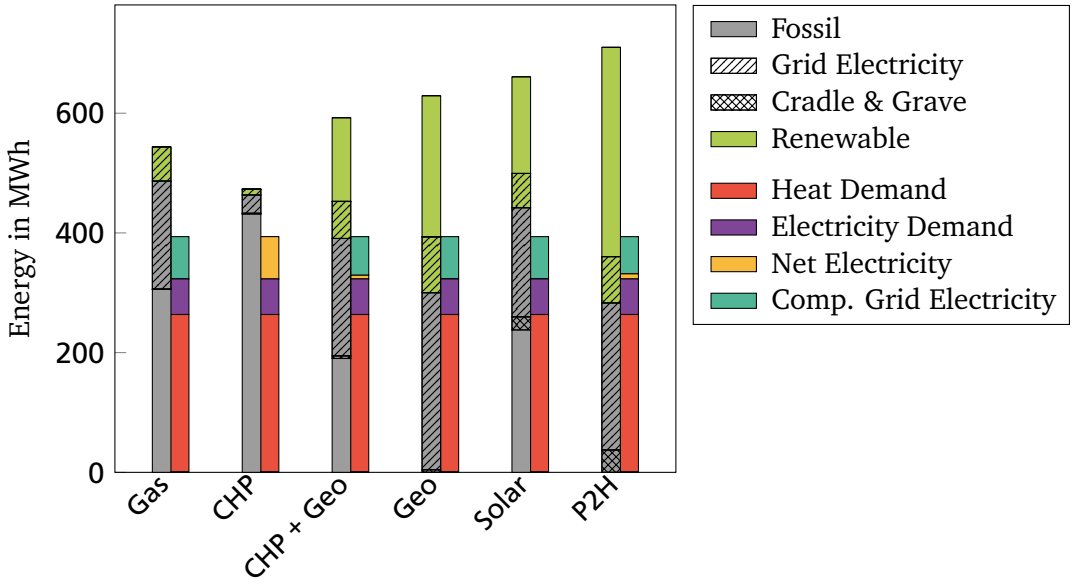

Figure 6.19: Energy input and output for the different scenarios.

same time, the P2H has the lowest fossil energy input and the Gas scenario the highest. The Geo scenario also has a low fossil energy input, but as well as the P2H a high grid electricity dependency. The C&G energy is only significant for the Solar and the P2H scenario, because of their large TES and their solar thermal collectors and PV modules, respectively. More detailed information regarding the individual C&G energies for each scenario is given in the appendix in tables A.3 till A.8.

Exergy

In figure 6.20 the exergy input and output of the individual scenarios are shown. The division is the same as in figure 6.19 with the input and output separated. However, the constant output is only at 140 MWh, because the exergy content of the heat demand is much lower than its energy content. The electricity output stays the same as in figure 6.19, because the energy content of electricity is equal to its exergy content. On the input side the fossil input almost stays the same as in figure 6.19, while the renewable input decreases because the exergy input in form of geothermal heat and solar thermal water is low. This leads to a different result regarding the input compared to figure 6.19. The Gas scenario has the highest exergy input of 550 MWh, while the Geo scenario has the lowest exergy input of 390 MWh. The P2H scenario also has a low overall exergy input. The exergy needed for cradle & grave is not known and therefore not displayed here. As seen in figure 6.19 this amount can be significant for the Solar and the P2H scenario and could lead to a higher overall exergy input.

Overall, the result is different from the energy analysis result in figure 6.19. The scenarios with combustion based heat generation systems have a higher exergy input than the two with only grid electricity input. While the Gas scenario had the second lowest overall energy input, it now has the highest overall exergy input, making it the worst choice exergy-wise.

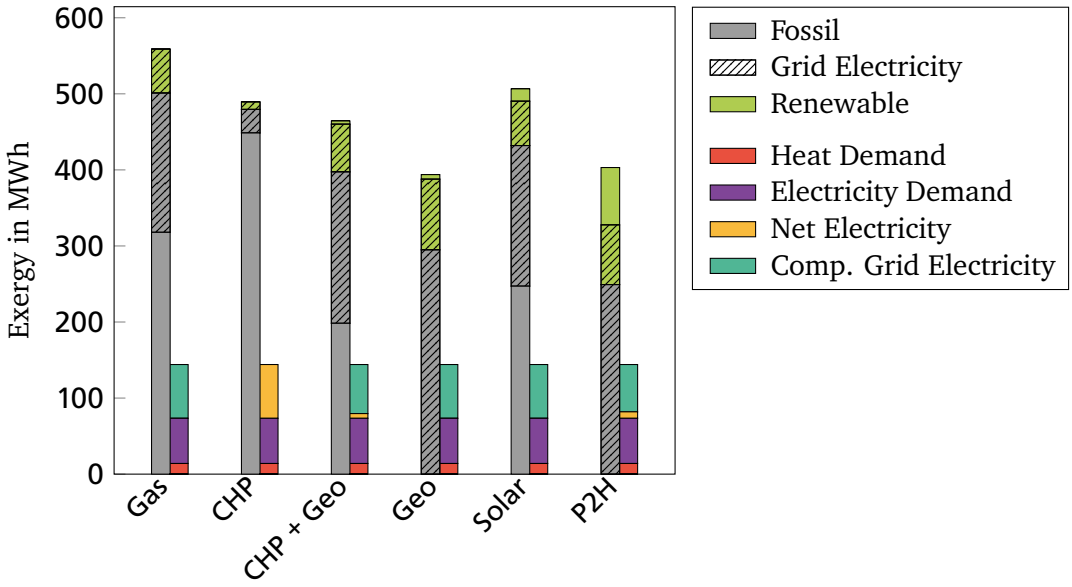

Figure 6.20: Exergy input and output for the different scenarios.

Efficiency

In figure 6.21 the energy and exergy efficiencies η and ψ of the individual scenarios are shown. The CHP scenario has the highest overall energy efficiency of 83 %, while the P2H scenario has the lowest at 55 %. Exergy-wise the Geo scenario and the P2H scenario have the highest efficiency at 36 % and the Gas scenario the lowest at 25 %. The other scenarios range in between according to their input shown in figure 6.19 and 6.20. While the energy efficiency is a measure for the quantity of energy used in a system, the exergy efficiency is a measure for the matching of the quality level between demand and supply. This is illustrated by the Gas and the CHP scenario. They are both very efficient in terms of matching the quantity level between demand and supply. However, their low exergy efficiency shows that there is still a large discrepancy between the high exergy supply in form of fossil fuels and the low exergy demand of the room heating and DHW.

Global Warming Potential

In figure 6.22 the global warming potential and the fossil energy input of the individual scenarios are shown. The GWP depends on the fossil fuel input in form of natural gas, grid electricity and cradle & grave energy. But it does not follow the trend of fossil energy input at first sight. As displayed in table 4.9 the GWP of the energy mix in the electricity grid is twice as high as the GWP of natural gas. This is illustrated in the results. Even though the fossil energy input of the CHP scenario is 160 MWh higher than the fossil energy input of the Geo scenario, their GWP is the same at 120 $t_{CO_2e}/(a)$. Only the P2H scenario has a lower GWP, but again with a significant share of cradle & grave. The Gas scenario has the highest GWP at 150 $t_{CO_2e}/(a)$ with the Solar scenario following closely. Also, here C&G only has an influence for the Solar and the P2H scenario and is negligible for the other scenarios.

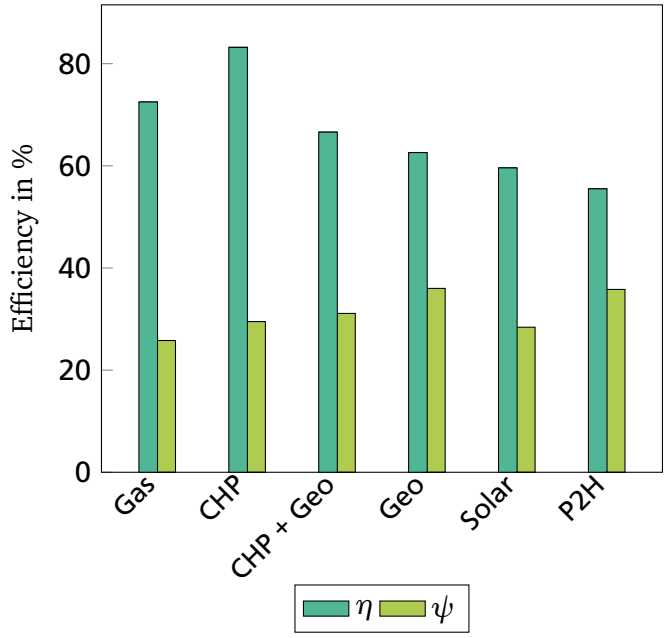

Figure 6.21: Energy efficiency η and exergy efficiency ψ for the different scenarios.

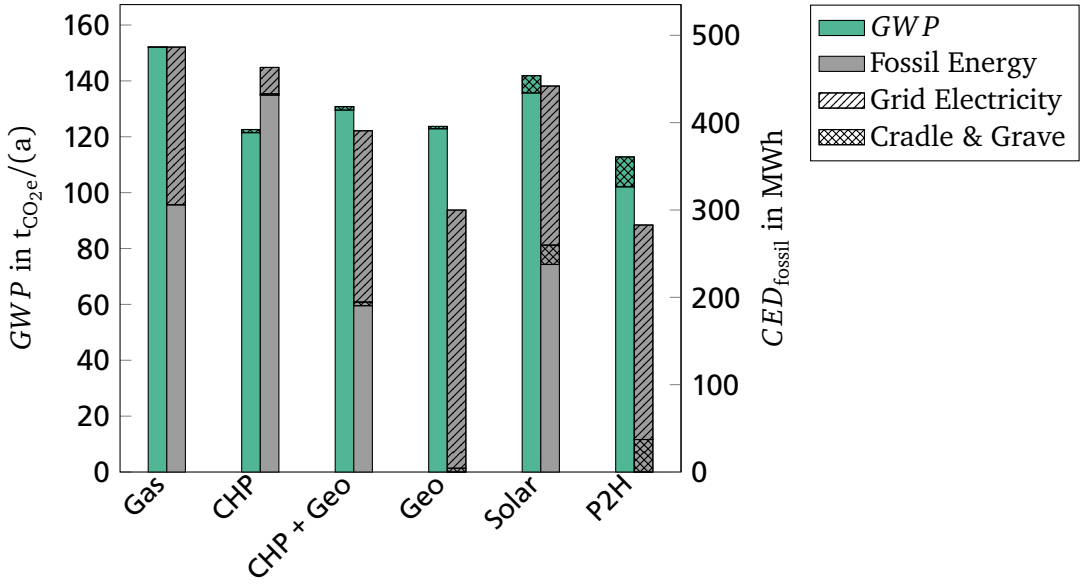

Figure 6.22: Global warming potential and fossil energy input for the different scenarios.

Annuity of total annual payments

In figure 6.23 the annuity of the individual scenarios is shown. The Gas and the CHP scenario have the same annuity for the costs at 45 000 €/(a), but the CHP scenario also has a revenue of 11 000 €/(a) making it the scenario with the lowest overall annuity. The revenue of the CHP+Geo and the P2H scenario are small compared to the costs. The demand-related costs for all scenarios are all in the same range, around 40 000 €/(a), making the capital-related costs the defining factor in the comparison. The CHP and the Gas scenario have the lowest capital-related costs, the CHP+Geo and the Geo scenario have slightly higher costs of 15 000 €/(a), while the capital-related costs of the Solar and the P2H scenario are much higher. This is due to the number of components used in the scenarios and especially the costs of the seasonal TES. More detailed information regarding the individual annuities for each scenario is given in the appendix in tables A.10 till A.15.

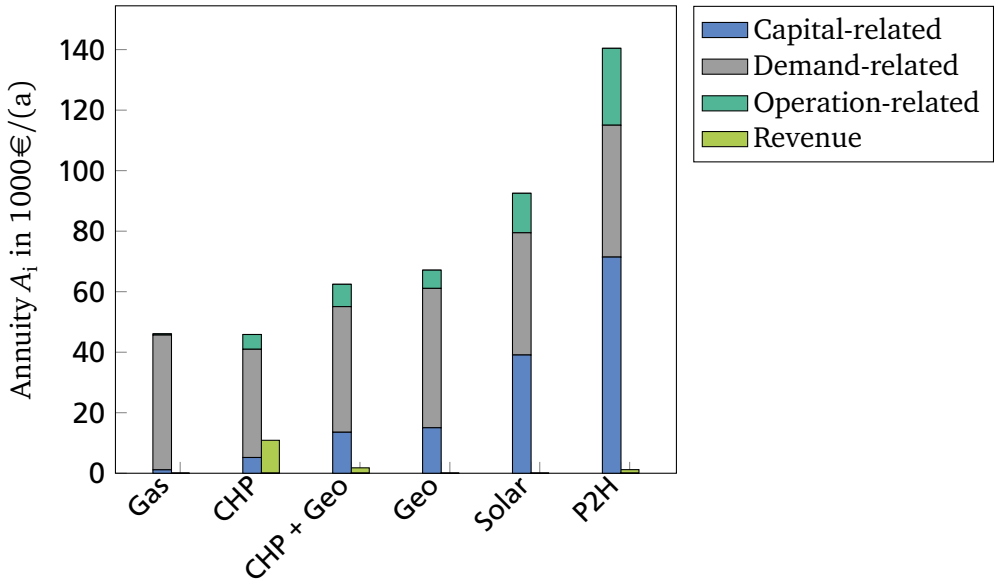

Figure 6.23: Composition of the total annuity for the different scenarios.

Overall, the CHP scenario has the lowest annuity, followed by the Gas scenario. The two CHP+Geo and the Geo scenario have comparable annuities in the range of 65 000 €/(a), while the Solar scenario has an annuity of 90 000 €/(a) and the P2H scenario of 140 000 €/(a).

Weighted multicriteria number

The results in figures 6.19 to 6.23 show opposing trends. The P2H scenario has the lowest fossil energy input and also the lowest GWP, but is the scenario with the highest annuity by far, while the Geo scenario has the lowest exergy input and the CHP scenario has the lowest annuity. This makes it difficult to draw an overall conclusion which of the six scenarios is the most favorable. For this reason, the weighted multicriteria number WMN is introduced in section 3.4.5. In figure 6.24 the WMN and the criteria numbers CN_i of the individual scenarios are illustrated. For the WMN all weighting factors are chosen as $\phi_i = 0.25$. The criteria numbers $CN_{CED_{fossil}}$, $CN_{EX_{in}}$, CN_{GWP} and CN_{A_N} show the results of the individual scenarios in relation to the best scenario for each CN. The Gas scenario has criteria numbers in the range of 0.58 to 0.75, which is rather low compared to the other scenarios. The CHP scenario has criteria numbers as low as 0.61 for $CN_{CED_{fossil}}$ and as high as 1 for CN_{A_N}. The CHP scenario criteria

number for EX_{in} is average, while the result for GWP is the second best. The CHP+Geo scenario shows better results for $CN_{\text{CED}_{\text{fossil}}}$ than the CHP scenario but the criteria number for $CN_{\text{A}_{\text{N}}}$ is below 0.6, while the other two are average. The Geo scenario shows good results for all criteria numbers, even scoring a 1 for $CN_{\text{EX}_{\text{in}}}$, except for $CN_{\text{A}_{\text{N}}}$ where it has a criteria number of only 0.5, making it twice as expensive as the CHP scenario. The Solar scenario has comparatively low criteria numbers for all categories. The P2H scenario has the highest criteria for almost three categories but is by far the most expensive one.

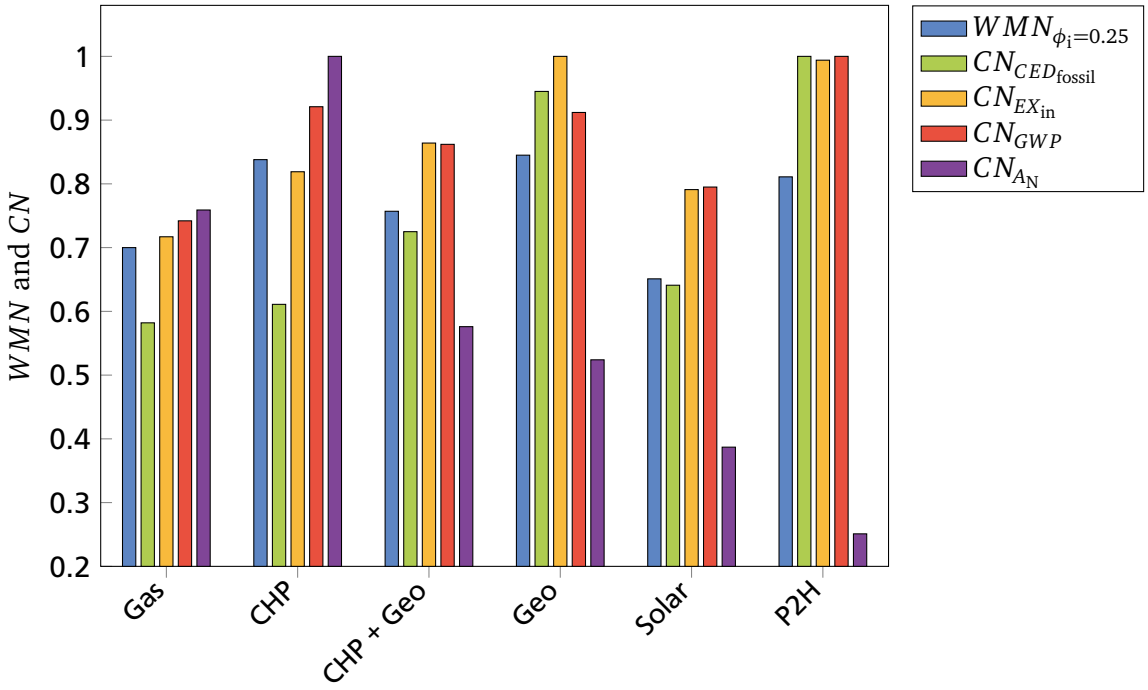

Figure 6.24: Weighted multicriteria number WMN and criteria numbers CN for the different scenarios.

Overall, the Gas scenario has a WMN of 0.7, the CHP scenario of 0.85, the CHP+Geo scenario of 0.75, the Geo scenario of 0.85, the Solar scenario of 0.65 and the P2H scenario of 0.8. This makes the CHP and the Geo scenario the most favorable choices, based on the chosen weighting factors. The CHP scenario is better annuity-wise, while the Geo scenario is better from a fossil energy input perspective. The P2H scenario also shows a good overall result even though its costs are four times the cost of the CHP scenario, because its scores in the other three categories are among the highest possible in this comparison.

7 Sensitivity analysis of the results

The results in section 6.1 and 6.2 show a dependency on the input parameters, such as TES parameters, electricity mix, costs and weighting factors. The capital-related costs are found to be the determining factor in the overall annuities in section 6.2, because even though the demand-related costs are the main costs for all but two scenarios, they are almost the same for each scenario. Some results are highly dependent on grid electricity, such as the Geo and the P2H scenario, while other scenarios like the CHP scenario have only a small share of grid electricity on the overall energy input. In the WMN the results of the four assessment categories introduced in section 3.4.5 are merged into one number with the help of equal weighting factors of $\phi_i = 0.25$.
This dependency leads to an investigation into the sensitivity of the results on the following parameters.

- Change of TES parameters
- Different composition of the electricity mix in 2030
- Changing capital costs and interest factor as well as changing operational costs and price change factor
- Changing weighting factors ϕ_i for the WMN

7.1 Influence of TES parameters

In this section the influence of different TES heat loss coefficients on the overall results is discussed using the Solar scenario as an example, followed by a scenario comparison.
In figure 7.1 the fossil energy input for three different heat loss coefficients k and three different sets of supply and return temperatures is shown for different TES volumes in the Solar scenario. The three sets of supply and return temperatures T_s/T_r are 70 °C/50 °C, 60 °C/40 °C and 50 °C/35 °C. The fossil energy input here is not to be confused with the cumulative energy demand CED, because the C&G energy is not included here.
Overall, the fossil energy input for a specific TES volume and k increases with increasing T_s. This is due to higher heat losses in the supply pipes, but also due to a smaller effective TES volume that can be used for the energy supply. The higher T_s, the higher the TES temperature has to be in order to feed into the DHS. And since the temperature in a TES is not homogeneous, but stratified, less temperature layers of the TES can actually be used to feed into the DHS with increasing T_s. A higher T_s therefore leads to a higher percentage of TES volume, which cannot be used for the heat supply of the district, thus leading to a higher fossil energy input into the backup boiler. In figure 6.1 it is shown that lowering the supply temperature leads to energy savings of 0.8 MWh/(K). In figure 7.1, the savings for lowering the supply temperature are around 1.5 MWh/(K) and higher depending on the TES volume and k. This is due to the better TES usage for lower supply temperatures.
For a given T_s the minimum of the fossil energy input shifts from higher TES volumes to smaller TES volumes with increasing k. This is true for all displayed result trends. However, for $T_s = 50$ °C and $k = 0.2\,\mathrm{W/(m^2K)}$ a minimum is reached at the end of the investigated TES volume range, and it is

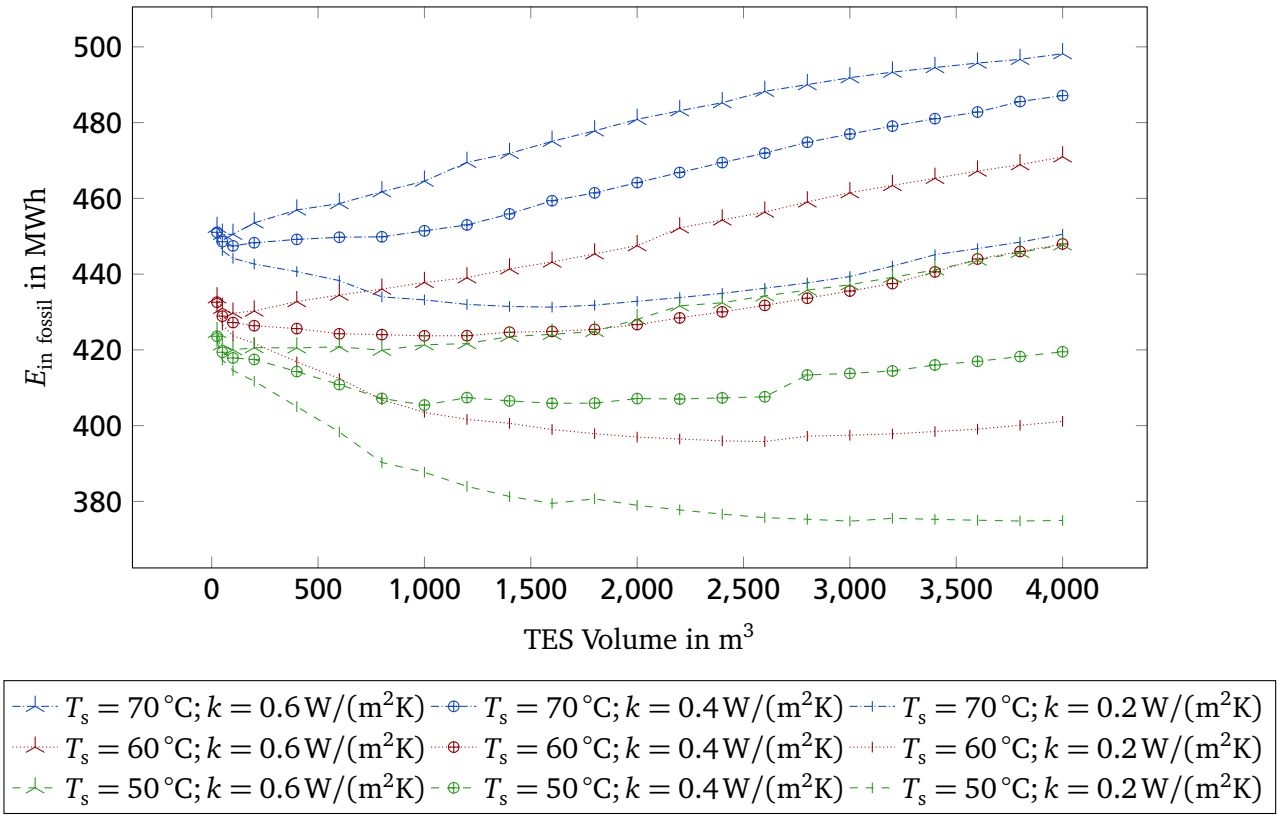

Figure 7.1: Dependency of the fossil energy input E_{fossil} on k, V and T_s for the Solar scenario.

possible that the energy input might decrease further for larger TES volumes.
The displayed results indicate that a larger TES volume does not necessarily mean a better performance in regards to fossil energy savings. Since the solar thermal collector size was kept constant in these simulations, the conclusion would rather be that a TES reacts sensitively to supply temperature and k and that it is important to design a TES in a way that its characteristics such as volume and heat loss correspond well to the given DHS temperatures and heat supply components. In order to analyze the influence of a smaller k on the performance of the scenarios, $k = 0.2\,\text{W}/(\text{m}^2\text{K})$ is chosen for the following sensitivity analysis in which the results displayed in figure 6.19 to figure 6.24 are recalculated. The TES size in each scenario is not changed, but kept at the volume specified for each individual scenario in section 4.4.

Energy

In figure 7.2 the energy input and output of the individual scenarios with $k = 0.2\,\text{W}/(\text{m}^2\text{K})$ for every TES is shown. The energy output does not change in comparison to the comparative case in figure 6.19, but the energy input of scenarios with a TES volume larger than $60\,\text{m}^3$ is smaller than in the comparative case. The Solar scenario displays the largest fossil energy reduction with 30 MWh less than in the comparative case in figure 6.19. The Gas scenario does not use a TES and the CHP scenario only uses a small TES, which is why no changes in the energy input can be observed. But not only fossil energy is saved, also the renewable energies are used more efficiently because not so much energy is lost through the TES.

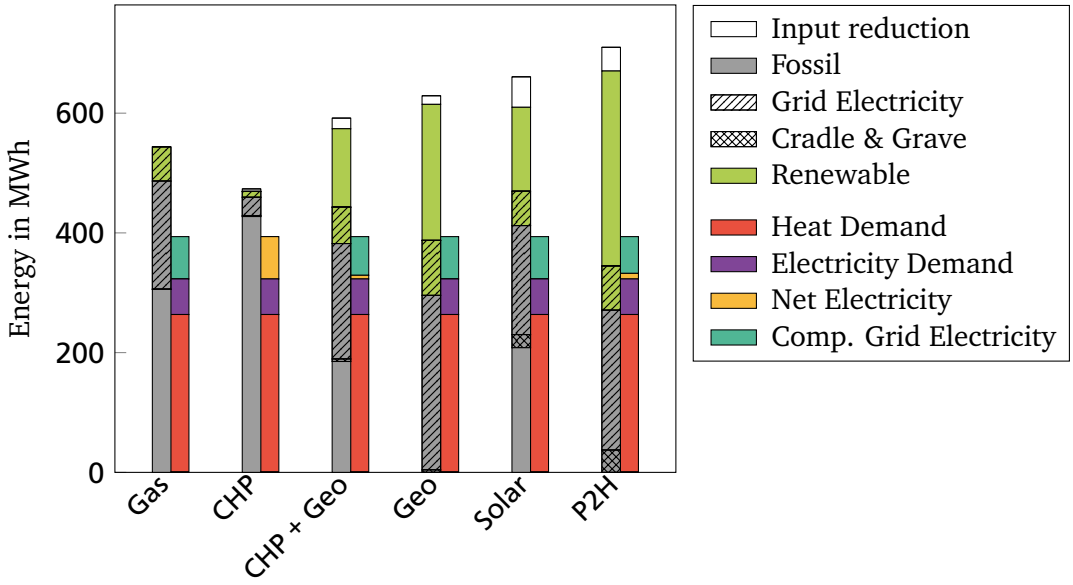

Figure 7.2: Energy input and output for the different scenarios with k = 0.2 W/(m^{2}K) and T_s/T_r = 50°C/35°C, compared to k = 0.6 W/(m^{2}K) in figure 6.19.

Exergy

In figure 7.3 the exergy input into the individual scenarios with $k = 0.2\,\mathrm{W/(m^2K)}$ is shown. Again, the largest reductions compared to figure 6.20 occur in the scenarios with the largest TES volumes. The exergy input of the Solar system is lowered beneath the input of the CHP scenario and the P2H now performs slightly better exergy-wise than the Geo scenario, making it the best scenario of the exergy comparison.

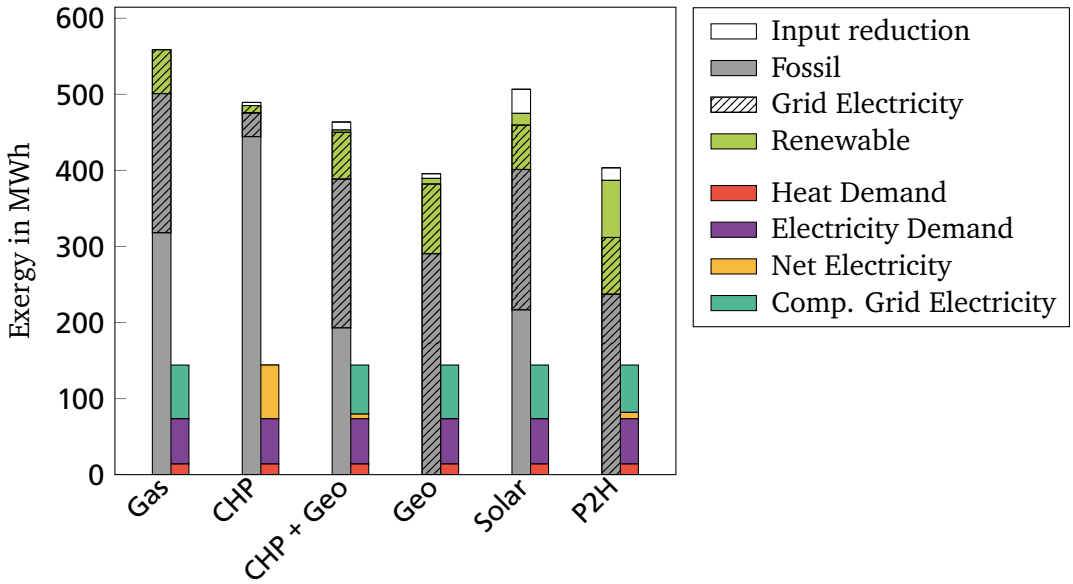

Figure 7.3: Exergy input and output for the different scenarios with k = 0.2 W/(m^{2}K) and T_s/T_r = 50°C/35°C, compared to k = 0.6 W/(m^{2}K) in figure 6.20.

Efficiency

In figure 7.4 the change of the energy and exergy efficiency $\Delta\eta$ and $\Delta\psi$ of the individual scenarios with $k = 0.2\,\mathrm{W/(m^2K)}$ is shown. Again, the biggest changes compared the comparative case displayed in figure 6.21 show the scenarios with a larger TES. The Solar scenario gains 5 percentage points in energy efficiency and 2 percentage points in exergy efficiency, while the P2H scenario gains 3 and 1.5 percentage points respectively.

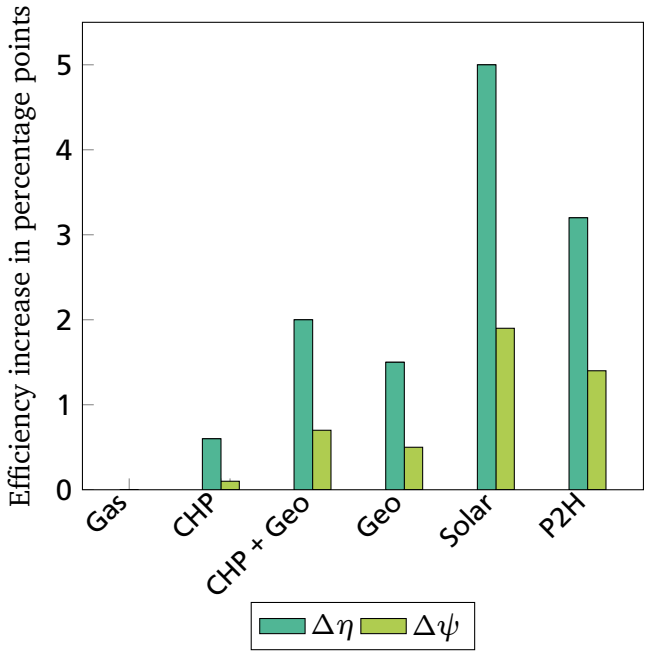

Figure 7.4: Increase of energy efficiency $\Delta\eta$ and exergy efficiency $\Delta\psi$ for the different scenarios with k = 0.2 W/(m^{2}K) and T_s/T_r = 50°C/35°C, compared to k = 0.6 W/(m^{2}K) in figure 6.21.

Global Warming Potential

In figure 7.5 the global warming potential and the fossil energy input of the individual scenarios with $k = 0.2\,\mathrm{W/(m^2K)}$ are shown. A reduction of GWP in the range of the energy efficiency increase in figure 7.4 is achieved. Again, the highest reductions are shown by the Solar and the P2H scenario with the larger TES, where the influence of a lower heat loss coefficient shows more effect.

Annuity

In figure 7.6, the annuity of the individual scenarios with $k = 0.2\,\mathrm{W/(m^2K)}$ is shown. Since the capital-related and the operation-related costs have been kept constant, the only savings possible are savings in demand-related costs. These savings are rather small, since the energy savings are mainly in natural gas, which is comparatively cheap per kWh. However, it can be assumed that a lower heat loss coefficient would result in higher capital-related costs, which would compensate the small demand-related savings. Overall, a higher insulation would probably not have any economical benefits.

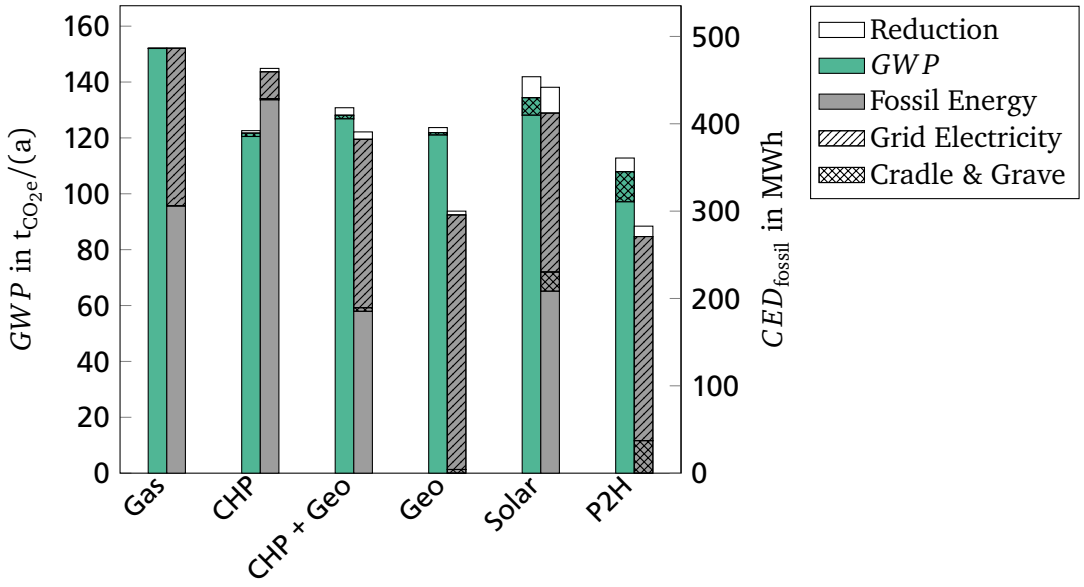

Figure 7.5: Global warming potential and fossil energy input for the different scenarios with k = 0.2 W/(m^{2}K) and T_s/T_r = 50°C/35°C, compared to k = 0.6 W/(m^{2}K) in figure 6.22.

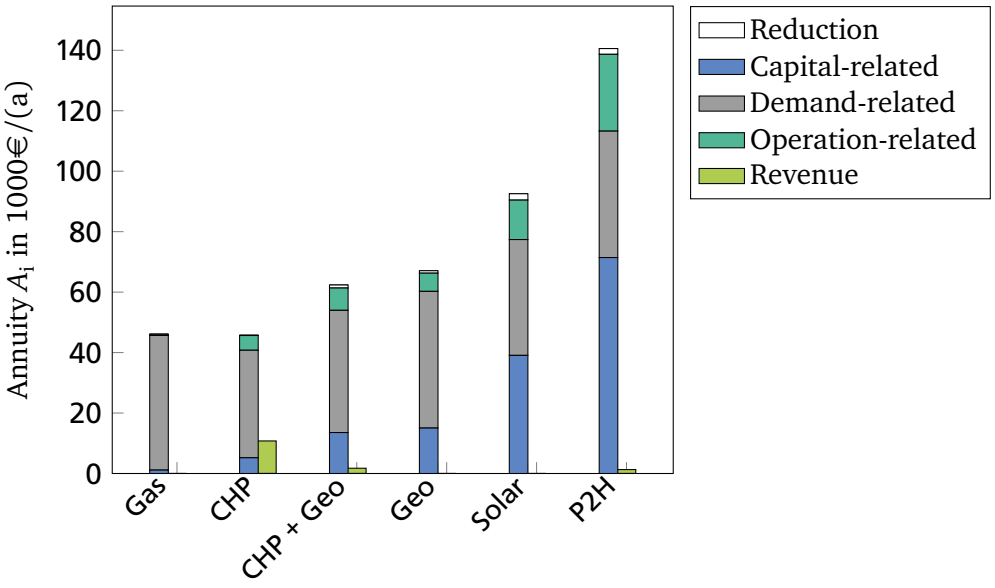

Figure 7.6: Composition of the total annuity for the different scenarios with k = 0.2 W/(m^{2}K) and T_s/T_r = 50°C/35°C, compared to k = 0.6 W/(m^{2}K) in figure 6.23.

Weighted Multicriteria Number

In figure 7.7 the weighted multicriteria number and the criteria numbers for the individual scenarios with $k = 0.2\,\mathrm{W/(m^2K)}$ are shown. Positive changes compared to figure 6.24 are marked with dots, while negative changes are marked by the white marks. The main change compared to the comparative case in figure 6.24 is that the P2H scenario now has the best performance in three out of four categories. The Solar and the P2H scenario improve slightly, both for the individual criteria numbers and the WMN, while the other scenarios lowered their performance for $CN_{\mathrm{CED_{fossil}}}$, $CN_{\mathrm{EX_{in}}}$ and CN_{GWP} in relation to the P2H scenario. This does not mean that their absolute performance is worse for $k = 0.2\,\mathrm{W/(m^2K)}$, but only that their relative performance for CN_{i} is lower than it is in the comparative case. The Geo scenario has the highest WMN of just above 0.8, closely followed by the CHP and the P2H scenario.

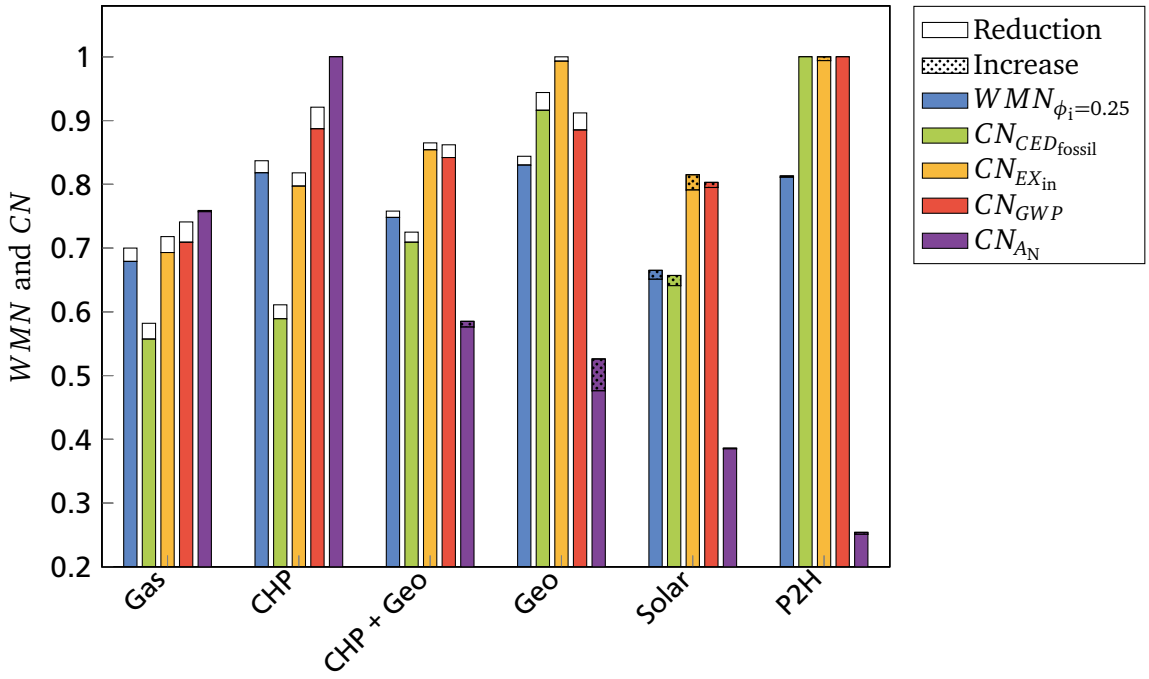

Figure 7.7: Weighted multicriteria number WMN and criteria numbers CN for the different scenarios with k = 0.2 W/(m^{2}K) and T_s/T_r = 50°C/35°C, compared to k = 0.6 W/(m^{2}K) in figure 6.24.

Summary

Overall, the influence of a lower k is higher for scenarios with larger TES, since the energy saving potential for the TES is higher there. A lower k lowers the fossil energy input, total exergy input and the global warming potential. However, since most of the saved fossil energy is natural gas, the saving potential in terms of costs is not as high. It is demonstrated in figure 7.1 that the TES design needs to be in accordance with the overall system parameters in order to use the TES effectively.

7.2 Influence of electricity mix

The composition of the energy sources in the German electricity grid is changing and will comprise of almost 50 % renewable energy in 2030 [64]. To investigate the influence of a changing electricity mix,

Table 7.1: Electricity mix in 2030.

	Hard coal	Gas	Oil	Renewable
σ_i	41.5 %	12 %	0.1 %	46.4 %
η_i	46 % [74]	54.7 % [55]	54.7 %	100 %
ψ_i	45 % based on [116]	52.6 % [55]	52.6 %	100 %

the results displayed in figure 6.19 to figure 6.24 are recalculated with the composition of the electricity mix of 2030 [64].

Electricity mix development

The values for σ_i, η_i and ψ_i are given in table 7.1. It is assumed that the exergy conversion efficiency of coal is one percentage point lower than its energy conversion efficiency based on [116]. It is further assumed that oil and gas have the same conversion efficiencies and that renewable energies have a conversion efficiency of 100% based on the chosen system boundary as discussed in section 3.1.1. With equation 3.7 and 3.8 the energy and exergy efficiency of the German electricity mix in 2030 can be calculated to $\eta_{el} = 72.1\,\%$ and $\psi_{el} = 71.4\,\%$. Since only the energy mix in the electricity grid is varied in the following sensitivity analysis, the differences to the comparative case should be bigger for scenarios with higher electricity grid dependency. A different electricity price is not part of this sensitivity analysis and therefore the annuity of the scenarios in 2030 is not shown in the following. It is assumed that the data for cradle & grave is still valid in 2030 because no data for 2030 was available. This assumption leads to conservative results because it can be assumed that with a higher share of renewable energies in the electricity mix the performance in regards to GWP and $E_{C\&G}$ would also improve.

Energy

In figure 7.8 the energy input and output for the individual scenarios with the electricity mix of 2030 are shown. The energy output is not affected by the sensitivity analysis and does not change compared to the comparative case in figure 6.19. As expected, the highest fossil energy savings of 130 MWh are achieved by the Geo scenario, which now has the lowest fossil energy input. The P2H scenario has fossil energy savings of 110 MWh. The CHP scenario now has the highest fossil fuel input, because due to its low share of grid electricity it is hardly influenced by a changing electricity mix. Changes in the scenarios are both a shift to a higher share of renewable energies in the grid electricity and a lower overall energy input through grid electricity due to the higher energy and exergy efficiency η_{el} and ψ_{el} of the German electricity grid in 2030 compared to 2012.

Exergy

In figure 7.9 the exergy input and output for the individual scenarios with the electricity mix of 2030 are shown. Again, the output side is not affected by the sensitivity analysis and does not change compared to the comparative case in figure 6.20. The changed energy mix in the electricity grid also changes the total exergy input of the scenarios, except for the CHP scenario, which is rather unchanged because of its low share of grid electricity. The Geo and the P2H scenario have the highest exergy savings with 85 MWh and 70 MWh due to their high share of grid electricity.

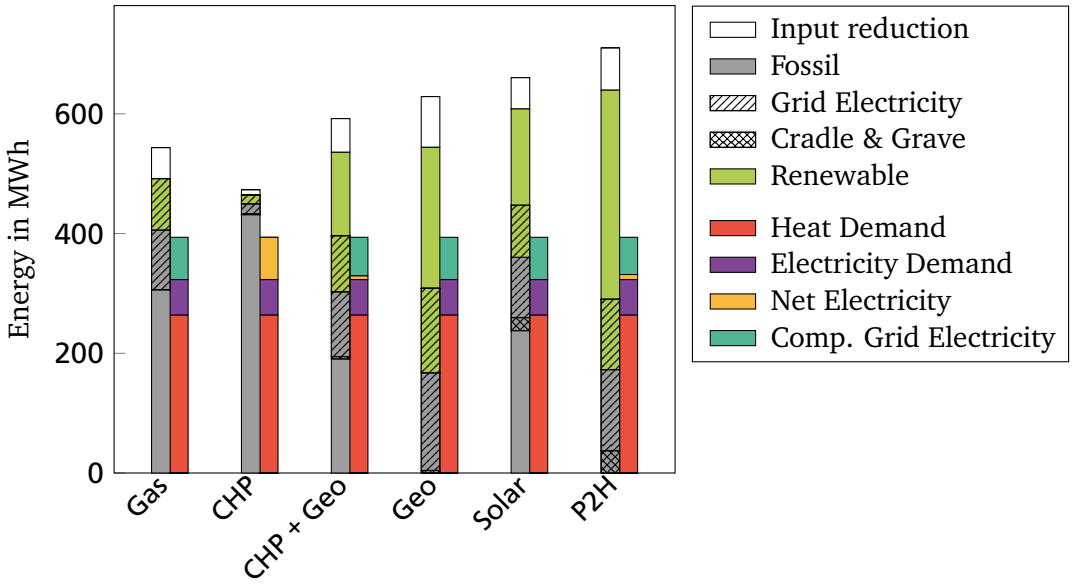

Figure 7.8: Energy input and output for the electricity mix in 2030, compared to the one in 2012 in figure 6.19.

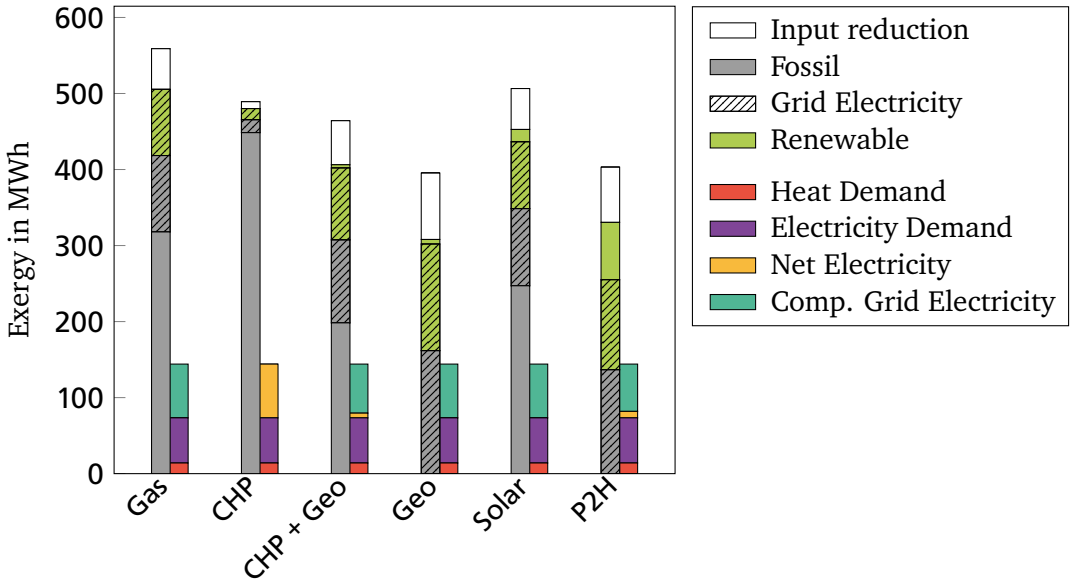

Figure 7.9: Exergy input and output for the electricity mix in 2030, compared to the one in 2012 in figure 6.20.

Efficiency

In figure 7.10 the change of the energy and exergy efficiency $\Delta\eta$ and $\Delta\psi$ for the individual scenarios with the electricity mix of 2030 are depicted. The Geo scenario has the highest efficiency gain of 10 percentage points energy- and exergy-wise. The Solar, P2H, CHP+Geo and Gas scenario also have energy efficiency improvements in the range of 5 and 7.5 percentage points. The CHP scenario has a very low efficiency increase due to its low share of grid electricity.

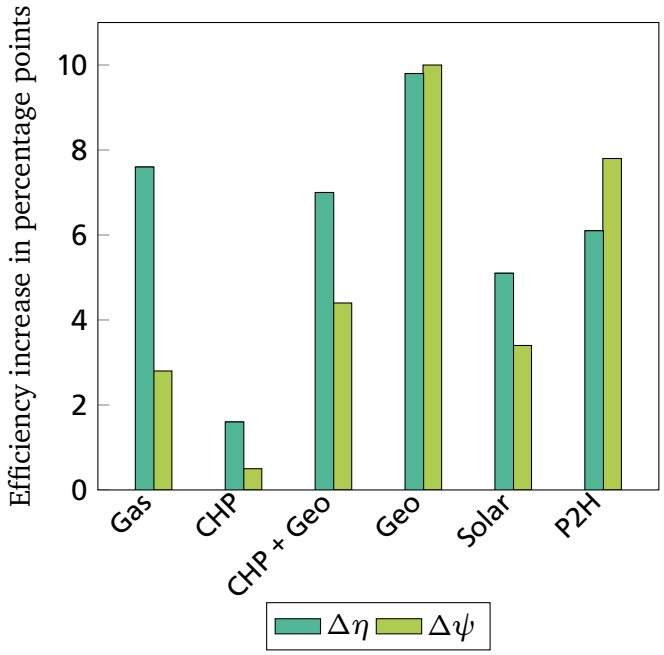

Figure 7.10: Increase of energy efficiency $\Delta\eta$ and exergy efficiency $\Delta\psi$ for the electricity mix in 2030, compared to the one in 2012 in figure 6.21.

Global Warming Potential

In figure 7.11 the global warming potential and the fossil energy input for the individual scenarios with the electricity mix of 2030 are shown. The change of the energy mix in the electricity grid has a large influence on the GWP for all scenarios except the CHP scenario. With a reduction of 130 MWh of fossil energy input the Geo scenario has a GWP reduction of 60 $t_{CO_2e}/(a)$, which is 50 % of the comparative case in figure 6.22. With the exception of the CHP scenario, all other scenarios show a GWP reduction between 35 $t_{CO_2e}/(a)$ and 50 $t_{CO_2e}/(a)$.

Weighted multicriteria number

In figure 7.12 the weighted multicriteria number and the criteria numbers for the individual scenarios with the electricity mix of 2030 are shown. Again, positive changes compared to figure 6.24 are marked with dots, while negative changes are highlighted by the white marks. Compared to figure 6.24, rather large changes are displayed. This is due to two factors. The first one being the reduction of fossil energy and total exergy input as well as the GWP reduction. Secondly, relative changes between the scenarios have a higher impact if the absolute characteristic numbers as introduced in section 3.4.5 are lowered,

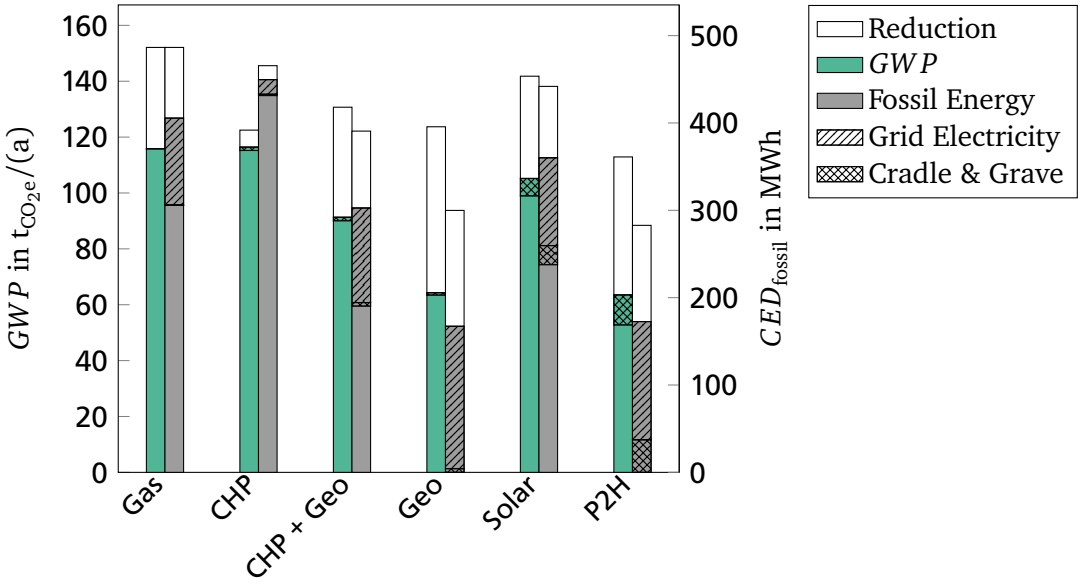

Figure 7.11: Global warming potential and fossil energy input for the electricity mix in 2030, compared to the one in 2012 in figure 6.22.

which is the case here. Except for the annuity, the criteria numbers and the WMN of the CHP scenario are significantly lower, now that the Geo scenario's performance has improved so much. The Geo scenario has improved in relation to the P2H scenario and now has the lowest fossil energy input and the lowest exergy input. The Geo scenario also has the highest WMN. While the WMN of the CHP scenario was as high as the WMN of the Geo and the P2H scenario in figure 6.24, it is now only at 0.6, while the other two are still above or around 0.8.

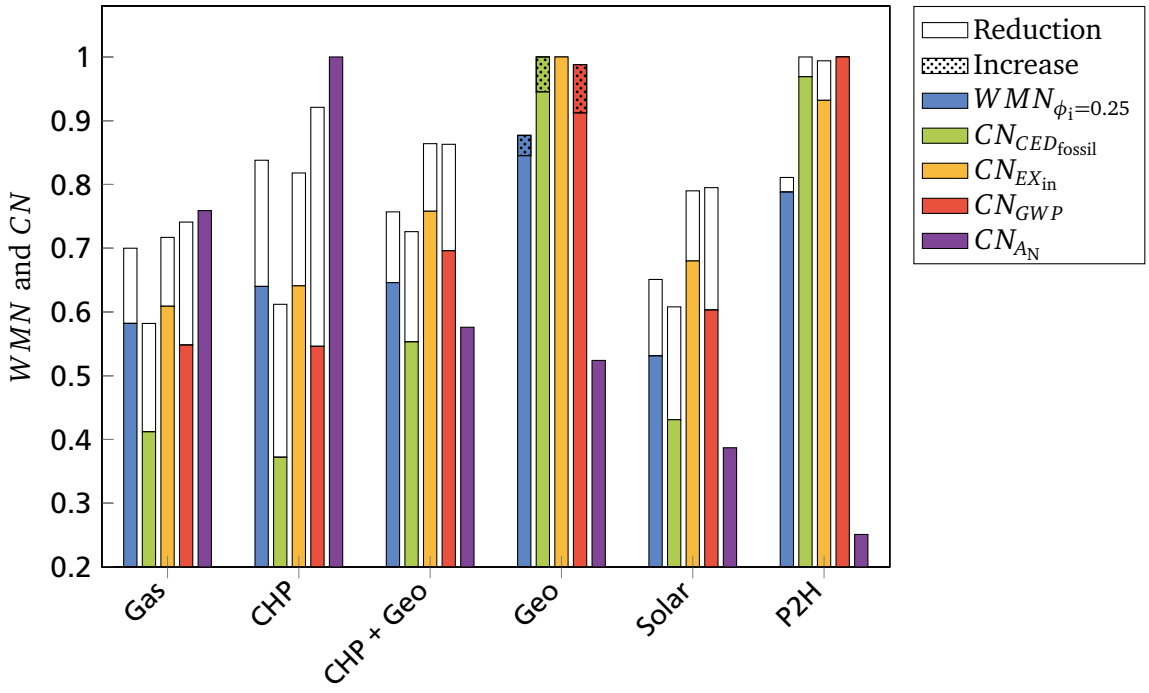

Figure 7.12: Weighted multicriteria number WMN and criteria numbers CN for the electricity mix in 2030, compared to the one in 2012 in figure 6.24.

Summary

Overall, the changing energy mix in the electricity grid is advantageous for all scenarios, although the CHP scenario is hardly influenced by it directly. But since the other scenarios improve a lot in terms of fossil energy and total exergy savings as well as GWP, the CHP performance decreases in relation to the other scenarios, which is emphasized in the WMN. The changing energy mix is therefore especially beneficial to scenarios with a high share of grid electricity, because the improvement potential the energy mix in the electricity grid has is passed on to the scenario and in return improves them. Particularly visible is the improvement in the GWP reductions of up to 50 %.

7.3 Influence of initial investment and operational costs

In the following, the sensitivity of the total annuity of the individual scenarios regarding the capital-related and demand-related costs is investigated. This is done by changing one parameter at a time in two different steps. The first step is to vary the initial investment costs A_0 and the natural gas and electricity price $A_{1,\text{gas}}$ and $A_{1,\text{el}}$ in the first year, as displayed in figure 7.13. In a second step, the initial investment and the prices for natural gas and electricity are kept constant and the interest factor ϵ and the price change factors for natural gas and electricity $r_{\text{D,gas}}$ and $r_{\text{D,el}}$ are varied as displayed in figure 7.14.

Initial investment, natural gas and electricity price

The natural gas and electricity price $A_{1,\text{gas}}$ and $A_{1,\text{el}}$ in the first year and the initial investment costs A_0 are varied between 0 % and 200 % in figure 7.13a to 7.13c. Since the Geo and the P2H scenario are independent from natural gas, their annuity does not change in figure 7.13a, while the annuity of the other scenarios increases with the price of natural gas. The slope of the increase shows the dependency on gas. The steeper the increase of the annuity of a scenario, the more natural gas is needed in that scenario. The annuity of the CHP+Geo would be higher than the annuity of the Geo scenario for a 60 % higher gas price than chosen in the current work. In figure 7.13b, the Geo and the P2H scenario show the greatest changes with changing electricity prices, while the CHP scenario also shows a slight increase with increasing electricity prices. The Geo scenario would have a lower annuity than the CHP+Geo scenario, if the electricity price would drop below 60 % of the current price. As displayed in figure 6.23, the Gas scenario has very little initial investments, which is why its annuity hardly changes in figure 7.13c. Also, the dependency of the annuity of the CHP+Geo and the Geo scenario on the initial investment is small compared to the P2H and the Solar scenario. The P2H and the Solar scenario react very sensitively to changes in the initial investment, because the initial investment is their biggest share in the annuity, as shown in figure 6.23.

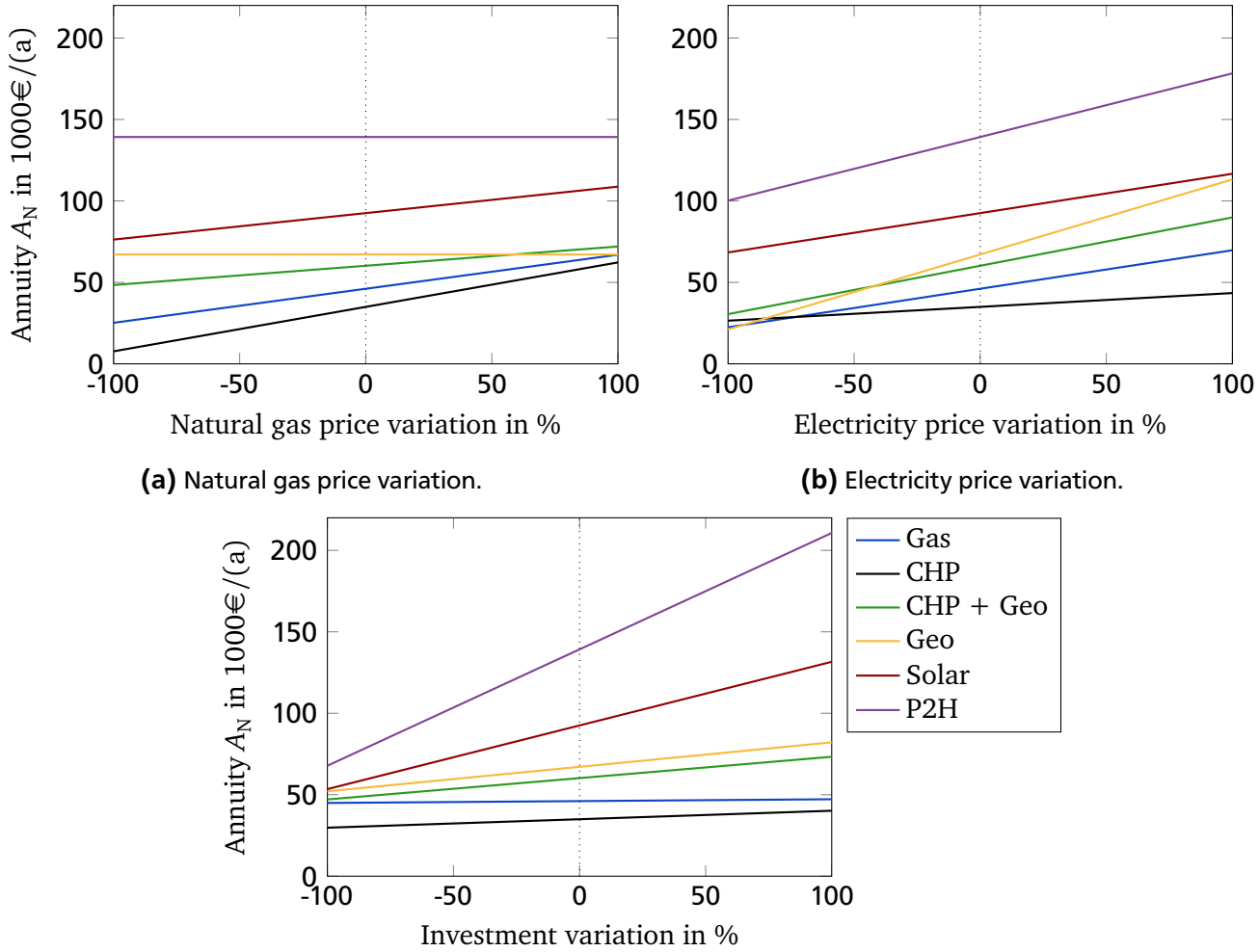

(a) Natural gas price variation.

(b) Electricity price variation.

(c) Initial investment variation.

Figure 7.13: Natural gas and electricity price and initial investment variation of ±100 %. Dotted lines correspond to the reference case.

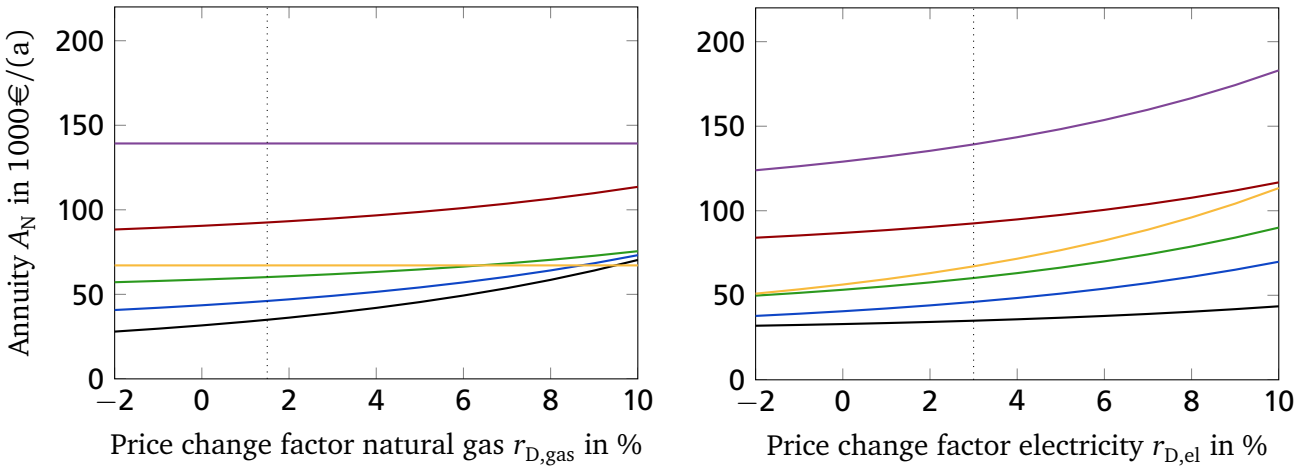

(a) Price change factor natural gas.

(b) Price change factor electricity.

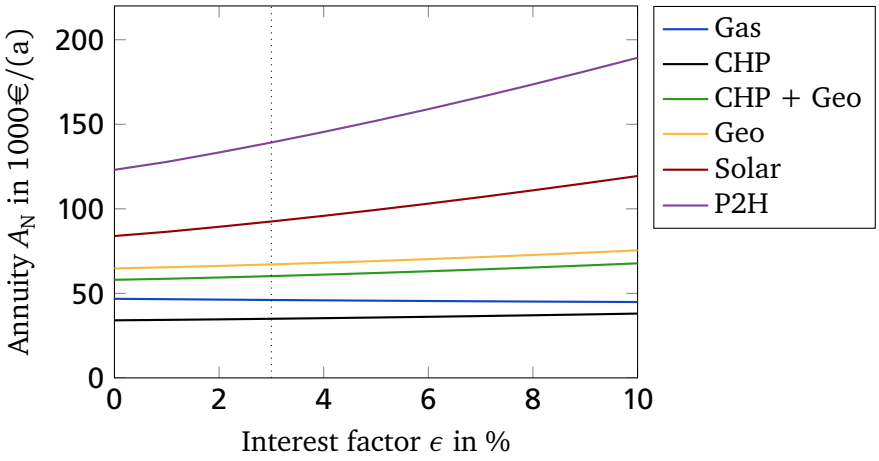

(c) Interest factor.

Figure 7.14: Variation of the price change factor for natural gas and electricity and interest factor. Dotted lines correspond to the reference case.

Interest factor and price change factor

The natural gas and electricity price change factors $r_{D,gas}$ and $r_{D,el}$ and the interest factor ϵ are varied between $-2\,\%$ and $10\,\%$ and between $0\,\%$ and $10\,\%$, respectively, in figure 7.14a to 7.14c. The Geo and the P2H scenario are independent from natural gas and stay constant for a changing natural gas price change factor in figure 7.14a. The annuity of the other scenarios is increased with increasing natural gas price change factor and the annuity of the CHP+Geo scenario becomes higher than the Geo scenario for $r_{D,gas} > 6\,\%$. For an increasing natural gas price change factor the annuities of the Gas, CHP and CHP+Geo scenario approach each other and almost have the same value at $r_{D,gas} = 10\,\%$. The Geo and the P2H scenario are very sensitive to a changing price change factor for electricity as shown in figure 7.14b, but the order of all scenarios regarding their annuity does not change in the investigated range. In figure 7.14c, only the P2H and the Solar scenario show an impact caused by a changing interest factor, because of their high initial investment, while the other scenarios stay rather constant.

Summary

Overall, the investigated parameter variations have an impact on the individual scenarios, which is shown especially for the Solar and the P2H scenario in regards to initial investment change and interest factor change. The same can be said for the Geo and the P2H scenario in regards to a changing electricity price and electricity price change factor. But in general the ranking in terms of total annuity stays the same as in figure 6.23 with the CHP always having the lowest annuity and the P2H having the highest. Only the ranking of the CHP+Geo and the Geo scenario can be interchanged for varying natural gas and electricity prices or a different natural gas price change factor.

7.4 Influence of weighting factors

The weighting factor for the WMN is chosen to be $\phi = 0.25$ for all four assessment categories. In order to show the influence of the chosen weighting factor on the WMN, a sensitivity analysis is conducted regarding the weighting factor in the following. Four different calculations are carried out. For each assessment category, the associated weighting factor is set to 0.4 while the others are set to 0.2 so that the sum of all weighting factors is still 1.
In figure 7.15 the results for $\phi_{\mathrm{CED_{fossil}}} = 0.4$, $\phi_{\mathrm{EX_{in}}} = 0.4$, $\phi_{\mathrm{GWP}} = 0.4$, $\phi_{\mathrm{A_N}} = 0.4$ and as comparative case $\phi_{\mathrm{i}} = 0.25$ are displayed for the individual scenarios. The WMN for the Gas scenario do not change significantly for different weighting factors. They always stay around 0.7. For the CHP scenario the WMN with the weight on costs increases, while it decreases when the weight is on the fossil energy input. The WMN of the CHP+Geo scenario increases slightly with the weight on exergy input and GWP, while it decreases for the weight on the costs. The WMN of the Geo scenario increases slightly with the weight either on fossil energy input, total exergy input or GWP, while it is significantly lowered when the weight is on the costs. The same can be said of the Solar scenario, except that the WMN with weight on fossil energy input is slightly lowered and that the WMN of the Solar scenario in general are on a much lower level than that of the Geo scenario. For the P2H scenario, the WMN with the weight either on fossil energy input, total exergy input or GWP is increased, while it is lowered by 0.2 when the weight is on the costs.

Summary

Overall, the impact of a changing weighting factor in the range considered in this study shows no high impact as far as fossil energy input, exergy input and GWP are concerned. The CHP, the Geo and the P2H scenario still score higher than the other scenarios. But with the weight on costs, the results change due to the high relative differences between the individual scenarios in terms of the annuity criteria number $CN_{\mathrm{A_N}}$ as shown in figure 6.24. The WMN is significantly lowered for the P2H, the Solar and the Geo scenario. The reason for this is that the relative differences in the absolute results for fossil energy input, exergy input and GWP are rather small compared to the relative differences in annuity. Therefore, when the weighting is more on the costs, the relative influence is bigger especially for the Geo, Solar and P2H scenario.
Overall, the Geo scenario shows the second best performance with the weight on the costs and shows the best performance for all other weighting factors.

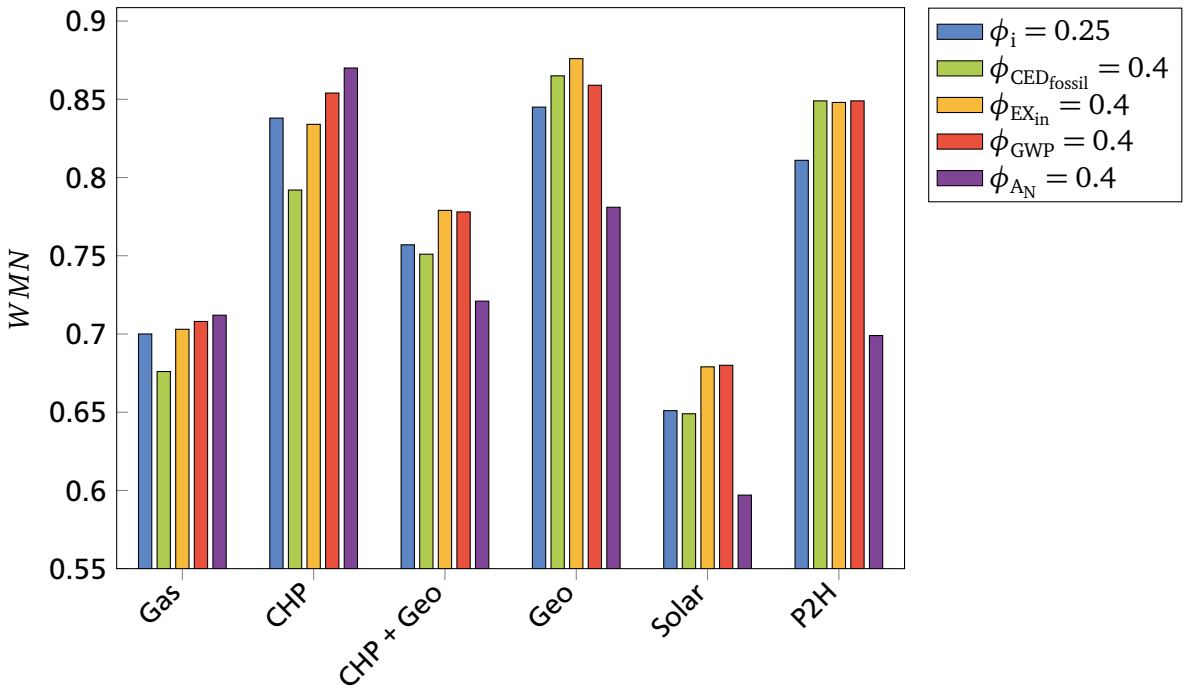

Figure 7.15: Weighted multicriteria number WMN for the different scenarios with different weighting factors.

8 Discussion and Conclusion

The developed simulation model is well suited to compare different heat supply scenarios with regard to their energy and exergy use. For the modeled system real demand data for 11 buildings in the area of Mannheim, Germany is used. But, in reality, the buildings are not connected with each other via a DHS. The modeled DHS in terms of pipe length is chosen arbitrarily. Since the individual buildings are not modeled, the heat distribution systems within the buildings are also not modeled. However, all assumptions and simplifications regarding the buildings and the DHS system are the same for each scenario, therefore eliminating a potential error in the comparison of the different scenarios with each other.
As renewable energies in this work, geothermal heat, solar heat, PV electricity, outside air heat and renewable energies in the German electricity grid are considered. Not taken into account is the possibility to substitute natural gas with biogas. If biogas was used for the combustion based processes, the results would change, because the GWP and the fossil energy input would be different for all scenarios except the Geo and the P2H scenario.
Specific real demand for 11 buildings is taken as the demand profile in the model. This begs the question of whether the results are only valid for this specific setting or whether the results are generally valid. In [8] the presented model is used to study the general validity. Several different demand profiles and sets of weather data are used. It is found that as long as the supply side stays the same, the actual demand profile does not have a big influence on the results. In the scenario comparison, the order of the different results in terms of energy and exergy use and efficiency does not vary. This is taken as an indicator that the results presented in this work are transferable to other systems as well.
The ecological analysis is done after the optimization of the different scenarios based on the energy and exergy analysis. Thist means that the results of the ecological analysis in this work do not lead to an optimization of the scenarios. There might be different scenarios and system configurations which have a better result in terms of GWP and CED. Data for the amount of exergy needed for producing and disposing of the system components was not available and therefore no cumulative exergy demand is calculated. The results of the ecological analysis are only comparative results between the individual scenarios, because components used in every scenario are not taken into account such as district pumps and the pipes. However, as shown in chapter 6, the influence of cradle & grave is negligible for most scenarios and only shows an influence for the Solar and the P2H scenario due to their seasonal TES and solar thermal collectors and PV modules.
Like the ecological analysis, the economical analysis is conducted after the optimization based on energy and exergy analysis. An economical optimization is not the aim of this work. The different scenarios are economically assessed, and common market components are used with the actual market price as input into the calculation. There might be other system configurations which are more advantageous in terms of economical efficiency. The TES for example is modeled as a cylindrical steel tank because of its good thermodynamic properties. However, cylindrical steel tanks are rather expensive compared to other concepts such as pit storage.
The developed method, in chapter 5, can be used to separate between the exergy change due to a varying reference temperature and the exergy destruction due to destratification. As written in section 4.5, CARNOT is well suited for the simulation of heating systems and for the integration of individual components into larger systems. It is not designed to study individual physical effects. The developed method

is only considered as a first step into further research regarding the method development and describing the phenomena of exergy change due to varying reference environment for a TES. Even though the presented method is not the exact solution, it is an approach that is still more accurate than not distinguishing between exergy change and exergy destruction at all.
The P2H system should be further optimized in terms of economic efficiency. Even though it shows good results for energy, exergy and ecological efficiency, its high investment costs make it unlikely to be used in its current design. The CHP scenario has the best result in terms of costs, but has a high fossil energy input as long has the CHP plant does not run on biogas. Despite the twice as high costs compared to the CHP scenario, the Geo scenario is considered to be the best alternative to the base case of a gas boiler DHS as it is introduced in section 2.3. The Geo scenario shows good overall results and with a changing composition of the electricity mix in the future its performance will improve even further.
In general, the combined and weighted results of this work show that geothermal systems can provide a good alternative to fossil fuel based heating systems for a small residential area with district heating. They combine a high heat generation efficiency with the possibility of using excess renewable electricity. They provide the option to lower the overall energy use of the building sector and to reduce CO_2 emissions. Especially with a changing electricity mix in the electricity grid towards a higher share of renewable energies the geothermal systems become even more favorable. However, the use of geothermal heat is dependent on local geological compositions and has to be assessed for each individual case. If geothermal heating is more widely used, the costs of such systems can be expected to decrease. The aforementioned remarks lead to the overall conclusion that more geothermal heating systems should be used in the building sector, as long as the geological conditions allow for it.

9 Summary and Outlook

In this chapter the presented work is summarized and an outlook is given for future tasks.

Summary

To study different heat generation technologies and the integration of a thermal energy storage (TES), six different heat supply scenarios are developed and simulated for a building cluster consisting of 11 buildings connected via a DHS. As input parameters real demand data for the room heating and DHW demand is used. To match the demand data, weather data for the same year and location is taken as input for the solar radiation calculation as well as for the reference temperature. The calculations of the individual components are based on specific data from the manufacturers of the components.
The different scenarios are: a gas boiler system as reference case (Gas scenario), a combined heat and power (CHP) plant with a gas boiler as backup (CHP scenario), a geothermal HP (Geo scenario), a geothermal heat pump (HP) combined with a CHP plant (CHP+Geo scenario), solar thermal collectors with a gas boiler as backup (Solar scenario) and a scenario consisting of a combination of an air HP and a geothermal HP (P2H scenario).
These six scenarios are analyzed and optimized using energy and exergy analysis. The results are then assessed regarding their ecological and economical efficiency and the individual scenarios are compared to each other.
It is found that the P2H scenario has the lowest fossil energy input with 283 MWh/(a) and the lowest global warming potential with 113 t_{CO_2e}/(a), but the highest annuity with 140 000 €/a. The CHP scenario has the lowest annuity with 35 000 €/a, but the second highest fossil energy input with 460 MWh/(a). The Geo scenario has the lowest total exergy input with 400 MWh/(a) and has the best overall performance.
For the individual scenarios it is found that the combustion based heat supply systems have the highest exergy losses and that the system pumps have a rather small share in the overall energy flow. Seasonal TES installed in the Solar and the P2H scenario show high heat losses. In a sensitivity analysis the influence of changing a TES heat loss coefficient is investigated and the importance of sound knowledge of the overall system parameters to choose an appropriate TES size is demonstrated. Regarding the change of the composition of the electricity mix in the German electricity grid it is found that both fossil energy input and global warming potential decrease and that the scenarios with a higher share of grid electricity have the highest improvement potential.
The phenomena of TES exergy change due to a changing reference environment is introduced and discussed. As a result a method is developed to describe the exergy change and to separate it from the exergy destruction due to destratification and the exergy loss due to heat loss. The exergy change is visualized in the exergy flow diagrams of the individual results.
Overall, the usefulness of exergy analysis in matching the quality level of the supply to the quality level of the demand could be demonstrated. Even though the developed model and evaluation methods were applied to several specific scenarios only within this work, they are applicable in a very general manner and can be applied to all kind of other scenarios beyond the Mannheim DHS example.

Outlook

In future works, the comparison of different heat supply systems should be extended to include more scenarios such as a combination of solar thermal collectors and a ground source HP. Further, a comparison of an air HP and a ground sourced HP could give insight into the optimal control strategy of both in order to use renewable energies effectively. Another possible scenario would be to use a vertical ground source heat exchanger and decentralized HP in every building and to omit a TES and instead use the DHS as buffer TES.
The possibility and effect of a DHS shutdown during the summer months should be investigated to clarify if energy savings are possible. In this work, the scenarios are optimized towards energy and exergy use. Future works should include an optimization towards ecological and economical efficiency during the design process of the scenarios.
The use of biogas should be investigated to study the improvement potential of the combustion based scenarios. As for the Solar and the P2H scenario, the use of PVT collectors could enhance the efficiency of both scenarios by producing electricity and heat at the same time and thus reducing the input from other energy sources.
The developed method to describe the exergy change of a TES due to a changing reference environment is considered to be only a first step towards a comprehensive method to describe this phenomenon. More research should be done to further develop the method and to describe the exergy change of a TES in further detail. In general, more exergy analyses of the residential sector should be conducted to make the concept of exergy, the matching of the quality level of demand and supply, more known to the public and decision makers.

Bibliography

[1] G. Abts. *Kunststoff-Wissen für Einsteiger*. Carl Hanser Verlag, München, 3 edition, 2016. ISBN 9783446439252.

[2] Agentur für Erneuerbare Energien. Strommix in Deutschland 2012, Retrieved January 2, 2014. URL http.//www.unendlich-viel-energie.de/mediathek/grafiken?cont=217.

[3] Anondi GmbH. PV Anschaffungskosten, 2017, Retrieved April 24, 2017. URL http://www.solaranlage-ratgeber.de/photovoltaik/photovoltaik-wirtschaftlichkeit/photovoltaik-anschaffungskosten.

[4] V. Badescu. Model of a solar-assisted heat-pump system for space heating integrating a thermal energy storage unit. *Energy and Buildings*, 34(7):715–726, 2002. ISSN 03787788. doi: 10.1016/S0378-7788(01)00139-6.

[5] V. Badescu. Model of a space heating system integrating a heat pump, photothermal collectors and solar cells. *Renewable Energy*, 27(4):489–505, 2002. ISSN 09601481. doi: 10.1016/S0960-1481(01)00191-4.

[6] V. Badescu. First and second law analysis of a solar assisted heat pump based heating system. *Energy Conversion and Management*, 43(18):2539–2552, 2002. ISSN 0196-8904. doi: 10.1016/S0196-8904(01)00192-3.

[7] V. Badescu. Model of a thermal energy storage device integrated into a solar assisted heat pump system for space heating. *Energy Conversion and Management*, 44(10):1589–1604, 2003. ISSN 0196-8904. doi: 10.1016/S0196-8904(02)00184-X.

[8] Balzer M. Simulation verschiedener Gebäudegruppen in CARNOT. *Master thesis, TU Darmstadt, Germany*, 2016.

[9] S. Bargel. *Entwicklung eines exergiebasierten Analysemodells zum umfassenden Technologievergleich von Wärmeversorgungssystemen unter Berücksichtigung des Einflusses einer veränderlichen Außentemperatur*. PhD thesis, Ruhr Universität Bochum, Germany, 2010, Retrieved March 1, 2013. URL http://www-brs.ub.ruhr-uni-bochum.de/netahtml/HSS/Diss/BargelStefan/diss.pdf.

[10] D. Bauer, R. Marx, J. Nußbicker-Lux, F. Ochs, W. Heidemann, and H. Müller-Steinhagen. German central solar heating plants with seasonal heat storage. *Solar Energy*, 84(4):612–623, 2010. ISSN 0038092X. doi: 10.1016/j.solener.2009.05.013.

[11] M. M. Becker, A. Dentel, B. Fuchs, and M. Faulstich. Dynamische Gebäudesimulation. *BWK - Das Energie-Fachmagazin*, (64), 2012.

[12] A. Bejan. *Entropy Generation Minimization: The Method of Thermodynamic Optimization of Finite-Size Systems and Finite-Time Processes*. CRC Press, 1 edition, 1995. ISBN 0849396514.

[13] A. Bejan, G. Tsatsaronis, and M. Moran. *Thermal Design and Optimization*. Wiley-Interscience, 1 edition, 1995. ISBN 0471584673.

[14] M. Benner and E. Hahne. *Solare Nahwärme: Ein Informationspaket ; ein Leitfaden für die Praxis*. BINE-Informationsdienst. TÜV-Verl., Köln, 1998. ISBN 3-8249-0470-5.

[15] Bernd Hafner. CARNOT_Manual: Conventional And Renewable eNergy systems Optimization Toolbox.

[16] Bianchi M. A. *Adaptive modellbasierte prädiktive Regelung einer Kleinwärmepumenanlage*. PhD thesis, ETH Zuerich, Switzerland, 2006.

[17] A. Bruns. Energetische, exergetische und ökonomische Analyse von Power-to-Heat Wärmeversorgungsszenarien in CARNOT. *Master thesis, TU Darmstadt, Germany*, 2016.

[18] Bundesamt für Wirtschaft und Ausfuhrkontrolle. Mini - KWK - Anlagen: Liste der förderfähigen KWK - Anlagen bis einschließlich 20 kWel, 2017, Retrieved April 24, 2017. URL http://www.bafa.de/SharedDocs/Downloads/DE/Energie/kwk_mini_kwk_liste_foerderfaehige_anlagen.pdf?__blob=publicationFile&v=7.

[19] Bundesfinanzhof. Urteil vom 16.11.2016, V R 1/15, Retrieved August 24, 2017. URL https://juris.bundesfinanzhof.de/cgi-bin/rechtsprechung/druckvorschau.py?Gericht=bfh&Art=en&nr=34095.

[20] Bundesministerium für Umwelt, Naturschutz, Bau und Reaktorsicherheit. Ökobaudat, Retrieved July 20, 2016. URL http://www.oekobaudat.de/.

[21] Bundesministerium für Wirtschaft und Energie. Richtlinien zur Förderung von Maßnahmen zur Nutzung erneuerbarer Energien im Wärmemarkt, 2015, Retrieved April 24, 2017. URL http://www.erneuerbare-energien.de/EE/Redaktion/DE/Downloads/Foerderbekanntmachungen/marktanreizprogramm-erneuerbare-energien.pdf?__blob=publicationFile&v=9.

[22] Bundesministerium für Wirtschaft und Energie. Die Energie der Zukunft - Vierter Monitoringbericht zur Energiewende, 2016, Retrieved October 6, 2017. URL https://www.umweltbundesamt.de/daten/klimawandel/klimaschutzziele-deutschlands#textpart-2.

[23] Bundesministeriums der Justiz und für Verbraucherschutz. Energiesteuergesetz: EnergieStG, 2008, Retrieved August 25, 2017. URL https://www.gesetze-im-internet.de/energiestg/EnergieStG.pdf.

[24] Bundesnetzagentur. EEG-Fördersätze für PV-Anlagen, 2016, Retrieved May 23, 2016. URL http://www.bundesnetzagentur.de/cln_1411/DE/Sachgebiete/ElektrizitaetundGas/Unternehmen_Institutionen/ErneuerbareEnergien/Photovoltaik/DatenMeldgn_EEG-VergSaetze/DatenMeldgn_EEG_VergSaetze.html?nn=414658#neuen.

[25] Bundesverband der Energie- und Wasserwirtschaft e.V. Strompreisanalyse Januar 2016, 2016, Retrieved August 24, 2017. URL https://www.bdew.de/internet.nsf/id/DC9ABD3F2D97604DC1257F42002E5075/$file/160122%20BDEW%20zum%20Strompreis%20der%20Haushalte%20Anhang.pdf.

[26] Bundesverband der Energie- und Wasserwirtschaft e.V. Standardlastprofile Strom, 2016, Retrieved May 24, 2017. URL https://www.bdew.de/internet.nsf/id/DE_Standartlastprofile.

[27] D. Buoro, P. Pinamonti, and M. Reini. Optimization of a Distributed Cogeneration System with solar district heating. *Applied Energy*, 124:298–308, 2014. ISSN 03062619. doi: 10.1016/j.apenergy.2014.02.062.

[28] J. Cervantes and E. Torres-Reyes. Experiments on a solar-assisted heat pump and an exergy analysis of the system. *Applied Thermal Engineering*, 22(12):1289–1297, 2002. ISSN 1359-4311. doi: 10.1016/S1359-4311(02)00055-8.

[29] T. T. Chow. A review on photovoltaic/thermal hybrid solar technology. *Applied Energy*, 87(2): 365–379, 2010. ISSN 03062619. doi: 10.1016/j.apenergy.2009.06.037.

[30] K. Çomaklı, B. Yüksel, and Ö. Çomaklı. Evaluation of energy and exergy losses in district heating network. *Applied Thermal Engineering*, 24(7):1009–1017, 2004. ISSN 1359-4311. doi: 10.1016/j.applthermaleng.2003.11.014.

[31] C. A. Cruickshank. *Evaluation of a Stratified Multi-tank Thermal Storage for Solar Heating Applications*. PhD thesis, Queen's University, Canada, 2009, Retrieved November 19, 2013. URL http://hdl.handle.net/1974/1969.

[32] C. A. Cruickshank and S. J. Harrison. Heat loss characteristics for a typical solar domestic hot water storage. *Energy and Buildings*, 42(10):1703–1710, 2010. ISSN 03787788. doi: 10.1016/j.enbuild.2010.04.013.

[33] D. Bauer, W. Heidemann, and H. Müller-Steinhagen. Central Solar Heating Plants with Seasonal Heat Storage, Presentation 04.-05.09.07, Retrieved October 13, 2015. URL http://www.itw.uni-stuttgart.de/dokumente/Publikationen/publikationen_07-07.pdf.

[34] A. Dalla Rosa and J. E. Christensen. Low-energy district heating in energy-efficient building areas. *Energy*, 36(12):6890–6899, 2011. ISSN 0360-5442. doi: 10.1016/j.energy.2011.10.001.

[35] Dehoust. Preisliste 2011, Retrieved April 21, 2017. URL http://www.dehoust.de/Files/download/preislisten/Deh_Preisliste_2011.pdf.

[36] Deubner Steuern & Praxis. Vorsteuer: Aufteilung für ein Blockheizkraftwerk, 2017, Retrieved August 25, 2017. URL https://www.deubner-steuern.de/news/umsatzsteuer/details/artikel/vorsteuer-aufteilung-fuer-ein-blockheizkraftwerk.html.

[37] Deutsche Gesellschaft für Geotechnik e.V. und Deutsche Gesellschaft für Geowissenschaften e.V. *Shallow geothermal systems - recommendations on design, construction, operation and monitoring: Of the Geothermal Energy Study Group at the specialist Hydrogeology Section of the German Geological Society (FH-DGGV) and the Engineering Geology Section of the German Geotechnical Society and the German Geological Society (FI-DGGT/DGGV)*. Ernst & Sohn GmbH & Co. KG., 2016. ISBN 978-3-433-03140-7.

[38] A. Dikici and A. Akbulut. Performance characteristics and energy–exergy analysis of solar-assisted heat pump system. *Building and Environment*, 43(11):1961–1972, 2008. ISSN 03601323. doi: 10.1016/j.buildenv.2007.11.014.

[39] Ecoinvent. Ecoinvent database version 3. URL http://www.ecoinvent.org/.

[40] K. Ellehauge and T. E. Pedersen. Solar heat storages in district heating networks, 2007, Retrieved October 13, 2015. URL https://www.energinet.dk/SiteCollectionDocuments/Danske%20dokumenter/Forskning%20-%20PSO-projekter/6750%20Europ%C3%A6isk%20samarbejde%20omkring%20udvikling%20af%20solvarmelagre%20til%20brug%20i%20kraftvarmesystemer.pdf.

[41] energie experten.org. Wechselrichter Preise, 2016, Retrieved April 24, 2017. URL http://www.energie-experten.org/erneuerbare-energien/photovoltaik/wechselrichter/zentralwechselrichter.html.

[42] Enerpipe. Datenblat, Caldopex, 2014, Retrieved May 17, 2017. URL http://www.enerpipe.de/produkte/pdl/?file=533e9bb1be9ba.pdf.

[43] Engelbart H. Erweiterung des Gebäudegruppenmodells in CARNOT. *Master thesis, TU Darmstadt, Germany*, 2015.

[44] P. M. Falk, F. Dammel, and P. Stephan. Exergy Analyses of Heat Supply Systems for a Building Cluster with CARNOT. *International Journal of Thermodynamics (IJoT)*, 2017(Vol. 20 (No. 4)): 191–198, 2017. URL http://dergipark.gov.tr/download/article-file/373061.

[45] C. Felsmann. *LowEx-Fernwärme: Multilevel District Heating ; Zusammenfassung*. TUDpress, Dresden, 2011. ISBN 978-3-942710-15-2.

[46] M. Fisch, M. Guigas, and J. Dalenbäck. A Review of large-scale Solar Heating Systems in Europe. *Solar Energy*, 63(6):355–366, 1998. ISSN 0038092X. doi: 10.1016/S0038-092X(98)00103-0.

[47] German Pipe - Industrie- und Fernwärmetechnik GmbH. Kunststoff-Mantelrohr, Retrieved April 21, 2017. URL http://www.germanpipe.de/domains/germanpipe_de/data/free_docs/gp_bauteile_kunststoffmantelrohr.pdf.

[48] Grundfos. Datenblatt Pumpe CR10-03 A-A-A-E-HQQE, 2013, Retrieved May 17, 2017. URL www.lenntech.com/uploads/grundfos/96500981/Grundfos_CR-10-3-A-A-A-E-HQQE.pdf.

[49] Grundfos. Datenblatt MAGNA 80-120 F, 2015, Retrieved May 17, 2017. URL http://product-selection.grundfos.com/product-detail.product-detail.html?productnumber=97924690&qcid=168268717.

[50] Grundfos. Datenblatt ALPHA 2 15-60, 2015, Retrieved May 17, 2017. URL http://www.ecopumpen.de/media/docs/datenheft-alpha2.pdf.

[51] Grundfos. Preisliste 2016, 2016, Retrieved April 21, 2017. URL http://www.stuewa.de/fileadmin/user_upload/preislisten/Grundfos_Gesamt-Preisliste_2016.pdf#page=1&zoom=auto,-202,842.

[52] H. Hackbusch. Modellierung und Validierung eines Blockheizkraftwerkes in CARNOT. *Bachelor thesis, TU Darmstadt, Germany*, 2015.

[53] M. Y. Haller, C. A. Cruickshank, W. Streicher, S. J. Harrison, E. Andersen, and S. Furbo. Methods to determine stratification efficiency of thermal energy storage processes – Review and theoretical comparison. *Solar Energy*, 83(10):1847–1860, 2009. ISSN 0038092X. doi: 10.1016/j.solener.2009.06.019.

[54] M. Y. Haller, E. Yazdanshenas, E. Andersen, C. Bales, W. Streicher, and S. Furbo. A method to determine stratification efficiency of thermal energy storage processes independently from storage heat losses. *Solar Energy*, 84(6):997–1007, 2010. ISSN 0038092X. doi: 10.1016/j.solener.2010.03.009.

[55] G. P. Hammond and Ondo Akwe, Serge S. Thermodynamic and related analysis of natural gas combined cycle power plants with and without carbon sequestration. *International Journal of Energy Research*, 31(12):1180–1201, 2007. ISSN 1099-114X. doi: 10.1002/er.1328.

[56] M. Hawlader, S. Chou, and M. Ullah. The performance of a solar assisted heat pump water heating system. *Applied Thermal Engineering*, 21(10):1049–1065, 2001. ISSN 1359-4311. doi: 10.1016/S1359-4311(00)00105-8.

[57] A. Hepbasli. Exergetic modeling and assessment of solar assisted domestic hot water tank integrated ground-source heat pump systems for residences. *Energy and Buildings*, 39(12):1211–1217, 2007. ISSN 03787788. doi: 10.1016/j.enbuild.2007.01.007.

[58] A. Hepbasli. A study on estimating the energetic and exergetic prices of various residential energy sources. *Energy and Buildings*, 40(3):308–315, 2008. ISSN 03787788. doi: 10.1016/j.enbuild.2007.01.023.

[59] A. Hepbasli and Y. Kalinci. A review of heat pump water heating systems. *Renewable and Sustainable Energy Reviews*, 13(6-7):1211–1229, 2009. ISSN 1364-0321. doi: 10.1016/j.rser.2008.08.002.

[60] J. T. Houghton, editor. *The scientific basis ; contribution of Working Group I to the third assessment report of the Intergovernmental Panel on Climate Change*. Climate change 2001. Cambridge Univ. Press, Cambridge, 2001. ISBN 0521807670.

[61] B. Huang, T. Lin, W. Hung, and F. Sun. Performance evaluation of solar photovoltaic/thermal systems. *Solar Energy*, 70(5):443–448, 2001. ISSN 0038092X. doi: 10.1016/S0038-092X(00)00153-5.

[62] A. Huber and O. Schuler. Berechnungsmodul für Erdwärmesonden (EWS). *ENET Bericht Nr. 9658807-1*, 1997.

[63] International Organization for Standardization. Environmental management - Life cycle assessment - Principles and framework - DIN EN ISO - 14040:2006, Retrieved September 13, 2016. URL `https://www.iso.org/obp/ui/#iso:std:iso:14040:ed-2:v1:en`.

[64] International Renewable Energy Agency. Renewable Energy Prospects: Germany, REmap 2030 analysis, 2015, Retrieved May 3, 2017. URL `www.irena.org/remap`.

[65] A. Jentsch. *A novel exergy-based concept of thermodynamic quality and its application to energy system evaluation and process analysis*. PhD thesis, TU Berlin, Germany, 2010, Retrieved March 1, 2013. URL `http://opus.kobv.de/tuberlin/volltexte/2010/2576/`.

[66] S. Kalogirou and Y. Tripanagnostopoulos. Hybrid PV/T solar systems for domestic hot water and electricity production. *Energy Conversion and Management*, 47(18-19):3368–3382, 2006. ISSN 0196-8904. doi: 10.1016/j.enconman.2006.01.012.

[67] S. A. Kalogirou. Solar thermal collectors and applications. *Progress in Energy and Combustion Science*, 30(3):231–295, 2004. ISSN 0360-1285. doi: 10.1016/j.pecs.2004.02.001.

[68] M. Kaltschmitt. *Erneuerbare Energien: Systemtechnik, Wirtschaftlichkeit, Umweltaspekte*. Springer, Berlin, 5. aufl., erw. und korr. nachdruck edition, 2014. ISBN 978-3-642-03248-6.

[69] K. Kaygusuz. Calculation of Required Collector Area of a Solar-Assisted Series Heat Pump for Domestic Heating. *Energy Sources*, 22(3):247–256, 2000. ISSN 0090-8312. doi: 10.1080/00908310050014036.

[70] R. Klemmer. Modellierung und Analyse von Wärmespeicherszenarien in CARNOT. *Master thesis, TU Darmstadt, Germany*, 2014.

[71] W. Klöpffer. Life cycle assessment: From the beginning to the current state. *Environmental science and pollution research international*, 4(4):223–228, 1997. ISSN 0944-1344. doi: 10.1007/BF02986351.

[72] J. K. Knigge. Ökonomische Analyse verschiedener Wärmeversorgungsszenearien. *Studienarbeit, TU Darmstadt, Germany*, 2015.

[73] Köhler D. Ganzheitliche energetische Bilanzierung der Energiebereitstellung (GaBiE): Teil VI Energetische Untersuchung von Blockheizkraftwerken, 1996, Retrieved July 20, 2016. URL `https://www.ffe.de/download/langberichte/FfE_GaBiE_Bilanzierung_Strombereitstellung.pdf`.

[74] J. Koornneef, T. van Keulen, A. Faaij, and W. Turkenburg. Life cycle assessment of a pulverized coal power plant with post-combustion capture, transport and storage of CO2. *International Journal of Greenhouse Gas Control*, 2(4):448–467, 2008. ISSN 17505836. doi: 10.1016/j.ijggc.2008.06.008.

[75] J. Krimmling. *Energieeffiziente Nahwärmesysteme: Grundwissen, Auslegung, Technik für Energieberater und Planer*. Fraunhofer IRB Verlag, Stuttgart, 2011. ISBN 9783816783428.

[76] Landesanstalt für Umwelt Messungen und Naturschutz. Wetterdaten 2013, Retrieved October 23, 2015. URL `http://udo.lubw.baden-wuerttemberg.de/public/`.

[77] LG. Datenblatt LG Neon2, 2016, Retrieved May 19, 2017. URL `http://www.lg-solar.com/downloads/products/LG-NeON-2/LGE-Data%20Sheet-LGxxxN1C-G4_DE_03.2016.pdf`.

[78] D. Lindenberger, T. Bruckner, H.-M. Groscurth, and R. Kümmel. Optimization of solar district heating systems: seasonal storage, heat pumps, and cogeneration. *Energy*, 25(7):591–608, 2000. ISSN 0360-5442. doi: 10.1016/S0360-5442(99)00082-1.

[79] Löbbe GmbH. Viessmann Vitotronic 300-K MW1: Digitale Kaskadenregelung, 2017, Retrieved April 24, 2017. URL `http://www.loebbeshop.de/viessmann/regelungen/regelung/viessmann-vitotronic-300-k-typ-mw1.htm`.

[80] S. Lohani. Energy and exergy analysis of fossil plant and heat pump building heating system at two different dead-state temperatures. *Energy*, 35(8):3323–3331, 2010. ISSN 0360-5442. doi: 10.1016/j.energy.2010.04.018.

[81] S. Lohani and D. Schmidt. Comparison of energy and exergy analysis of fossil plant, ground and air source heat pump building heating system. *Renewable Energy*, 35(6):1275–1282, 2010. ISSN 09601481. doi: 10.1016/j.renene.2009.10.002.

[82] Lorenz GmbH & Co KG. Groß-Pufferspeicher Typ PSG 2500 - 100000 l Preisliste, 2017, Retrieved April 24, 2017. URL http://lorenz-behaelterbau.de/wp-content/uploads/grosspuffer.pdf.

[83] V. Lottner, M. Schulz, and E. Hahne. Solar-Assisted District Heating Plants: Status of the German Programme Solarthermie-2000. *Solar Energy*, 69(6):449–459, 2000. ISSN 0038092X. doi: 10.1016/S0038-092X(00)00125-0.

[84] Lückel & Partner Steuerberatung. Photovoltaikanlagen Steuerliche Behandlung Stand Januar 2016: Merkblatt, Retrieved August 24, 2017. URL http://www.lueckel-partner-stb.de/merkblaetter.html.

[85] M. Bodmann, D. Mangold, J. Nußbicker, S. Raab, A. Schenke und T. Schmidt. Solar unterstützte Nahwärme und Langzeit-Wärmespeicher: Forschungsbericht zum BMWA / BMU-Vorhaben. *Solar- und Wärmetechnik Stuttgart (SWT)*, 2005, Retrieved October 27, 2015. URL http://www.solites.de/download/literatur/AB-SUN%20V%20FKZ%200329607F.pdf.

[86] D. Mangold, O. Miedaner, E. P. Tziggili, T. Schmidt, M. Unterberger, and B. Zeh. Technisch - Wirtschaftliche Analyse und Weiterentwicklung der Solaren Langzeit - Wärmespeicherung: Forschungebericht zum BMU -Vorhaben 0329607N, 2012, Retrieved April 21, 2017. URL http://www.solites.de/download/literatur/Solites_Technisch-wirtschaftliche%20Analyse%20und%20Weiterentwicklung%20der%20solaren%20Langzeit-W%C3%A4rmespeicherung_Forschungsbericht_FKZ%200329607N_2012.pdf.

[87] A. Morbach. Integration des Blockheizkraftwerkmodells in das CARNOT Gebäudegruppenmodell. *Studienarbeit, TU Darmstadt, Germany*, 2016.

[88] A. Morbach. Ökonomische Analyse zur Wärmeversorgung einer Gebäudegruppe anhand eines CARNOT-Modells. *Master thesis, TU Darmstadt, Germany*, 2016.

[89] A. Morbach. Integration of a combined heat and power plant model in the CARNOT building cluster model. *Documentation to Master-Thesis, TU Darmstadt, Germany*, 2016.

[90] MVV Energie AG Mannheim, Germany. URL https://www.mvv.de/de/.

[91] M. Noussan, G. Cerino Abdin, A. Poggio, and R. Roberto. Biomass-fired CHP and heat storage system simulations in existing district heating systems. *Applied Thermal Engineering*, 71(2):729–735, 2014. ISSN 1359-4311. doi: 10.1016/j.applthermaleng.2013.11.021.

[92] T. Nuytten, B. Claessens, K. Paredis, J. van Bael, and D. Six. Flexibility of a combined heat and power system with thermal energy storage for district heating. *Applied Energy*, 104:583–591, 2013. ISSN 03062619. doi: 10.1016/j.apenergy.2012.11.029.

[93] Öko-Institut e.V. Endenergiebezogene Gesamtemissionen für Treibhausgase aus fossilen Energieträgern unter Einbeziehung der Bereitstellungsvorketten: Kurzbericht im Auftrag des Bundesverbands der deutschen Gas- und Wasserwirtschaft e.V. (BGW), 2007, Retrieved July 20, 2016. URL http://www.iinas.org/tl_files/iinas/downloads/GEMIS/2007_thg_fossil_BGW.pdf.

[94] H. I. Onovwiona and V. I. Ugursal. Residential cogeneration systems: review of the current technology. *Renewable and Sustainable Energy Reviews*, 10(5):389–431, 2006. ISSN 1364-0321. doi: 10.1016/j.rser.2004.07.005.

[95] M. Ortiz, H. Barsun, H. He, P. Vorobieff, and A. Mammoli. Modeling of a solar-assisted HVAC system with thermal storage. *Energy and Buildings*, 42(4):500–509, 2010. ISSN 03787788. doi: 10.1016/j.enbuild.2009.10.019.

[96] P. A. Østergaard and H. Lund. A renewable energy system in Frederikshavn using low-temperature geothermal energy for district heating. *Applied Energy*, 88(2):479–487, 2011. ISSN 03062619. doi: 10.1016/j.apenergy.2010.03.018.

[97] L. Ozgener, A. Hepbasli, and I. Dincer. Energy and exergy analysis of geothermal district heating systems: an application. *Building and Environment*, 40(10):1309–1322, 2005. ISSN 03601323. doi: 10.1016/j.buildenv.2004.11.001.

[98] L. Ozgener, A. Hepbasli, and I. Dincer. Energy and exergy analysis of Salihli geothermal district heating system in Manisa, Turkey. *International Journal of Energy Research*, 29(5):393–408, 2005. ISSN 1099-114X. doi: 10.1002/er.1056.

[99] L. Ozgener, A. Hepbasli, and I. Dincer. Energy and exergy analysis of the Gonen geothermal district heating system, Turkey. *Geothermics*, 34(5):632–645, 2005. ISSN 03756505. doi: 10.1016/j.geothermics.2005.06.001.

[100] L. Ozgener, A. Hepbasli, and I. Dincer. Effect of reference state on the performance of energy and exergy evaluation of geothermal district heating systems: Balcova example. *Building and Environment*, 41(6):699–709, 2006. ISSN 03601323. doi: 10.1016/j.buildenv.2005.03.007.

[101] O. Ozgener and A. Hepbasli. Performance analysis of a solar-assisted ground-source heat pump system for greenhouse heating: an experimental study. *Building and Environment*, 40(8):1040–1050, 2005. ISSN 03601323. doi: 10.1016/j.buildenv.2004.08.030.

[102] O. Ozgener and A. Hepbasli. Experimental performance analysis of a solar assisted ground-source heat pump greenhouse heating system. *Energy and Buildings*, 37(1):101–110, 2005. ISSN 03787788. doi: 10.1016/j.enbuild.2004.06.003.

[103] O. Ozgener and A. Hepbasli. A review on the energy and exergy analysis of solar assisted heat pump systems. *Renewable and Sustainable Energy Reviews*, 11(3):482–496, 2007. ISSN 1364-0321. doi: 10.1016/j.rser.2004.12.010.

[104] O. Ozgener and A. Hepbasli. Modeling and performance evaluation of ground source (geothermal) heat pump systems. *Energy and Buildings*, 39(1):66–75, 2007. ISSN 03787788. doi: 10.1016/j.enbuild.2006.04.019.

[105] O. Ozgener and A. Hepbasli. A parametrical study on the energetic and exergetic assessment of a solar-assisted vertical ground-source heat pump system used for heating a greenhouse. *Building and Environment*, 42(1):11–24, 2007. ISSN 03601323. doi: 10.1016/j.buildenv.2005.07.003.

[106] V. Panthalookaran, W. Heidemann, and H. Müller-Steinhagen. A new method of characterization for stratified thermal energy stores. *Solar Energy*, 81(8):1043–1054, 2007. ISSN 0038092X. doi: 10.1016/j.solener.2006.11.012.

[107] D. P. Papadopoulos and P. A. Katsigiannis. Biomass energy surveying and techno-economic assessment of suitable CHP system installations. *Biomass and Bioenergy*, 22(2):105–124, 2002. ISSN 09619534. doi: 10.1016/S0961-9534(01)00064-2.

[108] B. Parida, S. Iniyan, and R. Goic. A review of solar photovoltaic technologies. *Renewable and Sustainable Energy Reviews*, 15(3):1625–1636, 2011. ISSN 1364-0321. doi: 10.1016/j.rser.2010.11.032.

[109] M. Pehnt and J. Henkel. Life cycle assessment of carbon dioxide capture and storage from lignite power plants. *International Journal of Greenhouse Gas Control*, 3(1):49–66, 2009. ISSN 17505836. doi: 10.1016/j.ijggc.2008.07.001.

[110] photovoltaik4all. LG Solarmodul LG320N1C-G4 NeON 2 Cello Preis, Retrieved April 24, 2017. URL http://www.photovoltaik4all.de/lg-solar-lg320n1c-g4-neon-2-cello.

[111] P.M. Falk, F. Meggers, P. Stephan, F. Dammel. Comparison of District Heating Systems and Distributed Geothermal Network for Optimal Exergetic Performance, Sustainable Built Environment (SBE) Regional Conference Zurich 2016, June 13 to 17 2016, doi 10.3218/3774-6_18.

[112] REGIERUNGSPRÄSIDIUM FREIBURG LANDESAMT FÜR GEOLOGIE, ROHSTOFFE UND BERGBAU:. LGRB Geothermie, Retrieved July 20, 2017. URL http://www.lgrb-bw.de/geothermie/grundlagen/allgemeine_grundlagen/.

[113] W. Retkowski and J. Thöming. Thermoeconomic optimization of vertical ground-source heat pump systems through nonlinear integer programming. *Applied Energy*, 114:492–503, 2014. ISSN 03062619. doi: 10.1016/j.apenergy.2013.09.012.

[114] A. Riedel. Sensitivitätsanalysen eines Wärmeversorgungsmodells einer Gebäudegruppe. *Bachelor thesis, TU Darmstadt, Germany*, 2015.

[115] M. Rosen and I. Dincer. Exergy methods for assessing and comparing thermal storage systems. *International Journal of Energy Research*, 27(4):415–430, 2003. ISSN 1099-114X. doi: 10.1002/er.885.

[116] M. A. Rosen. Energy- and exergy-based comparison of coal-fired and nuclear steam power plants. *Exergy, An International Journal*, 1(3):180–192, 2001. ISSN 1164-0235. doi: 10.1016/S1164-0235(01)00024-3.

[117] M. A. Rosen. The exergy of stratified thermal energy storages. *Solar Energy*, 71(3):173–185, 2001. ISSN 0038092X. doi: 10.1016/S0038-092X(01)00036-6.

[118] M. A. Rosen and M. Rosen. Energy and exergy analyses of electrolytic hydrogen production. *International Journal of Hydrogen Energy*, 20(7):547–553, 1995. ISSN 0360-3199. doi: 10.1016/0360-3199(94)00102-6. URL http://www.sciencedirect.com/science/article/pii/0360319994001026.

[119] M. A. Rosen, M. N. Le, and I. Dincer. Exergetic analysis of cogeneration-based district energy systems. *Proceedings of the Institution of Mechanical Engineers, Part A: Journal of Power and Energy*, 218(6):369–375, 2004. ISSN 0957-6509. doi: 10.1243/0957650041761892.

[120] M. A. Rosen, R. Tang, and I. Dincer. Effect of stratification on energy and exergy capacities in thermal storage systems. *International Journal of Energy Research*, 28(2):177–193, 2004. ISSN 1099-114X. doi: 10.1002/er.960.

[121] M. A. Rosen, M. N. Le, and I. Dincer. Efficiency analysis of a cogeneration and district energy system. *Applied Thermal Engineering*, 25(1):147–159, 2005. ISSN 1359-4311. doi: 10.1016/j.applthermaleng.2004.05.008.

[122] ROTEX. Datenblatt HPSU hitemp, 2016, Retrieved May 19, 2017. URL http://fachportal.rotex-heating.com/fileadmin/download/manuals/de/hpsu-bi-bloc/PH_HPSU_HPU_0081422349_02_1016_Web_DE.pdf.

[123] ROTEX. ROTEX-Paket-Preisliste, 2017, Retrieved April 24, 2017. URL http://www.heizungs-discount.de/Preislisten_Rabatte/Rotex_Preislisten_und_Rabatte/Rotex_Paket_Preisliste/rotex_paket_preisliste_oel_gas_brennwert_solar_waermepumpe_fussbodenheizungs_pakete_system_70_hybridcube_heizoeltanks_variosafe_watersafe.pdf.

[124] V. Schäfer. Machbarkeits- und Wirtschaftlichkeitsuntersuchung für Bau und Betrieb eines Heizwerkes oder Heizkraftwerkes mit Nahwärmenetz in Eschenfelden, 2011, Retrieved April 21, 2017. URL https://www.eschenfelden.de/spd/pdf/Nahwaerme_PraesentationMachbarkeit.pdf.

[125] Schiavoni S, D'Alessandro F, Bianchi F, Asdrubali F. Insulation materials for the building sector: A review and comparative analysis. *Renewable and Sustainable Energy Reviews*, 62:988–1011, 2016. ISSN 1364-0321. doi: 10.1016/j.rser.2016.05.045.

[126] T. Schmidt, D. Mangold, and H. Müller-Steinhagen. Central solar heating plants with seasonal storage in Germany. *Solar Energy*, 76(1-3):165–174, 2004. ISSN 0038092X. doi: 10.1016/j.solener.2003.07.025.

[127] K. Schwamberger. Modellbildung und Regelung von Gebäudeheizungsanlagen mit Wärmepumpen. *VDI Fortschrittsberichte Reihe 6*, (263), 1991.

[128] SES Energiesysteme GmbH. Technisches Datenblatt SES - HPC 50: NBHKW - Kompaktmodul, 2012, Retrieved November January 23, 2015. URL https://www.ses-energiesysteme.com/info/downloadbereich/.

[129] B. Sibbitt, D. McClenahan, R. Djebbar, J. Thornton, B. Wong, J. Carriere, and J. Kokko. The Performance of a High Solar Fraction Seasonal Storage District Heating System – Five Years of Operation. *Energy Procedia*, 30:856–865, 2012. ISSN 18766102. doi: 10.1016/j.egypro.2012.11.097.

[130] Solar Institut Jülich Germany. CARNOT 5.3: MATLAB SIMULINK Toolbox Extension, 1999. URL https://fh-aachen.sciebo.de/index.php/s/0hxub0iIJrui3ED.

[131] P. A. Sørensen, L. Holm, and N. A. Jensen. Water Storages, Solar thermal and Heat pumps in District Heating, Eurosun 2008, 1st International Congress on Heating, Cooling, and Buildings,October 7 to 10 2008, Retrieved October 13, 2015. URL http://www.solarthermalworld.org/sites/gstec/files/District%20Heating%20Planenergi_0.pdf.

[132] Statista. Beheizungsstruktur des Wohnungsbestandes in Deutschland in den Jahren 1995 bis 2016, 2017, Retrieved October 6, 2017. URL https://de.statista.com/statistik/daten/studie/162218/umfrage/beheizungsstruktur-des-wohnbestandes-in-deutschland-seit-1975/.

[133] Statistisches Bundesamt. Umweltnutzung und Wirtschaft, 2016, retrieved September 29, 2017. URL https://www.destatis.de/DE/Publikationen/Thematisch/UmweltoekonomischeGesamtrechnungen/Querschnitt/UmweltnutzungundWirtschaftTabelle5850007167006Teil_2.pdf?__blob=publicationFile.

[134] P. Stephan, K. Schaber, K. Stephan, and F. Mayinger. *Thermodynamik*. Springer Berlin Heidelberg, Berlin, Heidelberg, 2013. ISBN 978-3-642-30097-4. doi: 10.1007/978-3-642-30098-1.

[135] I. Stober and K. Bucher. *Geothermie*. Springer Berlin Heidelberg, Berlin, 2nd ed. edition, 2014. ISBN 978-3-642-41763-4.

[136] J. Szargut, D. Morris, and F. Steward. *Exergy analysis of thermal, chemical and metallurgical processes*. Hemisphere Publishing, New York, 1988. ISBN 3540188649.

[137] J. Terés-Zubiaga, S. Jansen, P. Luscuere, and J. Sala. Dynamic exergy analysis of energy systems for a social dwelling and exergy based system improvement. *Energy and Buildings*, 64:359–371, 2013. ISSN 03787788. doi: 10.1016/j.enbuild.2013.05.034.

[138] Thermal Energy System Specialists. TRNSYS, 1975. URL http://www.trnsys.com/.

[139] A. Thür, S. Furbo, and L. J. Shah. Energy savings for solar heating systems. *Solar Energy*, 80(11): 1463–1474, 2006. ISSN 0038092X. doi: 10.1016/j.solener.2006.03.007.

[140] H. Torío and D. Schmidt. Development of system concepts for improving the performance of a waste heat district heating network with exergy analysis. *Energy and Buildings*, 42(10):1601–1609, 2010. ISSN 03787788. doi: 10.1016/j.enbuild.2010.04.002.

[141] H. Torío and D. Schmidt. Development of system concepts for improving the performance of a waste heat district heating network with exergy analysis. *Energy and Buildings*, 42(10):1601–1609, 2010. ISSN 03787788. doi: 10.1016/j.enbuild.2010.04.002.

[142] H. Torío and D. Schmidt. *Exergy assessment guidebook for the built environment: ECBCS Annex 49 - low exergy systems for high-performancebBuildings and communities*. Fraunhofer Verlag, Stuttgart, 2011. ISBN 978-3-8396-0239-3.

[143] H. Torío and D. Schmidt. *Detailed Exergy Assessment Guidebook for the Built Environment: ECBCS Annex 49 - Low Exergy Systems for High-Performance Buildings and Communities*. Fraunhofer Verlag, Stuttgart, 2011. URL http://www.annex49.info/download/Annex49_guidebook.pdf.

[144] H. Torío, A. Angelotti, and D. Schmidt. Exergy analysis of renewable energy-based climatisation systems for buildings: A critical view. *Energy and Buildings*, 41(3):248–271, 2009. ISSN 03787788. doi: 10.1016/j.enbuild.2008.10.006.

[145] E. Torres R, M. Picon Nuñez, and J. Cervantes de G. Exergy analysis and optimization of a solar-assisted heat pump. *Energy*, 23(4):337–344, 1998. ISSN 0360-5442. doi: 10.1016/S0360-5442(97)00079-0.

[146] Umweltbundesamt. Endenergieverbrauch 2015 nach Sektoren und Energieträgern, 2015, Retrieved September 29, 2017. URL https://www.umweltbundesamt.de/sites/default/files/medien/384/bilder/dateien/4_abb_eev-sektoren-et_2017-02-17.pdf.

[147] Umweltbundesamt. Strom- und Wärmeversorgung in Zahlen, 2016, Retrieved July 20, 2016. URL https://www.umweltbundesamt.de/themen/klima-energie/energieversorgung/strom-waermeversorgung-in-zahlen?sprungmarke=Strommix.

[148] Umweltbundesamt. Nationale Trendtabellen für die deutsche Berichterstattung atmosphärischer Emissionen 1990 bis 2015, 2017, Retrieved October 4, 2017. URL https://www.umweltbundesamt.de/sites/default/files/medien/384/bilder/dateien/2_abb_entw-energiebed-thg-emi_2017-02-17.pdf.

[149] VDI Gesellschaft. VDI 4640 Blatt 1 Thermische Nutzung des Untergrunds - Grundlagen, Genehmigungen, Umweltaspekte, 2010.

[150] Vela Solaris AG, Schweiz. Polysun, 1992. URL http://www.velasolaris.com/.

[151] V. Verda and F. Colella. Primary energy savings through thermal storage in district heating networks. *Energy*, 36(7):4278–4286, 2011. ISSN 0360-5442. doi: 10.1016/j.energy.2011.04.015.

[152] Verein Deutscher Ingenieure. Wirtschaftlichkeit gebäudetechnischer Anlagen, VDI-Richtlinie 2067, 2016.

[153] Viessmann Deutschland GmbH. Vitocal - Planungsanleitung, 2012, Retrieved June 15, 2016. URL http://www.viessmann.com/vires/product_documents/5671883VPA00001_1.PDF.

[154] Viessmann Deutschland GmbH. Preisliste 2014 Teil 2, 2014, Retrieved April 21, 2017. URL http://www.heizungs-discount.de/Kataloge/Viessmann/viessmann_preisliste_mittel_und_grosskessel_vitoplex_vitocell_vitorond_vitotrans_vitoradial_vitomax_vitoplex_vitocontrol_kwt_vitocal_pyrot_pyrotec_mawera_vitocom_vitodata_vitohome.pdf.

[155] Viessmann Deutschland GmbH. Vitocal 300-G Pro - Planungsanleitung, 2014, Retrieved June 15, 2016. URL http://www.viessmann.com/vires/product_documents/5604040VSA00001_1.PDF.

[156] Viessmann Deutschland GmbH. Vitobloc 200 - Typ EM-20/39: Technische Beschreibung, 2014, Retrieved June 15, 2016. URL https://www.viessmann.de/de/wohngebaeude/kraft-waerme-kopplung/blockheizkraftwerk/vitobloc-200-em-20-39.html.

[157] Viessmann Deutschland GmbH. Vitobloc 200 - Typ EM-9/20: Technische Beschreibung, 2014, Retrieved June 15, 2016. URL https://www.viessmann.de/de/wohngebaeude/kraft-waerme-kopplung/blockheizkraftwerk/vitobloc-200-em-9-20.html.

[158] Viessmann Deutschland GmbH. Wärmepumpen bis 2000 kW, 2015, Retrieved May 17, 2017. URL https://www.viessmann.de/de/wohngebaeude/waermepumpe/grosswaermepumpen/vitocal-300-g_pro.html.

[159] Viessmann Deutschland GmbH. Datenblatt Vitobloc EM 20/39, 2015, Retrieved May 17, 2017. URL https://www.viessmann.de/de/wohngebaeude/kraft-waerme-kopplung/blockheizkraftwerk/vitobloc-200-em-20-39.html.

[160] Viessmann Deutschland GmbH. Datenblatt Vitobloc EM 9/20, 2015, Retrieved May 18, 2017. URL https://www.viessmann.de/de/wohngebaeude/kraft-waerme-kopplung/blockheizkraftwerk/vitobloc-200-em-9-20.html.

[161] Viessmann Deutschland GmbH. Datenblatt Vitocal 300 G BW 301.A45, 2015, Retrieved May 18, 2017. URL https://www.viessmann.de/de/wohngebaeude/waermepumpe/sole-wasser-waermepumpen/vitocal-300-g.html.

[162] Viessmann Deutschland GmbH. Datenblatt Vitosol-200-F, 2016, Retrieved June 17, 2017. URL https://www.viessmann.de/de/wohngebaeude/solaranlage/Flachkollektoren/vitosol-200-fm.html.

[163] Viessmann Deutschland GmbH. Datenblatt Vitocrossal 200, 2016, Retrieved May 17, 2017. URL https://www.viessmann.de/de/wohngebaeude/gas-heizkessel/gas-brennwertkessel/vitocrossal-200-cm2.html.

[164] Viessmann GmbH & Co. KG. Planungshandbuch Wärmepumpen, 2011, Retrieved, July 21, 2017. URL https://www.google.de/url?sa=t&rct=j&q=&esrc=s&source=web&cd=1&ved=0ahUKEwjQ8O2SqpPYAhWkJcAKHdJ2BtkQFggpMAA&url=https%3A%2F%2Fwww.viessmann.at%2Fcontent%2Fdam%2Fvi-brands%2FDE%2FPDF%2FPlanungshandbuch%2Fph-waermepumpen.pdf%2F_jcr_content%2Frenditions%2Foriginal.media_file.download_attachment.file%2Fph-waermepumpen.pdf&usg=AOvVaw059r8SK1xu8qLMgAbcuCGG.

[165] H. Wang, W. Yin, E. Abdollahi, R. Lahdelma, and W. Jiao. Modelling and optimization of CHP based district heating system with renewable energy production and energy storage. *Applied Energy*, 159:401–421, 2015. ISSN 03062619. doi: 10.1016/j.apenergy.2015.09.020.

[166] P. Wellbrock. Bewertung der CO2-Emissionen von Elektrofahrzeugen - Stand der wissenschaftlichen Debatte, 2011, Retrieved July 20, 2016. URL http://www.bremer-energie-institut.de/download/publications/BEI100-118_0397_Bericht.pdf.

[167] Wikibooks. Tabellensammlung Chemie/ Dichte fester Stoffe, 2014, Retrieved July 20, 2016. URL https://de.wikibooks.org/wiki/Tabellensammlung_Chemie/_Dichte_fester_Stoffe.

[168] Wikipedia. Beton, Retrieved July 20, 2016. URL https://de.wikipedia.org/wiki/Beton#Rohdichte.

[169] Wikipedia. Schaumglas, Retrieved July 20, 2016. URL https://de.wikipedia.org/wiki/Schaumglas#Eigenschaften.

[170] W. Winter, T. Haslauer, and Obernberger I. Untersuchungen der Gleichzeitigkeit in kleinen und mittleren Nahwärmenetzen. *Euroheat & Power*, 2001, Retrieved September 25, 2017. URL http://www.bios-bioenergy.at/uploads/media/Paper-Winter-Gleichzeitigkeit-Euroheat-2001-09-02.pdf.

[171] Wollersheim GmbH + Co. KG. Viessmann-Z011998-Vitobloc 200 EM-20/39 Preis, 2017, Retrieved April 24, 2017. URL http://www.uhs24.de/viessmann-z011998.html.

[172] Wollersheim GmbH + Co. KG. Viessmann-Z012964-Vitobloc 200 EM-9/20 Preis, 2017, Retrieved April 25, 2017. URL http://www.uhs24.de/viessmann-z012964.html.

[173] D. W. Wu and R. Z. Wang. Combined cooling, heating and power: A review. *Progress in Energy and Combustion Science*, 32(5-6):459–495, 2006. ISSN 0360-1285. doi: 10.1016/j.pecs.2006.02.001.

[174] R. Yumrutas and Ö. Kaska. Experimental investigation of thermal performance of a solar assisted heat pump system with an energy storage. *International Journal of Energy Research*, 28(2):163–175, 2004. ISSN 1099-114X. doi: 10.1002/er.959.

[175] R. Yumrutas, M. Kunduz, and T. Ayhan. Investigation of thermal performance of a ground coupled heat pump system with a cylindrical energy storage tank. *International Journal of Energy Research*, 27(11):1051–1066, 2003. ISSN 1099-114X. doi: 10.1002/er.932.

A Appendix

A.1 Ecological data

The calculation of the TES values is included in the appendix. The values for the CHP and the HP are interpolated between the nominal powers of the data given in the sources. “From-cradle-to-grave” data is used for all components except for the CHP. For the CHP only “from-cradle-to-gate” data was available, but it is assumed that the removal of the CHP has a negligible impact on the overall results. Only the components that are not installed in every scenario are taken into account in the calculation of the global warming potential and the energy demand for "cradle & grave". The district pipes, for example, are present in every scenario and are therefore not included in the calculations.

A.1.1 Ecological data - TES and Solar Pipes

The TES is modeled as a cylinder with a height to diameter ratio of $H/D = 19/26$ [114]. The volume and mass of each TES layer is calculated using the values in table A.1. The GWP and $E_{\mathrm{C\&G}}$ of the TES is calculated using table A.2. The values for reinforced concrete are calculated using a mass ratio of structural steel to concrete of $1/25$ [168].
The solar pipe length in the Solar scenario is 810 m and the pipe diameter is 0.032 m [70]. The GWP for the pipe is $0.2177\,\mathrm{kg_{CO_2e}/(m\,a)}$ and $E_{\mathrm{C\&G}}$ is $1.1868\,\mathrm{kWh/(m\,a)}$ [1; 39; 42; 47; 125].

A.1.2 Ecological data - Scenarios

In table A.3 till A.8 the annual global warming potential and the annual C&G energy of the individual components used in the scenarios are listed.

A.2 Economical data

In the following the data for the capital-related costs, the demand-related costs, the operation-related costs and the revenue is given.

Table A.1: TES wall thickness and layer density.

Material	Wall thickness in m	Density in $\mathrm{kg/(m^3)}$
Stainless steel	0.0005	7900 [167]
Reinforced Concrete	0.15	2500 [168]
Foam glass	0.5	150 [169]

Table A.2: TES material properties.

Material	GWP in $kg_{CO_2e}/(kg\,a)$	$E_{C\&G}$ in kWh/(kg a)
Stainless steel	0.17 [39]	0.56 [39]
Concrete	0.0067 [39]	0.013 [39]
Structural steel	0.078 [39]	0.23 [39]
Reinforced Concrete	0.0095 [39]	0.021 [39]
Foam glass	0.062 [39]	0.25 [39]

Table A.3: GWP and $E_{C\&G}$ of the Gas scenario components.

Component	GWP in $kg_{CO_2e}/(a)$	$E_{C\&G}$ in kWh/(a)	Source
Gas boiler 150 kW	122.3	479.8	[20]
Total	122.3	479.8	-

Table A.4: GWP and $E_{C\&G}$ of the CHP scenario components.

Component	GWP in $kg_{CO_2e}/(a)$	$E_{C\&G}$ in kWh/(a)	Source
CHP 39 kW_{th}	816.8	305.3	adapted from [39; 73]
Gas boiler 150 kW	122.3	479.8	[20]
TES 10 m^3	207	705.4	Calculated with [39]
CHP pump 1.1 kW	8.0	26.3	adapted from [39]
Total	1154.0	1516.8	-

Table A.5: GWP and $E_{C\&G}$ of the CHP+Geo scenario components.

Component	GWP in $kg_{CO_2e}/(a)$	$E_{C\&G}$ in kWh/(a)	Source
CHP 20.1 kW_{th}	382.9	143.1	adapted from [39; 73]
VGHX + HP 42.8 kW	146.6	1324.3	adapted from [20]
TES 90 m^3	790.1	2645.1	Calculated with [39]
CHP pump 1.1 kW	8.0	26.3	adapted from [39]
Primary pump 1.3 kW	9.4	31.1	adapted from [39]
Secondary pump 0.1 kW	0.7	2.4	adapted from [39]
Total	1344.2	4193.9	-

Table A.6: GWP and $E_{C\&G}$ of the Geo scenario components.

Component	GWP in $kg_{CO_2e}/(a)$	$E_{C\&G}$ in kWh/(a)	Source
VGHX + HP 93 kW	248.8	2201.9	adapted from [20]
TES 60 m^3	613.3 2058.5	Calculated with [39]	
Primary pump 1.3 kW	9.4	31.0	adapted from [39]
Secondary pump 0.1 kW	0.7	2.4	adapted from [39]
Total	872.2	4293.8	-

Table A.7: GWP and $E_{C\&G}$ of the Solar scenario components.

Component	GWP in $kg_{CO_2e}/(a)$	$E_{C\&G}$ in kWh/(a)	
Solar thermal collectors 500 m^2	2834.5	10 003.5	[39]
Gas boiler 150 kW	122.3	479.8	[20]
TES 800 m^3	3187.8	10 572.4	Calculated with [39]
Solar pump 1.1 kW	8.0	26.3	adapted from [39]
Solar Pipes 810m	176.3	961.2	See section A.1.1
Total	6328.8	22 043.2	-

Table A.8: GWP and $E_{C\&G}$ of the P2H scenario components.

Component	GWP in $kg_{CO_2e}/(a)$	$E_{C\&G}$ in kWh/(a)	Source
PV modules 98 kW_p	5175.0	17 106.9	adapted from [39]
VGHX + HP 93 kW	248.8	2201.9	adapted from [20]
Air HP 11*16 kW	472.5	1789.0	adapted from [20]
Seasonal TES 1200 m^3	4146.7	13 736.6	Calculated with [39]
Buffer TES 90 m^3	790.1	2645.1	Calculated with [39]
Primary pump 1.3 kW	9.4	31.0	adapted from [39]
Secondary pump 0.1 kW	0.7	2.4	adapted from [39]
Air/Water pump 1.3 kW	9.4	31.0	adapted from [39]
TES pump 90 W	0.7	2.2	adapted from [39]
Total	10 799.5	37 517.5	-

Table A.9: Data for the calculation of annuity and the price increase.

	%	Source
Interest factor ϵ	3.0	[88]
Price change factor natural gas $r_{D,gas}$	1.5	[88]
Price change factor electricity $r_{D,el}$	3.0	[88]
Price change factor operation r_O	1.5	[88]
Price change factor Revenue r_R	3	Assumption

Table A.10: Gas scenario gross investment.

Component	A_0 in €	Source
Gas boiler 150 kW	12 228.44	[154]
Subtotal	12 228.44	
Project planning 10 %	1222.84	[72; 124]
Installation 15 %	2131.30	[12; 72]
Uncertainty 10 %	1222.84	[12; 72]
Total	16 805.43	

Table A.11: CHP scenario gross investment.

Component	A_0 in €	Source
CHP 39 kW_{th}	46 695.00	[171]
Input tax deduction 86.0 %	−6411.73	[19]
Gas boiler 150 kW	12 228.44	[154]
Buffer TES 10 m^3	6182.05	[82]
Buffer TES Insolation 17.5 %	1081.86	[82; 86]
CHP pump 1.1 kW	1980.24	[51; 72]
Subtotal	61 755.86	
BAFA subsidy	−3500.00	[18]
BAFA bonus subsidiy	−875.00	[18]
Subtotal	57 380.86	
Project planning 10.0 %	5738.09	[72; 124]
Installation 15.0 %	8607.13	[12; 72]
Uncertainty 10.0 %	5738.09	[12; 72]
Total	77 464.16	

A.2.1 Capital-related costs

All components are assumed to have a life cycle of 20 years and the costs of disposal are neglected. It is further assumed that the whole DHS with all its components does not have any liquidation proceeds. Taken into account in the calculation of the capital-related costs are only the components which are not installed in every scenario. The district pipes, for example, are present in every scenario and are therefore not included in the calculations.

The two scenarios with a CHP are entitled to an input tax reduction for the CHP. According to the verdict of the supreme tax court (Bundesfinanzhof) from 16.11.2016 the input tax reduction is calculated dependent on the sale prices of heat and electricity, leading to a partitioning of 14 % and 86 % for heat and electricity [19] for the CHP.

In the geothermal scenario subsidies would be possible if the seasonal performance factor of the HP would be above 3.8. The current result is 3.75 which is very close to 3.8. Therefore, the subsidies are calculated for the geothermal scenario even though they are just below the needed value. The available subsidies are given in table A.13.

The P2H scenario is entitled to an input tax reduction of 100 % for the PV modules and their auxiliary components [84]. In table A.10 till A.15 the gross investment of the individual scenarios is listed.

Table A.12: CHP+Geo scenario gross investment.

Component	A_0 in €	Source
CHP 20.1 kW_{th}	31 653.00	[172]
Input tax deduction 86.0 %	−4346.30	[19]
HP 42.8 kW	23 382.31	[154]
VGHX	46 080.00	[88; 113]
TES 90 m^3	70 537.00	adapted from [35]
CHP pump 1.1 kW	1980.24	[51; 72]
Primary pump 1.3 kW	5870.95	[51]
Secondary pump 0.1 kW	809.74	[51; 72]
Subtotal	175 966.93	
BAFA subsidy	−3250.00	[18]
BAFA bonus subsidiy	−812.50	[18]
Basis subsidy 100.00 €/$kW_{HP\ power}$	−4280.00	[21]
Additional subsidy	−500.00	[21]
Clearance subsidy TES 30.0 % net	−17 782.44	[21]
Subtotal	149 342.00	
Project planning 10.0 %	14 934.20	[72; 124]
Installation 15.0 %	22 401.30	[12; 72]
Uncertainty 10.0 %	14 934.20	[12; 72]
Total	201 611.70	

Table A.13: Geo scenario gross investment.

Component	A_0 in €	Source
HP 93.0 kW	35 218.05	[154]
VGHX	92 160.00	[88; 113]
TES incl. Insolation 60 m^3	55 335.00	[35]
Primary pump 1.3 kW	5870.95	[51]
Secondary pump 0.1 kW	809.74	[51; 72]
Subtotal	189 393.73	
Basis subsidy 100.00 €/$kW_{HP\ power}$	−9300.00	[21]
Additional subsidy	−500.00	[21]
Clearance subsidy TES 30.0 % net	−13 950.00	[21]
Subtotal	165 643.73	
Project planning 10.0 %	16 564.37	[72; 124]
Installation 15.0 %	24 846.56	[12; 72]
Uncertainty 10.0 %	16 564.37	[12; 72]
Total	223 619.04	

Table A.14: Solar scenario gross investment.

Component	A_0 in €	Source
Solar thermal collectors 500 m^2	180 052.17	[154]
Gas boiler 150 kW	12 228.44	[154]
TES 800 m^3, net 350.00 €/m^3	333 200.00	[86]
Solar pump 1.1 kW	1980.24	[51; 72]
Solar pipes 810 m, 38.56 €/m	31 230.36	[72]
Pipe channel 405 m, average of costs beneath street and field 93.71 €/m	37 953.56	[72]
Subtotal	596 644.78	
Innovation subsidy 200.00 €/$m^2_{\text{collector area}}$	−100 000.00	[21]
Additional subsidy for DHS and gas boiler	−1000.00	[21]
TES subsidy 10 % net	−28 000.00	[21]
Subtotal	467 644.78	
Project planning 10.0 %	46 764.48	[72; 124]
Installation without TES 15.0 %	20 166.72	[12; 72]
Uncertainty 10.0 %	46 764.48	[12; 72]
Total	581 340.45	

A.2.2 Demand-related costs

In table A.16 the demand relates tariffs for natural gas and electricity are listed. There are two different tariffs for natural gas, because the energy tax can be omitted for natural gas used in CHP plants [23]. For HP, reduced tariffs for electricity exist and the tariff for PV electricity for own consumption consists of the turnover tax and of 40.0 % of the renewable energies law allocation (EEG Umlage) [17; 24].

A.2.3 Operation-related costs

In table A.20 till A.22 the operation-related costs of the different scenarios are listed.

A.2.4 Revenue

In table A.23 the tariffs for feed-in of PV and CHP electricity are listed. In contrast to the own consumption of PV electricity, the own consumption of CHP electricity also generates a revenue.

Table A.15: P2H scenario gross investment.

Component	A_0 in €	Source
PV modules 98 kW_p	84 336.66	[17; 110]
Inverter 100 kW	22 100.00	[17; 41]
Cable 1100 m, 2.5 €/m	3272.50	[3; 17]
Rack 148.75 €/kW_p	14 577.50	[3; 17]
Input tax deduction 100.0 %	−4346.30	[84]
HP 93.0 kW	35 218.05	[154]
VGHX	92 160.00	[88; 113]
Air HP 11*16 kW incl. necessary accessories	153 048.28	[123]
Cascade controller	1383.00	[79]
Buffer TES incl. Insolation 90 m^3	70 537.00	[35]
Seasonal TES 1200 m^3	428 400.00	[86]
Primary pump 1.3 kW	5870.95	[51]
Secondary pump 0.1 kW	809.74	[51]
Air/Water pump 1.3 kW	5870.95	[51]
TES pump 90 W	704.48	[51]
Subtotal	898 445.01	
Basis subsidy 100.00 €/$kW_{HP\ power}$	−9300.00	[21]
Additional subsidy	−500.00	[21]
Clearance subsidy TES 90 m^3 30 % net	−17 782.44	[21]
TES subsidy 1200 m^3 10.0 % net	−36 000.00	[21]
Subtotal	834 862.58	
Project planning 10.0 %	83 486.26	[72; 124]
Installation without seasonal TES 15.0 %	60 969.39	[12; 72]
Uncertainty 10.0 %	83 486.26	[12; 72]
Total	1 062 804.48	

Table A.16: Demand-related costs.

Component	in €/(kWh)	Source
Natural gas CHP tariff	0.0545	[88]
Natural gas	0.06	[88]
Electricity	0.2869	[25]
Electricity HP tariff	0.1975	[88]
PV electricity own consumption	0.0573	[17; 24]

Table A.17: Gas scenario operation-related costs.

Component	f_O in %	$A_0 f_O$ in €	Source
Gas boiler 150 kW	2.5	305.71	[152]
District pump 1.1 kW	3.0	59.41	[152]
Total		365.12	

Table A.18: CHP scenario operation-related costs.

Component	f_O in %	$A_0 f_O$ in €	Source
CHP 39 kW_{th}	8.0	3735.60	[152]
Gas boiler 150 kW	2.5	305.71	[152]
Buffer TES 10 m^3	2.5	181.60	[152]
District pump 1.1 kW	3.0	59.41	[152]
CHP pump 1.1 kW	3.0	59.41	[152]
Total		4282.32	

Table A.19: CHP+Geo scenario operation-related costs.

Component	f_O in %	$A_0 f_O$ in €	Source
CHP 20.1 kW_{th}	8.0	2532.24	[152]
HP 42.8 kW	2.5	584.56	[152]
VGHX	3.0	1382.40	[152]
TES 90 m^3	2.5	1763.43	[152]
District pump 1.1 kW	3.0	59.41	[152]
CHP pump 1.1 kW	3.0	59.41	[152]
Primary pump 1.3 kW	3.0	176.13	[152]
Secondary pump 0.1 kW	3.0	24.29	[152]
Total		6581.86	

Table A.20: Geo scenario operation-related costs.

Component	f_O in %	$A_0 f_O$ in €	Source
HP 93.0 kW	2.5	880.45	[152]
VGHX	3.0	2764.80	[152]
TES 60 m^3	2.5	1383.38	[152]
District pump 1.1 kW	3.0	59.41	[152]
Primary pump 1.3 kW	3.0	176.13	[152]
Secondary pump 0.1 kW	3.0	24.29	[152]
Total		5288.45	

Table A.21: Solar scenario operation-related costs.

Component	f_O in %	$A_0 f_O$ in €	Source
Solar thermal collectors 500 m^2	1.5	2700.78	[152]
Gas boiler 150 kW	2.5	305.71	[152]
TES 800 m^3, net 350 €/m^3	2.5	8330.00	[152]
District pump 1.1 kW	3.0	59.41	[152]
Solar pump 1.1 kW	3.0	59.41	[152]
Total		11 455.31	

Table A.22: P2H scenario operation-related costs.

Component	f_O in %	$A_0 f_O$ in €	Source
PV modules 98 kW_p	1.5	1864.30	Assumption
HP 93.0 kW	2.5	880.45	[152]
VGHX	3.0	2764.80	[152]
Air HP 11*16 kW incl. necessary accessories	2.5	3860.78	[152]
Buffer TES 90 m^3	2.5	1763.43	[152]
Seasonal TES 1200 m^3	2.5	10 710.00	[152]
District pump 1.1 kW	3.0	59.41	[152]
Primary pump 1.3 kW	3.0	176.13	[152]
Secondary pump 0.1 kW	3.0	24.29	[152]
Air/Water pump 1.3 kW	3.0	176.13	[152]
TES pump 90 W	3.0	21.13	[152]
Total		22 300.85	

Table A.23: Revenue.

Component	in €/(kWh)	Source
Feed-in tariff PV electricity	10.71	[24]
Feed-in tariff CHP electricity	10.79	[88]
CHP electricity own consumption	1.458	[88]